Wireless Communication

over Dispersive Channels

Wireless Communication
over Dispersive Channels

PROEFSCHRIFT

ter verkrijging van de graad van doctor
aan de Technische Universiteit Delft,
op gezag van de Rector Magnificus Prof. ir. K.C.A.M Luyben,
voorzitter van het College voor Promoties,
in het openbaar te verdedigen op maandag 1 maart 2010 om
10:00 uur
door

Kun FANG

MASTER OF SCIENCE ETH ZÜRICH
geboren te Tianjin, China.

Dit proefschrift is goedgekeurd door de promotor:

Prof. dr. ir. A.-J. van der Veen

Copromotor:

Dr. ir. G. Leus

Samenstelling promotiecommissie:

Rector Magnificus	voorzitter
Prof. dr. ir. A.-J. van der Veen	Technische Universiteit Delft, promotor
Dr. ir. G. Leus	Technische Universiteit Delft, copromotor
Prof. dr. M. C. Gastpar	Technische Universiteit Delft / University of California, Berkeley
Prof. dr. ir. J.W.M. Bergmans	Technische Universiteit Eindhoven
Prof. dr. G. Matz	Technische Universitaet Wien
Prof. dr. P. Banelli	Universita' degli Studi di Perugia
Prof. dr. U. Mitra	University of Southern California
Prof. dr. ir. I.G.M.M. Niemegeers	Technische Universiteit Delft, reservelid

ISBN 978-94-6113-006-8

To my family.

Summary

Broadband wireless communication systems require high transmission rates, where the bandwidth of the transmitted signal is larger than the channel coherence bandwidth. This gives rise to time dispersion of the transmitted symbols or frequency-selectivity with different frequency components exhibiting different gains. The time dispersion of the transmitted symbols induces intersymbol interference (ISI) due to multipath propagation, with multipath delays exceeding the transmitted symbol period. On the other hand, recent wireless communication standards such as WiMAX and Long Term Evolution (LTE) not only require high rates, but they also need to support high mobile speeds. High-mobility terminals and scatterers induce Doppler shifts which give rise to a fast fading channel, where the channel coherence time is smaller than the symbol period, and the channel changes rapidly within the symbol duration. The Doppler spreads induce frequency dispersion or time selectivity.

LTE is a major step in next generation wireless networks. The LTE physical layer relies on a multiple-access scheme based on orthogonal frequency-division multiplexing (OFDM) with a cyclic prefix (CP) in the downlink, and on single-carrier frequency-division multiple access (SC-FDMA) with a CP in the uplink. OFDM is one of the most important transmission schemes for wireless communications, and it has been used in many standards such as DVB-T/H, DAB, and IEEE 802.11. OFDM can eliminate ISI introduced in a static frequency-selective channel by turning it into a set of parallel frequency-flat channels, and therefore it enables simple one-tap equalization for each subcarrier. An SC system, which can also be viewed as a discrete Fourier transform (DFT) precoded OFDM system, has a smaller peak-to-average-power ratio than conventional OFDM, with complexity and performance comparable to OFDM, but with the complexity shifted from the transmitter to the receiver. Hence, it leads to more power-efficient terminals suitable for uplink transmission. However, both OFDM system and SC system using frequency-domain

equalization suffer from time-varying channels, where the orthogonality among the subcarriers is destroyed due to the Doppler shifts. The resulting intercarrier interference (ICI) severely degrades the performance of the one-tap equalizer. The ICI caused by Doppler spreading also makes the channel estimation problem more challenging, which is important for a coherent communication system, with the equalizer at the receiver relying on accurate channel state information. Therefore, advanced techniques are needed to accurately model time- and frequency-selective (i.e., doubly-selective) channels and to counteract the related performance degradation.

In the last decade, multi-antenna systems have attracted a lot of research interest for future wireless systems. Using multiple transmit and/or receive antennas can significantly enhance communication system performances such as channel capacity and reliability. Space-time block coding (STBC) has been introduced to achieve the spatial diversity offered by multiple transmit and/or receive antennas. However, as STBC is typically designed for flat-fading channels, the time- and frequency-selectivity will seriously degrade the system performance. Thus, it is crucial to design efficient STBC schemes to counteract its effects.

The first part of the thesis focuses on the receiver design for block transmission over doubly-selective channels, specifically, iterative channel estimation and low-complexity turbo equalization for OFDM and SC systems. The second part of the thesis focuses on STBC design for multi-antenna systems in doubly-selective channels. The proposed STBC is designed for a multiple-input single-output (MISO) system with 2 transmit antennas and 1 receive antenna, i.e., a 2×1 system, but it is straightforward to extend the ideas to a general multiple-input multiple-output (MIMO) system.

Contents

Acronyms and Abbreviations

BEM	Basis Expansion Model
BER	Bit Error Rate
BIE	Block Iterative Equalizer
BLE	Block Linear Equalizer
CA	Complex Addition
CD	Complex Division
CDMA	Code Division Multiple Access
CM	Complex Multiplications
CP	Cyclic Prefix
CSI	Channel State Information
DFT	Discrete Fourier Transform
DPS	Digital Phase Sweeping
FDKD	Frequency-Domain Kronecker Delta
FIR	Finite Impulse Response
GSM	Global System for Mobile
IBI	Inter Block Interference
ICI	Intercarrier Interference
ISI	Intersymbol Interference
LLR	Log-Likelihood Ratio
LTE	Long Term Evolution
LTV	Linear Time-Varying
MBAE-SOE	Minimum-Band-Approximation-Error Sum-of-Exponential
MIMO	Multiple-Input Multiple-Output
MISO	Multiple-Input Single-Output
ML	Maximum Likelihood
MMSE	Minimum Mean-Squared Error
MSE	Mean Square Error
OCE-BEM	Oversampled Complex Exponential BEM
OFDM	Orthogonal Frequency-Division Multiplexing
OFDMA	Orthogonal Frequency-Division Multiple Access
PAR	Peak-to-Average Ratio
PDF	Probability Density Function

QPSK	Quaternary Phase-Shift Keying
RLS	Recursive Least Squares
SC	Single Carrier
SC-FDMA	Single-Carrier Frequency-Division Multiple Access
SIE	Serial Iterative Equalizer
SISO	Single-Input Single-Output
SLE	Serial Linear Equalizer
SNR	Signal-to-Noise Ratio
STBC	Space-Time Block Coding
STF	Space-Time-Frequency
TDKD	Time-Domain Kronecker Delta
TDMA	Time Division Multiple Access
UAC	Underwater Acoustic Communication
UMTS	Universal Mobile Telecommunications System
WSSUS	Wide-Sense Stationary Uncorrelated Scattering
ZF	Zero Forcing

Chapter 1

Introduction

Guglielmo Marconi was awarded the Nobel Prize in Physics in recognition of his contributions to the development of wireless telegraphy in 1909, which involved the transmission of information messages without connecting wires. During the 100 years since Marconi received his Nobel Prize award, wireless communication technology has undergone many evolutions.

The first generation large scale commercial mobile communication systems relied on "analogue" technology, for example, the Analogue Mobile Phone System used in America. Later, second generation systems were developed, such as the Global System for Mobile communications (GSM) using time division multiple access (TDMA) and the Interim Standard 95 (IS-95) using code division multiple access (CDMA). Different from the first generation systems, they are all digital cellular standards. Nowadays, third generation systems have been deployed over the world, with representative systems such as the Universal Mobile Telecommunications System (UMTS) and CDMA2000. Besides commercial mobile communication systems, wireless transmission is also widely used in underwater communication, satellite communication, vehicular communication, etc. Since Nov. 2004, the 3rd Generation Partnership Project (3GPP) has started to develop the Long Term Evolution (LTE) of the UMTS system, which is a major step in next generation wireless networks, with the goal of achieving higher user data rates, improved spectral efficiency, greater flexibility of spectrum usage, and other improvements over the current mobile communication systems. The first version of LTE has been published in Release 8 of the 3GPP specification. The fundamental technologies for LTE physical layer design are orthogonal frequency-division multiple access (OFDMA) for the downlink and single-carrier frequency-division multiple ac-

cess (SC-FDMA) for the uplink, as well as multi-antenna technology.

1.1 Problem Statement and Research Objectives

Future mobile communication systems not only require high transmission rates, but they also need to support high mobile speeds. When the bandwidth of the transmitted signal is larger than the channel coherence bandwidth, it gives rise to time dispersion of the transmitted symbols and frequency selectivity with different frequency components exhibiting different gains. The time dispersion of the transmitted symbols induces intersymbol interference (ISI) due to multipath propagation. On the other hand, high-mobility terminals and scatterers induce Doppler shifts which give rise to a fast fading channel, where the channel coherence time is smaller than the symbol period, and the channel changes rapidly within the symbol duration. The Doppler spreads induce frequency dispersion or time selectivity.

OFDM is one of the most important transmission schemes for wireless communications, and it has been used in many standards such as DVB-T/H, DAB, and IEEE 802.11. Recently, OFDM transmission is also applied to underwater acoustic communication (UAC). As the sound speed is much slower than that of light in the water, which is approximately 1500m/s, it gives rise to a very large delay spread and frequency-selective fading. The low speed of the sound also leads to the problem of a large Doppler spread. Thus, the UAC channel can be regarded as a doubly-selective channel. OFDM can eliminate ISI introduced by a frequency-selective channel by turning it into a set of parallel frequency-flat channels, and therefore it enables simple one-tap equalization for each subcarrier. An SC system, which can also be viewed as a discrete Fourier transform (DFT) precoded OFDM system, has a smaller peak-to-average-power ratio than conventional OFDM, with complexity and performance comparable to OFDM, but with the complexity shifted from the transmitter to the receiver. Hence, it leads to more power-efficient terminals suitable for uplink transmission. However, both OFDM system and SC system using frequency-domain equalization suffer from doubly-selective channels, where the orthogonality among the subcarriers is destroyed due to the Doppler shifts, and the intercarrier interference (ICI) severely degrades the performance of the one-tap equalizer. The ICI caused by Doppler spreading also makes the channel estimation problem more challenging, which is important for a coherent communication system, with the equalizer at the receiver relying on

accurate channel state information. Doubly-selective channels can also provide multiplicative delay-Doppler diversity gains if the transceiver is properly designed, with diversity being an effective way to combat fading channels.

In order to counteract the effects of a time-varying channel, several different equalization techniques have been proposed [5–18] for OFDM systems. Among all the equalizers for OFDM in time-varying channels, one of the most promising approaches is the iterative MMSE serial linear equalizer (SLE) of [10]. This iterative approach is inspired by turbo equalization [19,20], where soft information is used in an iterative fashion to improve the bit error rate (BER) performance. Optimal joint processing of equalization and decoding at the receiver is prohibitive due to the heavy computational burden. Instead, the equalization and decoding tasks can be performed separately and carried out iteratively, with soft information being interchanged between these two parts. However, there is an error floor of the BER performance for the proposed SLE [10].

While turbo equalization for SC transmissions over frequency-selective channels has been originally applied in the time domain (see references in [19]), frequency-domain equalization has gained much interest due to its comparable complexity and performance to OFDM transceivers [33, 34, 47]. For SC systems in doubly-selective channels, a low-complexity iterative equalizer has been proposed in [35], which can be regarded as the time-domain counterpart of the iterative frequency-domain equalizer [40]. However, time-domain iterative equalizers are not suitable for long channels, since their complexity is quadratic in the channel length [35].

The above equalization algorithms require an accurate channel estimation at the receiver. Pilot-assisted channel estimation algorithms have been developed to model and estimate time-varying flat fading channels in [48, 49], and doubly-selective channels in [23, 39, 43, 44] for OFDM and SC systems. A superimposed training method has been developed in [38]. Besides pilot symbols, soft data estimates can be used to improve the quality of channel estimation, as shown in [24] using recursive least squares (RLS) algorithms.

In order to have reliable and efficient communications over a very hostile wireless medium, advanced techniques are needed to accurately model the doubly-selective channels and to counteract the related performance degradation. The first part of the thesis focuses on the receiver design, i.e, low-complexity turbo equalization and iterative channel estimation algorithms for block transmission. Algorithms are developed to effectively achieve the time

and frequency diversity offered by the doubly-selective channels.

In the last decade, multi-antenna systems have attracted a lot of research interest for future wireless systems. The use of multiple transmit and/or receive antennas can significantly enhance communication system performances such as channel capacity and reliability [53]. Space-time block coding (STBC) [54, 55] has been introduced to achieve the spatial diversity offered by multiple transmit and/or receive antennas. However, as STBC is typically designed for flat-fading channels, the time and frequency selectivity will seriously degrade the system performance. Thus, it is crucial to design efficient STBC schemes to counteract its effects. The second part of the thesis focuses on the design of STBC for multi-antenna systems under doubly-selective channels. Specifically, how to design a STBC which can jointly exploit the degrees of freedom in the time, frequency and spatial domains, while achieving a larger coding gain with higher spectral efficiency.

1.2 Contributions and Outline

The rest of the thesis is organized as follows.

In Chapter 2, we first briefly describe the wireless channel model, including the frequency-selective and time-varying (doubly-selective) channel approximation using a basis expansion model (BEM). Then we summarize the fundamental knowledge of OFDM and SC transmission systems, multi-antenna systems and the principle of MMSE estimation algorithms.

In Chapter 3 and Chapter 4, we develop new receivers for OFDM systems and SC systems in doubly-selective channels by embedding the channel estimation task within low-complexity block turbo equalizers. The presented equalizers are based on a soft MMSE block linear equalizer (BLE), and exploit both the banded structure of the frequency-domain channel matrix and receiver windowing. Therefore, their complexities will be linear in the block length. We derive iterative pilot-assisted channel estimators for both OFDM and SC systems. Specifically, in each channel estimation iteration, we also exploit the soft data estimates obtained from the turbo equalizer. These data estimates are used as additional virtual pilots, and their reliability, also obtained from the turbo equalizer, is included in the channel estimation process.

The publications related to these two chapters are the following:

- K. Fang, L. Rugini and G. Leus, "Block Transmission over Doubly-Selective Channels: Iterative Channel Estimation and Turbo Equalization," *Eurasip J. Advances in Signal Processing,* submitted.

- K. Fang, L. Rugini and G. Leus, "Low-complexity block turbo equalization for OFDM systems in time-varying channels," *IEEE Trans. Signal Processing,* vol. 56, no. 11, pp. 5555-5566, Nov. 2008.

- K. Fang, L. Rugini and G. Leus, "Low-Complexity Frequency-Domain Turbo Equalization for Single-Carrier Transmissions over Doubly-Selective Channels," in *Proc. IEEE International Conference on Acoustics, Speech, and Signal Processing (ICASSP),* Taipei, Taiwan, Apr. 2009.

- K. Fang, L. Rugini and G. Leus, "Iterative channel estimation and turbo equalization for time-varying OFDM systems," in *Proc. IEEE International Conference on Acoustics, Speech, and Signal Processing (ICASSP),* Las Vegas, NV, USA, Mar. 2008.

- K. Fang and G. Leus, "Low-Complexity Block Turbo Equalization for OFDM Systems in Time-varying Channels," in *Proc. IEEE International Conference on Acoustics, Speech, and Signal Processing (ICASSP),* Honolulu, Hawaii, Apr. 2007.

In Chapter 5, we develop a novel STBC for multi-antenna transmissions over doubly-selective channels. The proposed STBC is designed for a multiple-input single-output (MISO) system with 2 transmit antennas and 1 receive antenna, i.e., a 2×1 system, but it is straightforward to extend the ideas to a general multiple-input multiple-output (MIMO) system. The proposed technique can be interpreted as the extension of the Alamouti code to doubly-selective channels, and relies on a joint time-frequency reversal of the transmitted sequences.

The publications related to this chapter are the following:

- K. Fang and G. Leus, "Space-Time Block Coding for Doubly-Selective Channels," *IEEE Trans. Signal Processing,* Mar. 2009.

- K. Fang and G. Leus, "Space-Time Block Coding for Frequency-Selective and Time-Varying Channels," in *Proc. 43th Asilomar Conf. Signals, Systems, and Computers,* Pacific Grove, CA, Nov. 2009.

Besides the aforementioned research works presented in this thesis, other contributions have been presented in the following papers:

- L. Rugini, P. Banelli, K. Fang and G. Leus, "Enhanced Turbo MMSE Equalization for MIMO-OFDM over Rapidly Time-Varying Frequency-Selective Channels," in *Proc. of Intl. Workshop on Signal Processing Advances in Wireless Communication (SPAWC 2009),* Perugia, Italy, Jul. 2009.

- K. Fang and G. Leus, "Low-Complexity Block Turbo Equalization for OFDM Systems in Time- and Frequency-Selective Channels," in *Proc. 3rd Annual IEEE Benelux/DSP Valley Signal Processing Symposium,* Antwerp, Belgium, pp. 83-87, Mar. 2007.

- K. Fang, G. Leus, and L. Rugini, "Alamouti space-time coded OFDM systems in time- and frequency-selective channels," in *Proc. of Globecom Conf. (Globecom 2006),* St. Francisco, CA, Nov. 2006.

1.3 Notation

We use upper (lower) boldface letters to denote matrices (column vectors). $(\cdot)^T$, $(\cdot)^H$ and $(\cdot)^\dagger$ represent transpose, complex conjugate transpose (Hermitian), and pseudo-inverse, respectively. $[\mathbf{x}]_p$ indicates the $(p+1)$st element of $\mathbf{x}$, and $[\mathbf{A}]_{m,n}$ indicates the $(m+1, n+1)$th entry of the matrix $\mathbf{A}$. We use the symbol $\circ$ and $\otimes$ to denote the Hadamard (element-wise) product and Kronecker product between matrices, respectively. $\mathrm{diag}(\mathbf{a})$ is a diagonal matrix with the vector $\mathbf{a}$ on the diagonal. $\mathrm{E}(\cdot)$ stands for the statistical expectation. The covariance matrix between $\mathbf{x}$ and $\mathbf{y}$ is defined as $\mathrm{Cov}(\mathbf{x}, \mathbf{y}) = \mathrm{E}(\mathbf{x}\mathbf{y}^H) - \mathrm{E}(\mathbf{x})\mathrm{E}(\mathbf{y}^H)$. $\mathbf{F}_N$ denotes the unitary N-point DFT matrix with $[\mathbf{F}_N]_{p,q} = \frac{1}{\sqrt{N}} e^{-j\frac{2\pi}{N}pq}$. The $J \times J$ permutation matrices $\{\mathbf{P}_{\mathrm{er}_J}^{(n)}\}_{n=0}^{J-1}$ are defined to perform a reversed cyclic shift, i.e., $[\mathbf{P}_{\mathrm{er}_J}^{(n)}\mathbf{a}]_p = [\mathbf{a}]_{(J-p+n) \bmod J}$. Finally, $\mathbf{0}_{M\times N}$ and $\mathbf{I}_N$ denote the $M \times N$ all-zero matrix and the $N \times N$ identity matrix, respectively.

Chapter 2

Preliminaries

In this chapter, we first briefly describe the wireless channel model, and the doubly-selective channel approximation using the basis expansion model (BEM). Then we summarize the fundamentals of OFDM and SC transmission systems, multi-antenna systems and the principle of MMSE estimation algorithms.

2.1 Wireless Fading Channels

Modeling the electromagnetic wave propagation from Maxwell's equations is in general too complex. Wireless channel modeling usually resorts to a statistical approach, i.e., using a stochastic model and a few parameters to characterize the system input-output relationship.

An important part of wireless channel models is the fading effect, causing a variation of the received signal amplitude over time and frequency. There are mainly two types of fading that are used for describing the wireless channel. Large-scale fading, which arises due to path loss and shadowing effects, is in general a function of the distance between the transmitter and receiver and is relatively constant over time, and independent of frequency. Small-scale fading can be described as a random time-varying system due to the relative motion between the transmitter and receiver, and multipath propagation. It results in changes in signal amplitude and phase change over a very short moving distance, and is frequency dependent. In the remainder of this section, we will focus on the small-scale fading for a single-input single-output (SISO) system. In the thesis, *fading* always refers to small-scale fading, unless explicitly defined

otherwise. More detailed background information can be found in the the following references [46, 75, 79, 80].

2.1.1 General Linear Time-Varying Model

We first consider a continuous-time linear time-varying (LTV) system consisting of a wireless transmission channel perturbed by additive noise. The system is modeled as

$$y(t) = \int_{-\infty}^{\infty} h(t,\tau)x(t-\tau)d\tau + n(t), \tag{2.1}$$

where $x(t)$ and $y(t)$ are the transmitted and received signal, respectively, $h(t,\tau)$ is the channel impulse response, and $n(t)$ is the noise. Due to the finite time support, we can assume that $h(t,\tau) = 0$ for $\tau < 0$ and $\tau > \tau_{\max}$, with $\tau_{\max}$ the maximal delay spread. It is common to assume that the wireless channel has the wide-sense stationary (WSS) and uncorrelated scattering (US) properties. The correlation function of the impulse response under the WSSUS assumption can be expressed as

$$R_h(t,t';\tau,\tau') = \mathrm{E}[h(t,\tau)h^*(t',\tau')] = R_h(t-t',\tau)\delta(\tau-\tau'). \tag{2.2}$$

The delay-Doppler spreading function $S_H(\tau,\nu)$ is defined as

$$S_H(\tau,\nu) = \int_{-\infty}^{\infty} h(t,\tau)e^{-j2\pi\nu t}dt, \tag{2.3}$$

and we can rewrite (2.1) as

$$y(t) = \int_{\tau}\int_{\nu} S_H(\tau,\nu)x(t-\tau)e^{j2\pi\nu t}d\nu d\tau + n(t). \tag{2.4}$$

It can be seen from (2.4) that the received signal is the sum of time-frequency shifted and weighted transmitted signals. The time shifts arise due to the multipath propagation between the transmitter and receiver and the frequency shifts arise due to the relative motion between the transmitter and receiver. In a practical mobile radio channel, we have $\tau_{\max}\nu_{\max} \ll 1$, i.e., an underspread channel, with $\nu_{\max}$ the maximal Doppler spread.

Coherence bandwidth is used to measure the time dispersiveness of the wireless channel, which is inversely proportional to the delay spread. If the

input signal has a bandwidth less than the coherence bandwidth, the channel is said to be frequency-flat fading, i.e., narrowband; otherwise, it is a frequency-selective fading channel. Notice that whether it is a flat-fading channel or a frequency-selective fading channel depends on the wireless channel property, as well as the input signal bandwidth. Coherence time, which is the dual of coherence bandwidth, measures the frequency dispersiveness of the wireless channel, and is inversely proportional to the Doppler spread. If the input signal has a symbol period larger than the coherence time, the channel is said to be fast fading (time-varying), where the channel impulse response can change rapidly within the symbol duration; otherwise, the channel is said to be slow fading, where the channel impulse response can be regarded as constant within the symbol duration.

Sampling the received signal at the symbol rate T according to the sampling theorem, we get the discretized channel model corresponding to (2.1) as

$$y_n := y(nT) = \sum_{l=0}^{L} h_{n,l}^t x_{n-l} + n_n, \tag{2.5}$$

where $h_{n,l}^t$ is the baseband discrete-time channel, consists of channel impulse response taking into account the transmit filter, receive filter and the wireless propagation channel, represented by a time-varying FIR filter with limited time support, and $LT > \tau_{\max}$.

In this thesis, we consider the challenging case where the wireless channel is frequency-selective and time-varying (doubly-selective).

2.1.2 Modeling a Time-Varying Channel Using the Basis Expansion Model

In fast-fading channels, the Doppler shift is not negligible, and the channel impulse response changes rapidly within the symbol duration. The time-varying channel can be described by the second order moment statistics as

$$\mathrm{E}(h_{n,l}^t h_{n-m,l}^{t*}) = \sigma_l^2 \gamma_m, \tag{2.6}$$

where σ_l^2 is the energy of the lth channel tap and γ_m is in Fourier relation with Doppler spectrum. Specifically, we use Jakes' model in the later chapters, with

γ_m being expressed as [46]

$$\gamma_m = J_0\left(2\pi\frac{f_c v}{c}T|m|\right), \tag{2.7}$$

where $J_0(\cdot)$ is the zero-order Bessel function of the first kind, f_c the carrier frequency, v the moving velocity, and c the speed of the wave propagation.

We consider a block transmission which will be discussed in detail in the later chapters. Assume the block length is N and there are $L+1$ channel taps as in (2.5), and $\mathbf{h}_{t,l}$ is a $N \times 1$ vector collecting the channel coefficients from time index 0 to $N-1$ at the lth channel tap,

$$\mathbf{h}_{t,l} = [h^t_{0,l}, \ldots, h^t_{N-1,l}]^T. \tag{2.8}$$

Note that in total there are $N(L+1)$ parameters. In many cases, this number is too large to allow for accurate estimation and we need to reduce it using a more specific model. One possibility is as follows. Since the channel is assumed to be uncorrelated among different channel taps, and the time variation for each channel tap is continuous and smooth, the channel coefficients of the lth channel tap are correlated in the time index n. The $N \times 1$ vector $\mathbf{h}_{t,l}$ can be approximated using a basis expansion model (BEM) as [52]

$$\mathbf{h}_{t,l} \approx \mathbf{B}\mathbf{h}_l, \tag{2.9}$$

where $\mathbf{B} = [\mathbf{b}_{-Q}, \ldots, \mathbf{b}_Q]$ is a $N \times (2Q+1)$ matrix with $\mathbf{b}_q$ being the qth basis function, and $\mathbf{h}_l = [h_{-Q,l}, \ldots, h_{Q,l}]^T$ is a $(2Q+1) \times 1$ vector being the BEM coefficient vector related to the lth channel tap. Notice that $\mathbf{B}$ is a tall matrix as the block length N is much larger than the BEM order $2Q+1$. The accuracy of the BEM approximation depends on the choice of the BEM matrix $\mathbf{B}$ and the BEM order $2Q+1$.

The $(L+1)(2Q+1)$ BEM coefficients $\{\{h_{q,l}\}_{l=0}^{L}\}_{q=-Q}^{Q}$ remain constant during each length-N block, and are allowed to change over different length-N blocks. The $2Q+1$ basis functions used to capture the time variations are the same for every length-N block. Q can be regarded as the discrete Doppler spread index with frequency-domain resolution $1/(NT)$, and it needs to satisfy $Q/(NT) \geq \nu_{\max}$, in order to get an accurate BEM approximation. Usually $Q \leq 2$ is enough to get a good performance. By using the BEM to approximate the time-varying channel, we can reduce the number of unknowns from $N(L+1)$ to $(L+1)(2Q+1)$ with $Q \ll N$.

There are various kinds of basis functions, such as the discrete Karhunen-Loève BEM [89], discrete prolate spheroidal BEM [69], critically-sampled complex exponential BEM (CCE-BEM) [44], oversampled complex exponential BEM (OCE-BEM) [66], polynomial BEM [67], and so on. A detailed comparison of different BEMs can be found in [23, 69] and the references therein. In this thesis, the CE-BEM is used later for channel estimation, with the basis function $\mathbf{b}_q$ being written as

$$\mathbf{b}_q = \left[1, \ldots, e^{j\frac{2\pi}{K}n(q-Q)}, \ldots, e^{j\frac{2\pi}{K}(N-1)(q-Q)}\right]^T. \tag{2.10}$$

When $K = N$, it becomes the CCE-BEM, which is a truncated Fourier expansion. When the function period K is greater than the block length N, for example $K = 2N$, we have the OCE-BEM, which results in a better approximation than the CCE-BEM. Despite its poorer modeling performance, the CCE-BEM gained a lot of attention due to the nice algebraic structure which can be used to prove the achievable diversity for specific coding schemes and receiver algorithms [44, 65].

Besides the BEM approach, [90] has used a Gauss-Markov process to describe the time-varying channel, which is a stochastic model used for time-domain sequential processing.

2.1.3 Underwater Acoustic Communication Channel

For underwater communications it is better to transmit sound signals, since electromagnetic waves experience high attenuation in water. However, the speed of sound (around 1500m/s) is much slower than that of light, which leads to a very large delay spread and frequency-selective fading. The low speed of sound also gives rise to the problem of large Doppler spreads. Thus, the underwater acoustic communication (UAC) channel can be regarded as a doubly-selective channel as discussed before. More details about UAC channel modeling can be found in [81]. OFDM transmissions for UAC have been investigated in [82, 83] and the references therein. Specifically, [82] also uses a BEM to approximate the UAC channel and a low-complexity block banded equalizer which corresponds to the non-iterative version of the channel estimation and equalization algorithms discussed in the later chapters in this thesis.

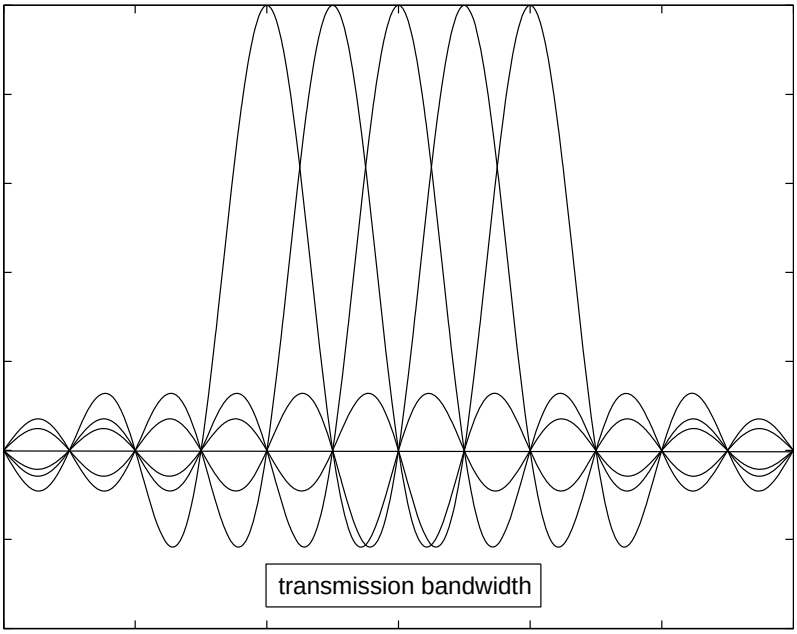

Figure 2.1: Overlapping spectrum of orthogonal subcarriers.

2.2 OFDM and SC Transmission

The block transmission system considered in this thesis includes OFDM and SC cases. OFDM is one of the most important modulation schemes for wireless communications, since it is widely used in many standards such as DVB-T/H, DAB, IEEE 802.11 and IEEE 802.16. OFDM can eliminate intersymbol interference (ISI) introduced by a frequency-selective channel by turning it into a set of parallel frequency-flat channels, and therefore renders possible simple one-tap equalization for each subcarrier. Recently, LTE has been proposed as a major 3GPP step in next generation wireless networks. The LTE physical layer relies on a multiple-access scheme based on OFDM with a cyclic prefix (CP) in the downlink, and on SC-FDMA with a CP in the uplink [32]. Using FDMA, different users are allocated different subcarriers for data modulation and to access the system simultaneously. In order to achieve higher spectrum efficiency, the system is designed to maintain orthogonality between subcarriers but their spectrum is overlapping in the frequency domain as shown in Fig. 2.1.

2.2.1 CP-OFDM System

In this subsection, we give a brief introduction of the CP-OFDM system, while other OFDM systems with zero-padding and known symbol padding approaches can be found in [3, 87].

In OFDM systems, a high-rate data stream is serial-to-parallel converted to N parallel low-rate data streams, where N is the number of subcarriers in one OFDM symbol, with each data stream being modulated to a subcarrier. In this way, a frequency-selective channel can be converted to a set of parallel frequency-flat channels, and ISI can be eliminated. We denote the $N \times 1$ vector $\mathbf{s}_i = [s_{iN}, \ldots, s_{(i+1)N-1}]^T$ as the ith block of data symbols. At the transmitter, $\mathbf{s}_i$ is firstly transformed to the time domain by an IFFT operation, then a length-G CP is added. The resulting $(N+G) \times 1$ transmitted signal $\mathbf{x}_i = [x_{i(N+G)}, \ldots, x_{(i+1)(N+G)-1}]^T$ can be expressed as

$$\mathbf{x}_i = \mathbf{T}_{\text{cp}} \mathbf{F}^H \mathbf{s}_i, \tag{2.11}$$

where $\mathbf{F}$ denotes the $N \times N$ unitary DFT matrix, and $\mathbf{T}_{\text{cp}}$ is the $(N+G) \times N$ CP padding matrix which can be written as

$$\mathbf{T}_{\text{cp}} = \left[\frac{\mathbf{0}_{G \times (N-G)} \ \mathbf{I}_G}{\mathbf{I}_N} \right]. \tag{2.12}$$

The receiver groups $N+G$ received samples into one block. We denote the ith block of the received signal as $\mathbf{y}_i = [y_{i(N+G)}, \ldots, s_{(i+1)(N+G)-1}]^T$. It can be shown [3] that if the length of the CP is larger than the maximal channel order L, and we drop the first G samples from $\mathbf{y}_i$, there will be no interference between successive blocks, and the equalizer can be designed separately for each block. Thus, we can omit the block index i from the notation, and focus on the first block. An FFT operation is applied after discarding the CP. The resulting frequency-domain received signal can be written as

$$\begin{aligned} \mathbf{y}_f &= \mathbf{F}\mathbf{R}_{\text{cp}} \mathbf{H}_t' \mathbf{T}_{\text{cp}} \mathbf{F}^H \mathbf{s} + \mathbf{F}\mathbf{R}_{\text{cp}} \mathbf{n} \\ &= \mathbf{F}\mathbf{H}_t \mathbf{F}^H \mathbf{s} + \mathbf{F}\mathbf{n}_t \end{aligned} \tag{2.13}$$

where $\mathbf{R}_{\text{cp}} = [\mathbf{0}_{N \times G} \ \mathbf{I}_N]$ is the CP discarding matrix, $\mathbf{H}_t'$ is the $(N+G) \times (N+G)$

matrix

$$\mathbf{H}'_t = \begin{pmatrix} h^t_{0,0} & & & & \\ \vdots & \ddots & & & 0 \\ h^t_{L,L} & \cdots & h^t_{L,0} & & \\ & \ddots & \vdots & \ddots & \\ 0 & & h^t_{N+G-1,L} & \cdots & h^t_{N+G-1,0} \end{pmatrix}, \tag{2.14}$$

with $h_{n,l}$ being defined in (2.8), $\mathbf{H}_t = \mathbf{R}_{\text{cp}}\mathbf{H}'_t\mathbf{T}_{\text{cp}}$ is the $N \times N$ time-domain channel matrix with a pseudo-circulant form

$$\mathbf{H}_t = \begin{pmatrix} h^t_{G,0} & & 0 & h^t_{G,L} & \cdots & h^t_{G,1} \\ \vdots & \ddots & & & \ddots & \vdots \\ h^t_{G+L,L} & & \ddots & \ddots & & h^t_{G+L-1,L} \\ & \ddots & & \ddots & 0 & \\ & & \ddots & & \ddots & 0 \\ 0 & & & h^t_{N+G-1,L} & \cdots & h^t_{N+G-1,0} \end{pmatrix}, \tag{2.15}$$

and $\mathbf{n}_t$ stands for the $N \times 1$ noise vector.

In the time-invariant case, the time-domain channel matrix $\mathbf{H}_t$ is circulant, and consequently the frequency-domain channel matrix $\mathbf{H}_f = \mathbf{F}\mathbf{H}_t\mathbf{F}^H$ is diagonal. This triggers the use of the simple traditional OFDM one-tap equalizer. However, in a time-varying scenario, $\mathbf{H}_t$ is no longer circulant, and $\mathbf{H}_f$ becomes a non-diagonal matrix, giving rise to ICI that corresponds to the non-zero off-diagonal elements of $\mathbf{H}_f$. Fortunately, $\mathbf{H}_f$ is almost banded, with the most significant elements around the main diagonal [8]. This permits the use of low-complexity equalization, as explained in [8–11]. The banded structure turns out to be very useful, since easy equalization is one of the main advantages of OFDM over single-carrier communications. Moreover, with an appropriate time-domain receiver window design $\mathbf{W} = \text{diag}(\mathbf{w})$, where $\mathbf{w}$ is the $N \times 1$ time-domain window, the banded character of $\mathbf{H}_f = \mathbf{F}\mathbf{W}\mathbf{H}_t\mathbf{F}^H$ can even be enforced.

Despite the above advantage, OFDM systems also have challenges. The following ones are the mostly discussed in literature:

- an OFDM system is very sensitive to carrier frequency offsets, which arise due to relative motion between the transmitter and receiver and/or implementation imperfections.

- an OFDM system has a high Peak-to-Average Ratio (PAR). Since the power amplifier is linear only within limited dynamic range, it causes a non-linear distortion of the OFDM signal. Thus, the power amplifier need to have a large power back-off to avoid the non-linearity, which leads to inefficient and expensive power amplifiers.

2.2.2 SC System

In this subsection, we are particularly interested in SC systems with frequency-domain processing. Similar to the OFDM system, a CP is added at the transmitter in order to eliminate the ISI. Assume the $N \times 1$ vector $\mathbf{s}$ contains the data symbols, the transmitted signal with CP can be written as $\mathbf{x} = \mathbf{T}_{\text{cp}}\mathbf{s}$. The input-output relationship can be derived as

$$\begin{aligned} \mathbf{y}_t &= \mathbf{R}_{\text{cp}}\mathbf{H}_t'\mathbf{T}_{\text{cp}}\mathbf{s} + \mathbf{R}_{\text{cp}}\mathbf{n} \\ &= \mathbf{H}_t\mathbf{s} + \mathbf{n}_t, \end{aligned} \tag{2.16}$$

where we have assumed that the CP length is larger than the maximal channel order, i.e., $G > L$, so that there is no interference between successive blocks. Transforming the time-domain received signal to the frequency-domain, we obtain

$$\begin{aligned} \mathbf{y}_f &= \mathbf{F}\mathbf{H}_t\mathbf{F}^H\mathbf{F}\mathbf{s} + \mathbf{F}\mathbf{n}_t \\ &= \mathbf{H}_f\mathbf{s}_f + \mathbf{n}_f. \end{aligned} \tag{2.17}$$

From (2.17), we can see that the frequency-domain equalization for SC systems is the same as that for OFDM systems, despite that the estimated symbols are in the frequency-domain, and need to be transformed back to time-domain for final decision. Compared to OFDM transmission, a SC system has a much lower PAR which makes it suitable for uplink transmission. The complexity of frequency-domain equalization for SC systems is independent of the channel length, which leads to significant complexity savings for time-domain equalization in long delay spread channels.

2.3 Linear MMSE Estimation

In this thesis, we use a linear MMSE estimator to derive the turbo equalization and iterative channel estimation algorithms. This subsection gives a brief

review of MMSE estimation methods. This summary is primarily adapted from [86].

Given a $N \times 1$ observation vector $\mathbf{y}$, we want to estimate the scalar parameter s. Assuming that s and $\mathbf{y}$ are statistically dependent, the linear estimator can be expressed as

$$\hat{s} = \mathbf{w}_0^H \mathbf{y} + w_0, \tag{2.18}$$

where $\mathbf{w}_0$ and w_0 are chosen to minimize the mean square error (MSE)

$$\text{mse}(\hat{s}) = \text{E}[(s - \hat{s})^2]. \tag{2.19}$$

We rewrite (2.19) using (2.18), which leads to

$$\text{mse}(\hat{s}) = \text{E}[(s - \mathbf{w}_0^H \mathbf{y} - w_0)^2]. \tag{2.20}$$

Differentiating with respect to w_0 and setting it to zero, we can obtain w_0 as

$$w_0 = \text{E}(s) - \mathbf{w}_0^H \text{E}(\mathbf{y}). \tag{2.21}$$

Substituting (2.21) into (2.20), we get the following equation

$$\begin{aligned} \text{mse}(\hat{s}) &= \text{E}\{[s - \mathbf{w}_0^H \mathbf{y} - (\text{E}(s) - \mathbf{w}_0^H \text{E}(\mathbf{y}))]^2\} \\ &= \text{E}\{[\mathbf{w}_0^H (\mathbf{y} - \text{E}(\mathbf{y})) - (s - \text{E}(s))]^2\} \\ &= \mathbf{w}_0^H \text{Cov}(\mathbf{y}, \mathbf{y}) \mathbf{w}_0 - \mathbf{w}_0^H \text{Cov}(\mathbf{y}, s) - \text{Cov}(s, \mathbf{y}) \mathbf{w}_0 + \text{Cov}(s, s). \end{aligned} \tag{2.22}$$

Taking the derivative with respect to $\mathbf{w}_0$ and setting the result to 0 leads to

$$\mathbf{w}_0 = \text{Cov}(\mathbf{y}, \mathbf{y})^{-1} \text{Cov}(\mathbf{y}, s). \tag{2.23}$$

Thus the linear MMSE estimator can be expressed as

$$\hat{s} = \text{E}(s) + \text{Cov}(s, \mathbf{y}) \text{Cov}(\mathbf{y}, \mathbf{y})^{-1} (\mathbf{y} - \text{E}(\mathbf{y})). \tag{2.24}$$

The vector linear MMSE estimator can be derived in a similar way.

2.4 Multi-Antenna Systems

In addition to the time and frequency domain, we can add more antennas at the transmitter and/or receiver to exploit the spatial dimension resources for

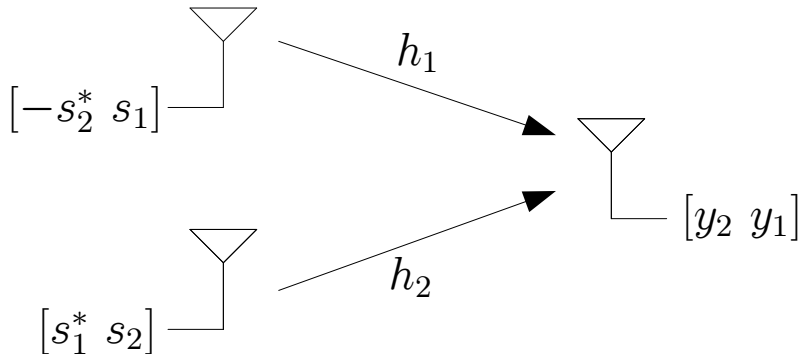

Figure 2.2: Alamouti coding scheme.

potential performance improvement. In the last decade, multi-antenna systems have attracted a lot of research interest for future wireless systems. The use of multiple transmit and/or receive antennas can significantly enhance communication system performances such as channel capacity and reliability. The channel capacity C is characterized by the multiplexing gain, which is approximately linear in the minimum of the number of the transmit and receive antennas [77] in the ideal case. The bit error rate performance P_e is characterized by the diversity gain d which is at most the product of the number of transmit and receive antennas [54]. Specifically, the upper bounds on the capacity C and bit error rate performance P_e are given by

$$C \simeq \min(M_t, M_r) \log \mathrm{SNR} \tag{2.25}$$

$$P_e \simeq \alpha\ \mathrm{SNR}^{-d} \tag{2.26}$$

where M_t and M_r are the number of transmit and receive antennas respectively, and α is a constant which does not affect the diversity gain. The system can also exploit spatial diversity gain and spatial multiplexing gain simultaneously, with a diversity-multiplexing gain tradeoff [53].

STBC [54,55] has been introduced to achieve the spatial diversity offered by multiple transmit and/or receive antennas. In this subsection, we give a brief introduction of the Alamouti code, which is the first and the most fundamental STBC. More advanced coding schemes and other issues about multi-antenna systems can be found in [88].

For a system with two transmit antennas and one receive antenna, i.e., a 2 by 1 system as shown in Fig. 2.2, the Alamouti code achieves full diversity

and full rate. The system input-output relationship can be written as

$$\begin{aligned} y_1 &= h_1 s_1 + h_2 s_2 + n_1, \\ y_2 &= -h_1 s_2^* + h_2 s_1^* + n_2, \end{aligned} \tag{2.27}$$

where s_1 and s_2 are the transmitted signal from antenna 1 and antenna 2 at time slot 1, $-s_2^*$ and s_1^* are the transmitted signal from antenna 1 and antenna 2 at time slot 2, h_1 and h_2 are the channel coefficients from transmit antenna 1 and transmit antenna 2 to the receive antenna, respectively, y_1 and y_2 are the received signal at the receive antenna at time slot 1 and time slot 2, respectively, and finally n_1 and n_2 are the noise at the receive antenna at time slot 1 and time slot 2, respectively. The channel is assumed to be static over the two time slots, i.e., h_1 and h_2 are constant for receiving y_1 and y_2.

Stacking y_1 and y_2^* together, we obtain

$$\begin{aligned} \mathbf{y} &= \begin{bmatrix} y_1 \\ y_2^* \end{bmatrix} \\ &= \begin{bmatrix} h_1 & h_2 \\ h_2^* & -h_1^* \end{bmatrix} \begin{bmatrix} s_1 \\ s_2 \end{bmatrix} + \begin{bmatrix} n_1 \\ n_2^* \end{bmatrix} \\ &= \mathbf{H}\mathbf{s} + \mathbf{n}, \end{aligned} \tag{2.28}$$

where $\mathbf{H}$ is a scaled unitary matrix regardless of the channel realization,

$$\mathbf{H}^H \mathbf{H} = (|h_1|^2 + |h_2|^2)\mathbf{I}_2. \tag{2.29}$$

Thus, we can multiply the received signal $\mathbf{y}$ with $\mathbf{H}^H$, which leads to

$$\begin{bmatrix} y_1' \\ y_2' \end{bmatrix} = \mathbf{H}^H \mathbf{y} = (|h_1|^2 + |h_2|^2) \begin{bmatrix} s_1 \\ s_2 \end{bmatrix} + \mathbf{n}', \tag{2.30}$$

where each data symbol can be decoded separately and maximum-likelihood decoding becomes very simple.

However, as STBC is typically designed for flat-fading channels, the time and frequency selectivity will seriously degrade the system performance. Thus, it is crucial to accurately model the doubly-selective channel and to design efficient STBC schemes to counteract its effects. Doubly-selective channels can also provide multiplicative delay-Doppler diversity gains if the transceiver is properly designed [51, 52], with diversity being an effective way to combat fading channels.

Chapter 3

Turbo Equalization

3.1 Introduction

In order to counteract the effects of a time-varying channel, several different equalization techniques have been proposed for OFDM systems [5–18]. These techniques range from linear equalizers, based on the ZF or the MMSE criterion [5–14], to decision-directed equalizers based on decision-feedback or ICI cancellation [10–15]. Also near maximum-likelihood approaches have been proposed [17, 18]. ICI cancellation with transmitter optimization is proposed in [16]. Similar to the situation in single-carrier communications subject to ISI channels, or in multiuser detection for CDMA, each equalization technique is characterized by a different performance-complexity tradeoff. However, the specific structure of the Doppler-induced ICI in OFDM systems presents some distinctive features that can be exploited by the equalizer. The first feature is the limited support of the Doppler spread, which makes the frequency-domain channel matrix almost banded, i.e., the most significant elements occur around the main diagonal. For example, the equalization methods in [7–11] exploit the banded character of the frequency-domain channel matrix to reach a complexity that is only linear in the number of subcarriers. This is in contrast with more complex equalization methods that rely on the full (i.e., non-banded) frequency-domain channel matrix. Indeed, for non-banded methods, the complexity is quadratic [14] or even cubic [13] in the number of subcarriers, and therefore can be too high for standards with a large number of subcarriers like DVB. In a certain sense, the assumption of a banded frequency-domain channel matrix is a natural extension of the time-invariant channel case, where

the frequency-domain channel matrix is diagonal and hence banded with the smallest possible bandwidth. A second feature that can be exploited in the equalization is the knowledge of the Doppler spectrum shape, typically a U-shaped spectrum, a bell-shaped spectrum, or a combination thereof. This knowledge can be used to design simple time-domain receiver windows that enforce the banded assumption and improve the performance of equalization schemes [10, 11].

Among all the equalizers for OFDM in time-varying channels, one of the most promising approaches is the iterative MMSE serial linear equalizer (SLE) of [10]. This iterative approach is inspired by turbo equalization [19,20], where soft information is used in an iterative fashion to improve the bit error rate (BER) performance, and it will therefore also be labeled as the serial turbo MMSE equalizer in the sequel. Optimal joint processing of equalization and decoding at the receiver is prohibitive due to the heavy computational burden. Instead, the equalization and decoding tasks can be performed separately and carried out iteratively, with soft information being interchanged between these two parts. Compared to the receivers that make hard decisions as to which symbols and which bits are transmitted, the receivers can employ soft information to express the probabilities that each of the received symbols and bits take on a specific value. For example, turbo MMSE equalizers iteratively improve the mean and the covariance of the estimated symbol vector by exploiting extrinsic information and performing soft cancelation. Different turbo MMSE equalizers exist in the technical literature, such as serial or block versions [19–22]. The difference between a serial and a block approach is that in the serial case each symbol is equalized separately using a sliding window MMSE equalizer [19, 20], whereas in the block case all the symbols in a block are jointly equalized [21, 22].

While turbo equalization for SC transmissions over frequency-selective channels has been originally applied in the time domain (see references in [19]), frequency-domain equalization has gained much interest due to its comparable complexity and performance to OFDM transceivers [33, 34, 47]. For SC systems in doubly-selective channels, a low-complexity iterative equalizer has been proposed in [35], which can be regarded as the time-domain counterpart of the iterative frequency-domain equalizer [40]. However, time-domain iterative equalizers are not suitable for long channels, since their complexity is quadratic in the channel length [35].

In this chapter, we first derive *block* turbo MMSE equalizers for OFDM systems in time-varying channels, as an alternative to the *serial* turbo MMSE

equalization [10]. The presented equalizers are based on a soft MMSE block linear equalizer (BLE), and exploit both the banded structure of the frequency-domain channel matrix and receiver windowing. Therefore, their complexities will be linear in the number of subcarriers, like the methods in [7–11]. Three different algorithms are proposed, and their complexities are investigated. In addition, we establish some insightful mutual relations among the different methods as well as connections to existing turbo methods. The performances of the proposed block turbo MMSE equalizers are compared with that of the serial turbo MMSE equalizer of [10]. In [11], it has been shown that the non-iterative block MMSE equalizer outperforms the non-iterative serial MMSE equalizer. The simulation results in this chapter will display that their iterative versions have a similar performance difference. Specifically, our block equalizers are able to reduce the error floor of the BER performance due to the ICI. In order to establish a fair comparison with [10], we do not consider channel coding at first. However, it is clear that the performance can be further improved by incorporating error correction codes into the turbo loop. This is also illustrated in the simulations section.

Later, we apply the block philosophy to design a soft MMSE turbo equalizer for SC systems in doubly-selective channels. It should be noted that most of the existing equalizers for SC systems in doubly-selective channels mainly focus on serial equalization, either in time domain [35] or in frequency domain [40]. However, when a CP is present, block equalization becomes a valid alternative. Therefore, similarly to the OFDM case [37], we perform block equalization in the frequency domain, exploiting the banded structure of the frequency-domain channel matrix. Optionally, receiver windowing can be included. Note that [40] also includes a time-domain receiver window which is designed over the entire block, but the equalization is performed serially in frequency domain, as for the OFDM counterpart [10]. An interesting feature of the proposed equalizer is its reduced computational complexity, which scales only linearly with the block length. As a result, in doubly-selective channels with significant multipath delay spread, our frequency-domain approach is less complex than time-domain equalizers like [35].

Notice that in this chapter, the receiver is assumed to have perfect channel state information (CSI). A channel estimation algorithm is discussed in the next chapter.

3.2 System Model

We consider a single-user communication system with block-wise transmission, and a channel that is both frequency- and time-selective. The structure of both transmitter and receiver is shown in Fig. 3.1. At the transmitter, a sequence of bits is encoded with error correction coding, and the coded bits are interleaved and mapped into N_d complex symbols, represented by the $N_d \times 1$ vector $\mathbf{s}^d$, and the data symbols are assumed to be uncorrelated. We define $\mathbf{s}^p$ as the $N_p \times 1$ vector that stands for the pilot symbols, which are multiplexed with $\mathbf{s}^d$ to form a block of $N = N_d + N_p$ transmitted symbols $\mathbf{s}$. For simplicity, we consider unit-energy quaternary phase-shift keying (QPSK) with the symbol alphabet shown in Table 3.1. However, the equalizers and channel estimators proposed herein can be easily extended to other constellations, like in [20]. As far as the

Table 3.1: QPSK symbol alphabet

k	1	2	3	4
$(\alpha_{k,1}, \alpha_{k,2})$	(0,0)	(1,0)	(0,1)	(1,1)
α_k	$\frac{(+1+i)}{\sqrt{2}}$	$\frac{(-1+i)}{\sqrt{2}}$	$\frac{(+1-i)}{\sqrt{2}}$	$\frac{(-1-i)}{\sqrt{2}}$

time dispersion of the channel is concerned, we adopt the standard assumption that the maximal channel order is equal to the CP length, both denoted by L, where $L < N$. This way, there is no interference between successive blocks, and the equalizer can be designed separately for each block. As a consequence, we can omit the block index from our notation. In the following, we also omit the details of inserting and removing the CP, it is implemented by the CP padding matrix $\mathbf{T}_{\text{cp}}$ and the CP discarding matrix $\mathbf{R}_{\text{cp}}$ (2.13).

At the receiver, after removing the CP, the $N \times 1$ received vector $\mathbf{y}_t$ can be expressed as

$$\mathbf{y}_t = \mathbf{H}_t \mathbf{P} \mathbf{s} + \mathbf{n}_t, \tag{3.1}$$

where $\mathbf{H}_t$ is the $N \times N$ time-domain channel matrix, $\mathbf{P}$ denotes the $N \times N$ precoder matrix. The precoder is set to $\mathbf{P} = \mathbf{I}_N$ for SC systems, and $\mathbf{P} = \mathbf{F}^H$ for OFDM systems, where $\mathbf{F}$ denotes the $N \times N$ unitary DFT matrix. $\mathbf{s}$ represents the $N \times 1$ symbol vector consisting of the multiplexed pilot and data symbols, and $\mathbf{n}_t$ stands for the $N \times 1$ noise vector, which is uncorrelated with the data symbols. For simplicity, we assume that $\mathbf{n}_t$ is a circularly symmetric complex Gaussian noise vector, with zero mean and covariance matrix $\mathbf{R}_{\mathbf{n}_t} =$

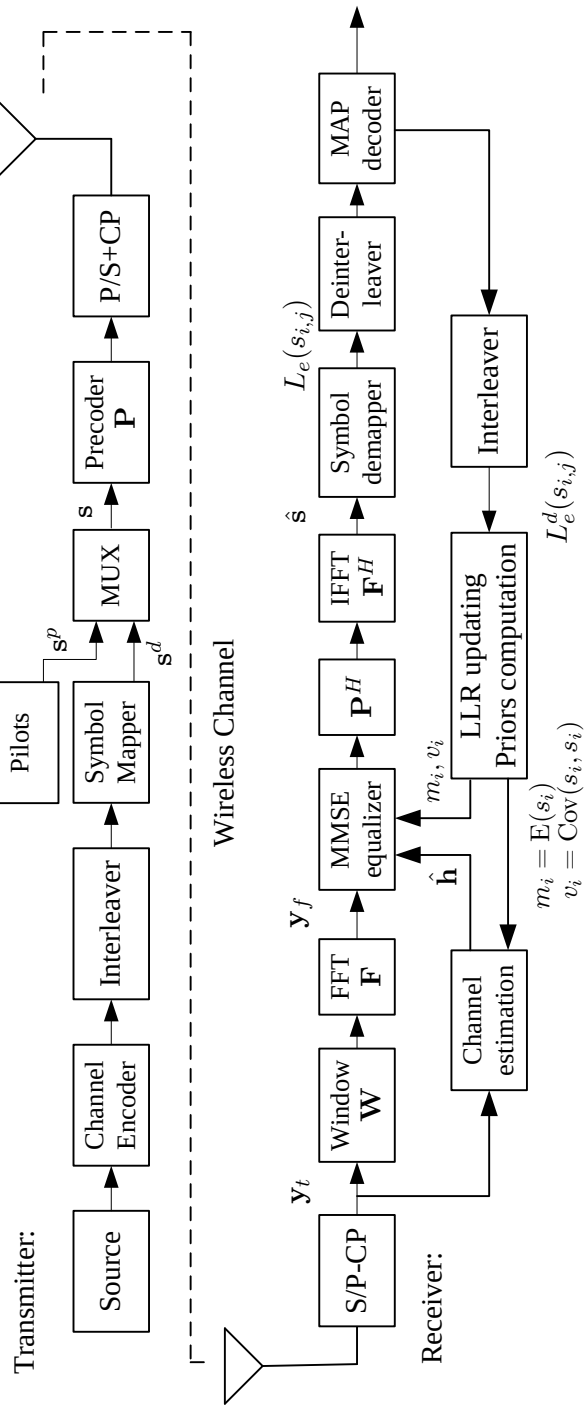

Figure 3.1: System model.

$E(\mathbf{n}_t\mathbf{n}_t^H) = \sigma_n^2\mathbf{I}_N$. At the receiver, an N-length time-domain window can be applied after CP removal and before the DFT operation. In this case, the output vector after the DFT operation can be expressed as

$$\mathbf{y}_f = \mathbf{FWH}_t\mathbf{F}^H\mathbf{FPs} + \mathbf{FWn}_t = \mathbf{H}_f\mathbf{FPs} + \mathbf{n}_f, \tag{3.2}$$

where $\mathbf{y}_f = \mathbf{FWy}_t$, $\mathbf{n}_f = \mathbf{FWn}_t$, $\mathbf{H}_f = \mathbf{FWH}_t\mathbf{F}^H$, and $\mathbf{W} = \text{diag}(\mathbf{w})$, with $\mathbf{w}$ the $N \times 1$ vector denoting the time-domain receiver window. Note that classical systems do not include windowing, i.e., $\mathbf{W} = \mathbf{I}_N$. Details about the time-domain receiver window is explained later in this subsection.

When the channel is time-invariant and no windowing is employed, i.e., $\mathbf{W} = \mathbf{I}_N$, the time-domain channel matrix $\mathbf{H}_t$ is circulant, and consequently the frequency-domain channel matrix $\mathbf{H}_f$ is diagonal. This triggers the use of the simple traditional OFDM one-tap equalizer. However, when the channel is time varying, $\mathbf{H}_t$ is no longer circulant, and the $N \times N$ frequency-domain channel matrix $\mathbf{H}_f$ becomes a non-diagonal matrix, giving rise to ICI, where the ICI coupling is summarized by the non-zero off-diagonal elements of $\mathbf{H}_f$. However, with a proper window design, $\mathbf{H}_f$ is practically banded, with the most significant elements around the main diagonal [10, 11] as shown in Fig. 3.2. In this thesis, we employ the minimum band approximation error sum-of-exponentials windowing developed in [11]. This choice permits the use of low-complexity equalization algorithms specially tailored to banded matrices, as explained in [9–11, 37]. We remark that the receiver windowing in [11] only requires some statistical knowledge about the channel time variation. Therefore, the channel Doppler spectrum is assumed known, whereas the power-delay profile information is not required.

As shown later, the equalization process requires to invert the $N \times N$ frequency-domain channel matrix $\mathbf{H}_f$. In time-varying channels, $\mathbf{H}_f$ is a full matrix and the standard computation of a matrix reverse requires a complexity of $\mathcal{O}(N^3)$, which is too complicated for a system with large block length N. To simplify the equalization procedure, the matrix $\mathbf{H}_f$ is further approximated by its banded version

$$\mathbf{H} = \mathbf{H}_f \circ \mathbf{\Theta}, \tag{3.3}$$

where we use the symbol $\circ$ to denote the Hadamard (element-wise) product between matrices, and $\mathbf{\Theta}$ is the $N \times N$ circulant matrix, which has ones on the main diagonal, and on the B_c super- and B_c sub-diagonals, while the remaining entries are zeros. The banded approximation allows for a low complexity equalization algorithm shown in the later sections in this chapter. The

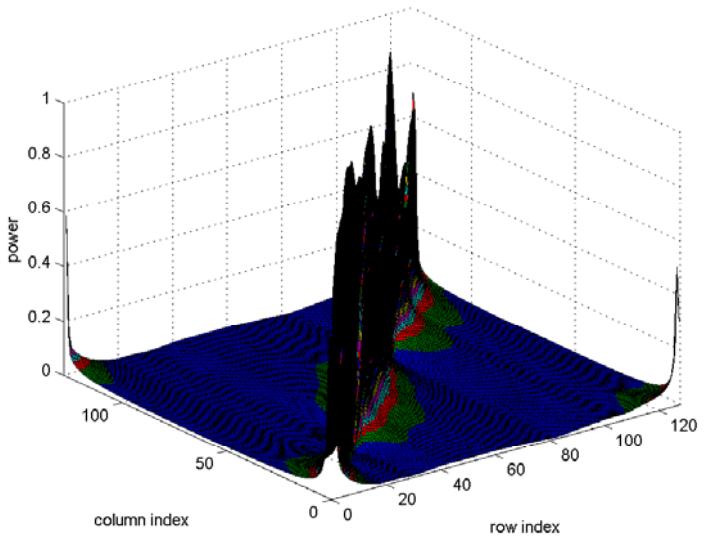

Figure 3.2: An example of a frequency-domain channel matrix.

matrix bandwidth parameter B_c allows for a trade-off between equalization complexity and performance, and it can be chosen according to some rules of thumb [10]. When windowing is included, B_c is usually much smaller than the number of subcarriers N, usually $1 \leq B_c \leq 3$ is enough to achieve a good performance. Note that B_c also determines the design of the window $\mathbf{W}$ [10, 11]. In this thesis, we use the minimum band-approximation-error sum-of-exponentials (MBAE-SOE) windows [11], the window is designed to make the banded approximation (3.3) as good as possible. We give an example in Fig. 3.3, where $fdmax$ is the maximal normalized Doppler shifts. It can be shown that the receiver window mainly depends on the matrix bandwidth parameter B_c, and is insensitive to the maximal Doppler shifts.

It can be observed that the transmitted data block $\mathbf{s}$ represents a time-domain signal in SC systems, while it represents a frequency-domain signal in OFDM systems. This clearly explains why SC systems are more prone to multipath effects, which mix the data due to the associated ISI, while OFDM systems suffer from Doppler effects, which mix the data due to the associated ICI. For both systems, our equalizers are designed in the frequency domain, with the goal of mitigating both the ICI, caused by the non-zero off-diagonal elements of $\mathbf{H}$, and the ISI, represented by the different elements in the main diagonal of $\mathbf{H}$.

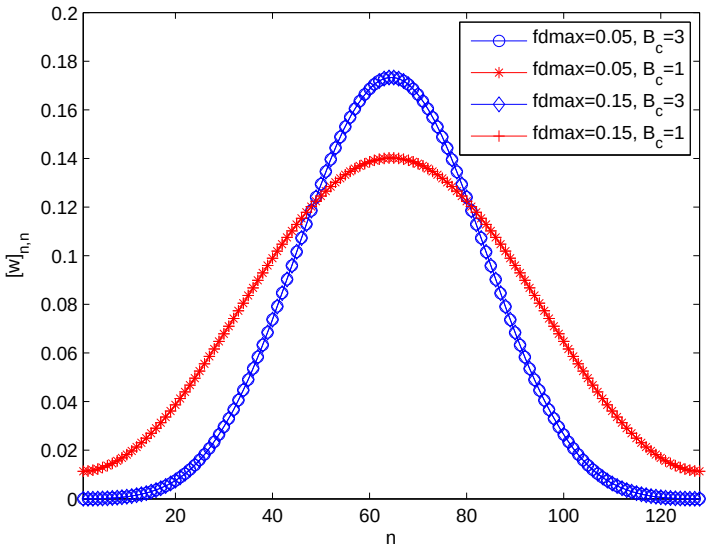

Figure 3.3: An example of a time-domain receiver window.

3.3 Low-Complexity Block Turbo Equalization

In order to derive frequency-domain block turbo equalizers for doubly-selective channels, let us define s_i as the ith QPSK symbol of $\mathbf{s}$, and $(s_{i,1}, s_{i,2})$ as the related bits. The mean and the variance of the symbol s_i are denoted as $m_i = \mathrm{E}(s_i)$ and $v_i = \mathrm{Cov}(s_i, s_i)$, respectively. Similarly, we have $\mathbf{m} = \mathrm{E}(\mathbf{s}) = [m_1, \ldots, m_N]^T$ and $\mathbf{V} = \mathrm{Cov}(\mathbf{s}, \mathbf{s}) = \mathrm{diag}([v_1, \ldots, v_N]^T)$, where we assume the transmitted signals s_i are always independent. As far as the N_d data symbols are concerned, the means and the variances are initialized with zeros and ones, respectively. But in every iteration of the turbo equalizer, they are updated using soft information from the estimated symbols. On the other hand, for each of the N_p pilot symbols, the mean is set to the pilot symbol value, while the variance is zero, for all the iterations.

After each iteration of the equalizer, we update the means and the variances using the soft estimated symbols. Specifically, we need to calculate the extrinsic log-likelihood ratio (LLR), $L_e(s_{i,j}) = L(s_{i,j}|\hat{s}_i) - L(s_{i,j})$, where $L(s_{i,j})$ is the *a priori* LLR and $L(s_{i,j}|\hat{s}_i)$ is the *a posteriori* LLR [19], which are defined

as

$$
\begin{aligned}
L(s_{i,j}) &= \ln\frac{P(s_{i,j}=0)}{P(s_{i,j}=1)},\\
L(s_{i,j}|\hat{s}_i) &= \ln\frac{P(s_{i,j}=0|\hat{s}_i)}{P(s_{i,j}=1|\hat{s}_i)},\\
L_e(s_{i,j}) &= L(s_{i,j}|\hat{s}_i) - L(s_{i,j})\\
&= \ln\frac{\sum\limits_{\alpha_k:\alpha_{k,j}=0} p(\hat{s}_i|s_i=\alpha_k)P(s_i=\alpha_k)}{\sum\limits_{\alpha_k:\alpha_{k,j}=1} p(\hat{s}_i|s_i=\alpha_k)P(s_i=\alpha_k)} - \ln\frac{P(s_{i,j}=0)}{P(s_{i,j}=1)} \qquad (3.4)\\
&= \ln\frac{\sum\limits_{\alpha_k:\alpha_{k,j}=0} p(\hat{s}_i|s_i=\alpha_k)P(s_{i,1}=\alpha_{k,1})P(s_{i,2}=\alpha_{k,2})}{\sum\limits_{\alpha_k:\alpha_{k,j}=1} p(\hat{s}_i|s_i=\alpha_k)P(s_{i,1}=\alpha_{k,1})P(s_{i,2}=\alpha_{k,2})} - \ln\frac{P(s_{i,j}=0)}{P(s_{i,j}=1)} \qquad (3.5)\\
&= \ln\frac{\sum\limits_{\alpha_k:\alpha_{k,j}=0} p(\hat{s}_i|s_i=\alpha_k)P(s_{i,j'}=\alpha_{k,j'})}{\sum\limits_{\alpha_k:\alpha_{k,j}=1} p(\hat{s}_i|s_i=\alpha_k)P(s_{i,j'}=\alpha_{k,j'})}, \qquad (3.6)
\end{aligned}
$$

where $j, j' = 1, 2$, with $j \neq j'$, $\hat{s}_i$ is the estimated symbol at the current iteration, $P(s_{i,j}=0)$ and $P(s_{i,j}=1)$ are the a prior probabilities, $P(s_{i,j}=0|\hat{s}_i)$ and $P(s_{i,j}=1|\hat{s}_i)$ are the a posteriori probabilities, and $p(\hat{s}_i|s_i=\alpha_k)$ is the conditional probability.

To perform the calculation of $L_e(s_{i,j})$, we should derive the probability density function (PDF) $p(\hat{s}_i|s_i=s)$, which can be approximated as Gaussian: $p(\hat{s}_i|s_i=s) = \frac{1}{\pi\sigma_i^2}\cdot e^{-|\hat{s}_i-\mu_i|^2/\sigma_i^2}$, with mean $\mu_i = \mathrm{E}(\hat{s}_i|s_i=s)$ and variance $\sigma_i^2 = \mathrm{Cov}(\hat{s}_i, \hat{s}_i|s_i=s)$ [19,20]. This approximation is extensively used in turbo equalization, because it highly simplifies the LLR updating (see, e.g., [19]). Note that this choice is not only made for convenience reasons. In a CDMA scenario, the results presented in [26] clearly show that the random variables at the output of a linear MMSE estimator are quite close to be Gaussian distributed. Since our OFDM system can be viewed as a special case of a CDMA system, where each carrier acts as a user, we may assume that the Gaussian approximation also holds in our case. As shown in Fig. 3.1, the extrinsic LLR $L_e(s_{i,j})$ generated by the equalizer is passed to the decoder to

generate a new extrinsic LLR $L_e^d(s_{i,j})$, which is added to the a priori LLR to form the a posteriori LLR $L_{new}(s_{i,j})$ or the new version of the a priori LLR for the next iteration. The means m_i and the variances v_i of the estimated symbol can be updated as in [19, 37]:

$$\begin{aligned} L_{new}(s_{i,j}) &= L(s_{i,j}) + L_e^d(s_{i,j}), \\ m_{i,new} &= \mathrm{E}(s_i) \\ &= \sum_{k=1}^{4} \alpha_k \cdot P(s_i = \alpha_k) \\ &= \frac{\tanh(\frac{L_{new}(s_{i,1})}{2}) + i \cdot \tanh(\frac{L_{new}(s_{i,2})}{2})}{\sqrt{2}}, \\ v_{i,new} &= \sum_{k=1}^{4} |\alpha_k - \mathrm{E}(s_i)|^2 \cdot P(s_i = \alpha_k) \\ &= 1 - |m_{i,new}|^2. \end{aligned} \tag{3.7}$$

The whole procedure described above can then be repeated, depending on the chosen number of iterations.

We now introduce the equalization procedure and the calculation of $L_e(s_{i,j})$ for OFDM systems. The obtained results are subsequently used to derive the block turbo equalizer for SC systems. We assume the receiver has perfect CSI here, the channel estimation algorithm is discussed in the next chapter.

3.3.1 Block Turbo Equalization for OFDM systems

In this subsection, we derive three block turbo MMSE equalizers for OFDM systems subject to time-varying channels, relying on the banded approximation expressed by (3.3). The precoder is set to $\mathbf{P} = \mathbf{F}^H$ for OFDM systems, and (3.2) can be rewritten as

$$\mathbf{y}_f = \mathbf{F}\mathbf{W}\mathbf{H}_t\mathbf{F}^H\mathbf{s} + \mathbf{F}\mathbf{W}\mathbf{n}_t = \mathbf{H}_f\mathbf{s} + \mathbf{n}_f \approx \mathbf{H}\mathbf{s} + \mathbf{n}_f, \tag{3.8}$$

where we approximate $\mathbf{H}_f$ by its banded version as in (3.3) and $\mathbf{n}_f = \mathbf{F}\mathbf{W}\mathbf{n}_t$.

Block Turbo Equalizer I

The first equalizer we propose, which will be called *equalizer I*, is based on a linear MMSE criterion that produces biased symbol estimates. We adopt the

subscript I to denote quantities obtained by this equalizer.

Using a priori information

$$\begin{aligned} \mathbf{m}_I &= [m_{I,1}, m_{I,2}, \ldots, m_{I,N}]^T, \\ \mathbf{V}_I &= \mathrm{diag}([v_{I,1}, v_{I,2}, \ldots, v_{I,N}]^T), \end{aligned} \tag{3.9}$$

the linear MMSE estimate of the symbol on the ith subcarrier is given by [25]

$$\hat{s}_{I,i} = m_{I,i} + \mathbf{g}_{I,i}^H(\mathbf{y}_f - \mathbf{H}\mathbf{m}_I), \tag{3.10}$$

$$\mathbf{g}_{I,i} = v_{I,i}\mathbf{A}_I^{-1}\mathbf{h}_i, \tag{3.11}$$

where

$$\mathbf{A}_I = \mathbf{H}\mathbf{V}_I\mathbf{H}^H + \mathbf{R}_{\mathbf{n}_f}, \tag{3.12}$$

with $\mathbf{h}_i$ being the ith column of $\mathbf{H}$, and $\mathbf{R}_{\mathbf{n}_f} = E(\mathbf{n}_f\mathbf{n}_f^H)$ representing the frequency-domain noise covariance matrix. In the first iteration, when no a priori information is available, we have $m_{I,i} = 0$ and $v_{I,i} = 1$ for the data symbols, and the equalizer becomes the non-iterative MMSE BLE of [11].

After the equalization, the next step is the extrinsic LLR updating. To perform this calculation, we should derive the PDF $p(\hat{s}_{I,i}|s_i = \alpha_k)$. In general, the exact derivation of this PDF is not easy. However, the PDF $p(\hat{s}_{I,i}|s_i = \alpha_k)$ can be approximated as Gaussian, with mean $\mu_{I,i,k}$ and variance $\sigma_{I,i,k}^2$. Therefore, $p(\hat{s}_{I,i}|s_i = \alpha_k)$ can be written as

$$\begin{aligned} p(\hat{s}_{I,i}|s_i = \alpha_k) &= \frac{1}{\pi\sigma_{I,i,k}^2} \cdot e^{-|\hat{s}_{I,i} - \mu_{I,i,k}|^2/\sigma_{I,i,k}^2}, \\ \mu_{I,i,k} &= \mathrm{E}(\hat{s}_{I,i}|s_i = \alpha_k) \\ &= m_{I,i} + \mathbf{g}_{I,i}^H\mathbf{h}_i(\alpha_k - m_{I,i}) \\ &= m_{I,i} + v_{I,i}\mathbf{h}_i^H(\mathbf{H}\mathbf{V}_I\mathbf{H}^H + \mathbf{R}_{\mathbf{n}_f})^{-1}\mathbf{h}_i(\alpha_k - m_{I,i}) \\ &= m_{I,i} + v_{I,i}t_{I,i}(\alpha_k - m_{I,i}), \end{aligned} \tag{3.13}$$

$$\begin{aligned}
\sigma^2_{I,i,k} &= \mathrm{Cov}(\hat{s}_{I,i}, \hat{s}_{I,i}|s_i = \alpha_k) \\
&= \mathbf{g}^H_{I,i}\mathrm{Cov}(\mathbf{y}_f, \mathbf{y}_f|s_i = \alpha_k)\mathbf{g}_{I,i} \\
&= \mathbf{g}^H_{I,i}(\mathbf{H}\mathbf{V}_I\mathbf{H}^H + \mathbf{R}_{\mathbf{n}_f} - v_{I,i}\mathbf{h}_i\mathbf{h}^H_i)\mathbf{g}_{I,i} \\
&= v_{I,i}\mathbf{h}^H_i(\mathbf{H}\mathbf{V}_I\mathbf{H}^H + \mathbf{R}_{\mathbf{n}_f})^{-1}(\mathbf{H}\mathbf{V}_I\mathbf{H}^H + \mathbf{R}_{\mathbf{n}_f} \\
&\quad - v_{I,i}\mathbf{h}_i\mathbf{h}^H_i)(\mathbf{H}\mathbf{V}_I\mathbf{H}^H + \mathbf{R}_{\mathbf{n}_f})^{-1}\mathbf{h}_i v_{I,i} \\
&= v_{I,i}\mathbf{h}^H_i(\mathbf{H}\mathbf{V}_I\mathbf{H}^H + \mathbf{R}_{\mathbf{n}_f})^{-1}[\mathbf{I} - v_{I,i}\mathbf{h}_i\mathbf{h}^H_i(\mathbf{H}\mathbf{V}_I\mathbf{H}^H + \mathbf{R}_{\mathbf{n}_f})^{-1}]\mathbf{h}_i v_{I,i} \\
&= v_{I,i}\mathbf{h}^H_i(\mathbf{H}\mathbf{V}_I\mathbf{H}^H + \mathbf{R}_{\mathbf{n}_f})^{-1}\mathbf{h}_i v_{I,i} - v^2_{I,i}[\mathbf{h}^H_i(\mathbf{H}\mathbf{V}_I\mathbf{H}^H + \mathbf{R}_{\mathbf{n}_f})^{-1}\mathbf{h}_i]^2 v_{I,i} \\
&= v^2_{I,i}t_{I,i} - v^3_{I,i}t^2_{I,i} \\
&= v^2_{I,i}t_{I,i}(1 - v_{I,i}t_{I,i}),
\end{aligned} \tag{3.14}$$

with

$$t_{I,i} = \mathbf{h}^H_i(\mathbf{H}\mathbf{V}_I\mathbf{H}^H + \mathbf{R}_{\mathbf{n}_f})^{-1}\mathbf{h}_i. \tag{3.15}$$

Based on the above equations, the extrinsic information can be calculated from (3.6), as detailed in Appendix 3.1, which leads to the following result:

$$\begin{aligned}
L_e(s_{I,i,1}) &= \frac{\sqrt{8}\mathrm{Re}(\hat{s}_{I,i} - m_{I,i}(1 - v_{I,i}t_{I,i}))}{v_{I,i}(1 - v_{I,i}t_{I,i})}, \\
L_e(s_{I,i,2}) &= \frac{\sqrt{8}\mathrm{Im}(\hat{s}_{I,i} - m_{I,i}(1 - v_{I,i}t_{I,i}))}{v_{I,i}(1 - v_{I,i}t_{I,i})}.
\end{aligned} \tag{3.16}$$

Block Turbo Equalizer II

In turbo equalization and turbo decoding, it is a good rule to have the extrinsic information $L_e(s_{i,j})$ independent from the a priori LLR $L(s_{i,j})$ [19, 20]. Otherwise, it would create a feedback loop in the equalization and decoding process, i.e., the equalizer sends information for a given bit to the decoder, and the decoder simply sends back the information that the equalizer already knows. Indeed, the extrinsic information represents only the new information gained by equalization or decoding, and should not depend on the a priori LLR, which is added separately during the LLR update. Thus, the equalizer only sends the decoder new information for a given bit obtained from other bits due to the interleaving operation, and the decoder performs similarly.

In the previous equalizer, however, the estimated symbol $\hat{s}_{I,i}$ depends on the a priori mean $m_{I,i}$ and variance $v_{I,i}$. Therefore, in our equalizer I, the

prior knowledge is in a certain way overrated, because it also contributes to the extrinsic LLR. In this subsection, we modify the previously proposed equalizer to make the extrinsic LLR independent from the a priori LLR. To achieve this goal, we design our *equalizer II* in such a way that the equalizer output $\hat{s}_{II,i}$ at the ith subcarrier is independent from the specific values of $m_{II,i}$ and $v_{II,i}$ [19]. In this way, the extrinsic LLR $L_e(s_{II,i,j})$, which is obtained from the equalizer output at the ith subcarrier, does not depend on the prior knowledge of the specific ith QPSK symbol, but depends only on the prior knowledge of the QPSK symbols with indices $\{i' : i' \neq i\}$.

To obtain a mathematical expression for equalizer II, let us recall the equalizer I expressions (4.1) and (3.11), derived in the previous subsection. In order to make the estimated symbol on the ith subcarrier independent from the prior knowledge of the ith symbol itself, we should set $m_{II,i}$ equal to zero and $v_{II,i}$ equal to one. However, when estimating the symbols on the other subcarriers, we should maintain $m_{II,i}$ and $v_{II,i}$ equal to their original values, obtained from the previous iteration. To achieve these two requirements, we adopt a similar modification as in [19], and we express the equalizer as

$$\hat{s}_{II,i} = \mathbf{g}_{II,i}^H(\mathbf{y}_f - \mathbf{H}\mathbf{m}_{II} + m_{II,i}\mathbf{h}_i), \tag{3.17}$$

$$\mathbf{g}_{II,i} = (\mathbf{A}_{II} + (1 - v_{II,i})\mathbf{h}_i\mathbf{h}_i^H)^{-1}\mathbf{h}_i, \tag{3.18}$$

where $\mathbf{A}_{II} = \mathbf{H}\mathbf{V}_{II}\mathbf{H}^H + \mathbf{R}_{\mathbf{n}_f}$ is similarly defined as in (3.12). At a first look, this block MMSE equalizer seems much more complicated than the first one, because a matrix inverse for each subcarrier is required in (3.17), whereas a single inverse is shared by all the subcarriers in (3.10). However, it is possible to show that also equalizer II can use a unique shared inverse. Indeed, from the matrix inversion lemma, we obtain

$$\begin{aligned}
&(\mathbf{A}_{II} + (1 - v_{II,i})\mathbf{h}_i\mathbf{h}_i^H)^{-1} \\
&= \mathbf{A}_{II}^{-1} - \frac{1 - v_{II,i}}{1 + (1 - v_{II,i})\mathbf{h}_i^H\mathbf{A}_{II}^{-1}\mathbf{h}_i}\mathbf{A}_{II}^{-1}\mathbf{h}_i\mathbf{h}_i^H\mathbf{A}_{II}^{-1} &(3.19)\\
&= \mathbf{A}_{II}^{-1} - \frac{1 - v_{II,i}}{1 + (1 - v_{II,i})t_{II,i}}\mathbf{A}_{II}^{-1}\mathbf{h}_i\mathbf{h}_i^H\mathbf{A}_{II}^{-1}, &(3.20)
\end{aligned}$$

where $t_{II,i} = \mathbf{h}_i^H(\mathbf{H}\mathbf{V}_{II}\mathbf{H}^H + \mathbf{R}_{\mathbf{n}_f})^{-1}\mathbf{h}_i$ is similarly defined as in (3.15). Consequently, $\mathbf{g}_{II,i}$ becomes

$$\begin{aligned}
\mathbf{g}_{II,i} &= \mathbf{A}_{II}^{-1}\mathbf{h}_i - \frac{1 - v_{II,i}}{1 + (1 - v_{II,i})t_{II,i}}t_{II,i}\mathbf{A}_{II}^{-1}\mathbf{h}_i \\
&= \frac{1}{1 + (1 - v_{II,i})t_{II,i}}\mathbf{A}_{II}^{-1}\mathbf{h}_i. &(3.21)
\end{aligned}$$

Hence, from (3.17), the estimated symbol becomes

$$\hat{s}_{II,i} = \frac{1}{1+(1-v_{II,i})t_{II,i}}\mathbf{h}_i^H \mathbf{A}_{II}^{-1}(\mathbf{y}_f - \mathbf{H}\mathbf{m}_{II}) + \frac{t_{II,i}m_{II,i}}{1+(1-v_{II,i})t_{II,i}}. \quad (3.22)$$

From (3.22), it is clear that the same inverse $\mathbf{A}_{II}^{-1}$ can be used for every subcarrier. Hence, the structure of equalizer II is quite similar to that of equalizer I. We highlight that a similar procedure has also been presented in [22] but in a CDMA context. The main difference with [22] is that we are using an alternative expression for the MMSE equalizer.

Also the LLR calculation can be derived similarly to that for equalizer I. The PDF $p(\hat{s}_{II,i}|s_i = \alpha_k)$ is again assumed Gaussian, with mean and variance expressed by

$$\begin{aligned} \mu_{II,i,k} &= \frac{1}{1+(1-v_{II,i})t_{II,i}} t_{II,i}\alpha_k, \\ \sigma^2_{II,i,k} &= \mathbf{g}_{II,i}^H(\mathbf{H}\mathbf{V}_{II}\mathbf{H}^H - v_{II,i}\mathbf{h}_i\mathbf{h}_i^H + \mathbf{R}_{\mathbf{n}_f})\mathbf{g}_{II,i} \\ &= \frac{1}{[1+(1-v_{II,i})t_{II,i}]^2} t_{II,i}(1-v_{II,i}t_{II,i}). \end{aligned} \quad (3.23)$$

Therefore, by using the same procedure of Appendix A for Equalizer I, the extrinsic LLR can be calculated as

$$\begin{aligned} L_e(s_{II,i,1}) &= \frac{[1+(1-v_{II,i})t_{II,i}]\sqrt{8}\mathrm{Re}(\hat{s}_{II,i})}{1-v_{II,i}t_{II,i}}, \\ L_e(s_{II,i,2}) &= \frac{[1+(1-v_{II,i})t_{II,i}]\sqrt{8}\mathrm{Im}(\hat{s}_{II,i})}{1-v_{II,i}t_{II,i}}. \end{aligned} \quad (3.24)$$

Block Turbo Equalizer III

The two previous equalizers are biased, since $\mathrm{E}\{\hat{s}_i\} \neq s_i$. However, an unbiased equalizer can be derived by simply removing the bias term from equalizer I or equalizer II, as done in [27] for a decision-feedback equalizer. From (3.10), we observe that the bias term for equalizer I can be expressed by

$$\mathrm{E}(\hat{s}_{I,i}) - s_i = m_{I,1} + (v_{I,i}t_{I,i} - 1)s_i - m_{I,i}v_{I,i}t_{I,i}, \quad (3.25)$$

and, from (3.22), the bias for equalizer II is

$$\mathrm{E}(\hat{s}_{II,i}) - s_i = \left(\frac{t_{II,i}}{1+(1-v_{II,i})t_{II,i}} - 1\right) s_i. \quad (3.26)$$

Please observe that $\mathrm{E}(\hat{s}_{I,i})$ and $\mathrm{E}(\hat{s}_{II,i})$ are a posteriori expected values performed after equalization, and should not be confused with the a priori means $m_{I,i} = \mathrm{E}(s_{I,i})$ and $m_{II,i} = \mathrm{E}(s_{II,i})$, which are the corresponding expected values before equalization. By compensating for the bias, we obtain one and the same expression for the unbiased equalizer, which we call *equalizer III*. More specifically, for equalizer I and II, the ith unbiased estimated symbol can be written as

$$\frac{\hat{s}_{I,i} - (1 - v_{I,i}t_{I,i})m_{I,i}}{v_{I,i}t_{I,i}} \quad \text{and} \quad \frac{1 + (1 - v_{II,i})t_{II,i}}{t_{II,i}}\hat{s}_{II,i} \tag{3.27}$$

respectively, which both lead to the following expression

$$\hat{s}_{III,i} = \frac{1}{t_{III,i}}\mathbf{h}_i^H \mathbf{A}_{III}^{-1}(\mathbf{y}_f - \mathbf{H}\mathbf{m}_{III}) + m_{III,i}, \tag{3.28}$$

where $t_{III,i}$ and $\mathbf{A}_{III}$ are similarly defined as in (3.15) and (3.12), respectively. The mean and variance can be expressed by

$$\begin{aligned} \mu_{III,i,k} &= \alpha_k, \\ \sigma^2_{III,i,k} &= \frac{1 - v_{III,i}t_{III,i}}{t_{III,i}}. \end{aligned} \tag{3.29}$$

The extrinsic information can be calculated in the same way as in (3.16) or (3.24), leading to

$$\begin{aligned} L_e(s_{III,i,1}) &= \frac{t_{III,i}\sqrt{8}\mathrm{Re}(\hat{s}_{III,i})}{1 - v_{III,i}t_{III,i}} \\ L_e(s_{III,i,2}) &= \frac{t_{III,i}\sqrt{8}\mathrm{Im}(\hat{s}_{III,i})}{1 - v_{III,i}t_{III,i}}. \end{aligned} \tag{3.30}$$

3.3.2 Comparisons

We now compare the extrinsic LLR's of the three equalizers by inserting (3.10), (3.22), and (3.28), into (3.16), (3.24), and (3.30), respectively. By focusing on

the first bit of subcarrier i, we obtain

$$\begin{aligned}
L_e(s_{I,i,1}) &= \sqrt{8}\mathrm{Re}\left[\frac{1}{1-v_{I,i}t_{I,i}}\mathbf{h}_i^H\mathbf{A}_I^{-1}(\mathbf{y}_f-\mathbf{H}\mathbf{m}_I)+\frac{m_{I,i}}{v_{I,i}(1-v_{I,i}t_{I,i})}-\frac{m_{I,i}}{v_{I,i}}\right] \\
&= \sqrt{8}\mathrm{Re}\left[\frac{1}{1-v_{I,i}t_{I,i}}\mathbf{h}_i^H\mathbf{A}_I^{-1}(\mathbf{y}_f-\mathbf{H}\mathbf{m}_I)+\frac{t_{I,i}m_{I,i}}{1-v_{I,i}t_{I,i}}\right], \\
L_e(s_{II,i,1}) &= \sqrt{8}\mathrm{Re}\left[\frac{1}{1-v_{II,i}t_{II,i}}\mathbf{h}_i^H\mathbf{A}_{II}^{-1}(\mathbf{y}_f-\mathbf{H}\mathbf{m}_{II})+\frac{t_{II,i}m_{II,i}}{1-v_{II,i}t_{II,i}}\right], \\
L_e(s_{III,i,1}) &= \sqrt{8}\mathrm{Re}\left[\frac{1}{1-v_{III,i}t_{III,i}}\mathbf{h}_i^H\mathbf{A}_{III}^{-1}(\mathbf{y}-\mathbf{H}\mathbf{m}_{III})+\frac{t_{III,i}m_{III,i}}{1-v_{III,i}t_{III,i}}\right].
\end{aligned} \tag{3.31}$$

From the above equations, we can notice that the extrinsic LLR expressions are the same for all three equalizers. In other words, for all iterations, the means (and the variances) are the same for all three equalizers. Hence, in equalizers I and II, the extrinsic LLR calculation is able to compensate for the bias introduced by the equalizer. However, in an uncoded system, since the symbol decision is taken at the equalizer output (i.e., before the LLR updating), a residual bias will be present at the final symbol estimates of equalizers I and II. For equalizer II, the residual bias only contains a positive scaling factor that does not affect the QPSK BER, which therefore is the same as the BER of the unbiased equalizer III. On the contrary, for equalizer I, the residual bias also contains an additive term that produces a BER performance loss with respect to equalizers II and III.

The equivalence between the extrinsic LLR's for the biased equalizer II and the unbiased equalizer III is a nice result, because it establishes a clear link with non-iterative equalizers, for which it is well known that biased and unbiased equalizers are equivalent, for constant-modulus constellations. This also justifies the use of the biased MMSE equalizer, instead of the unbiased one, in other turbo scenarios, e.g., those in [19, 20, 22]. We remark that, in general, the equivalence between biased and unbiased equalizers does not hold for nonconstant-modulus constellations, e.g., 16-QAM. An example of this behavior has already been shown in [21], where an unbiased minimum variance (i.e., unbiased MMSE) equalizer outperforms the biased MMSE equalizer. It is worth noting that the unbiased MMSE equalizer of [21] has been derived using interference cancelation, i.e., in a different way with respect to our equalizer. When also channel coding is incorporated into the turbo loop, our unbiased equalizer III can be interpreted as the corresponding version of [21] for OFDM communications over time-varying channels.

Note that the proposed iterative BLE's also have their serial counterparts, as for instance discussed in [10]. In the serial case, the equalizer is updated from subcarrier to subcarrier and a different matrix inverse has to be computed for each subcarrier, which actually could be carried out in a recursive fashion as explained in [20]. The advantage of this subcarrier by subcarrier processing is that one can choose between updating the priors from one subcarrier to the next (sequential iterative estimation (SIE) in [10]) or from one OFDM symbol to the next (block iterative estimation (BIE) in [10]). On the contrary, the proposed iterative BLE's remain fixed for the entire OFDM symbol, since the matrix inverse contained in $\mathbf{g}$ is the same for all the subcarriers. Therefore, we can only update our priors from one OFDM symbol to the next.

3.3.3 Low-Complexity Algorithms

In this subsection, we investigate the computational complexity of the proposed equalizers. Our aim is to show some useful techniques that render this complexity linear in the number of active subcarriers N.

In order to calculate $\hat{s}_i$ in (3.10), (3.22), and (3.28), and t_i in (3.15), a matrix inverse $\mathbf{A}^{-1}$ is required. The standard computation of a matrix inverse requires a complexity of $O(N^3)$, which is too much for an OFDM system, even with a moderate number of active subcarriers. However, [9, 11] show how to exploit the banded structure of the approximated frequency-domain channel matrix $\mathbf{H}$ to reduce complexity. Specifically, instead of computing the matrix inverse, the equalization is performed by applying a band LDL^H factorization [28] to the matrix to be inverted, as expressed by

$$\mathbf{A} = \mathbf{H}\mathbf{V}\mathbf{H}^H + \mathbf{R}_{\mathbf{n}_f} = \mathbf{L}\mathbf{D}\mathbf{L}^H, \tag{3.32}$$

where $\mathbf{L}$ is a unit lower triangular matrix and $\mathbf{D}$ is diagonal, followed by a linear system solver that exploits this matrix decomposition to solve (4.1), (3.22), and (3.28) in one step for all i's. Instead of inverting the matrix $\mathbf{A}$ in (3.32), we solve the linear system $\mathbf{A}\mathbf{c} = \mathbf{b}$, which can be written as $\mathbf{L}\mathbf{D}\mathbf{L}^H\mathbf{c} = \mathbf{b}$ by (3.32). As explained in [9], this can be solved in three steps: first, $\mathbf{L}\mathbf{c}' = \mathbf{b}$ is solved for $\mathbf{c}'$, then $\mathbf{D}\mathbf{c}'' = \mathbf{c}'$ is solved for $\mathbf{c}''$, and eventually $\mathbf{L}^H\mathbf{c} = \mathbf{c}''$ is solved for $\mathbf{c}$. Overall, this leads to a complexity of $O(N)$. Note that this is valid only when the frequency-domain noise covariance matrix $\mathbf{R}_{\mathbf{n}_f}$ is banded. In this thesis, we adopt the minimum band-approximation-error sum-of-exponentials (MBAE-SOE) windows [11], which are able to fulfill the banded constraint of the frequency-domain noise covariance matrix.

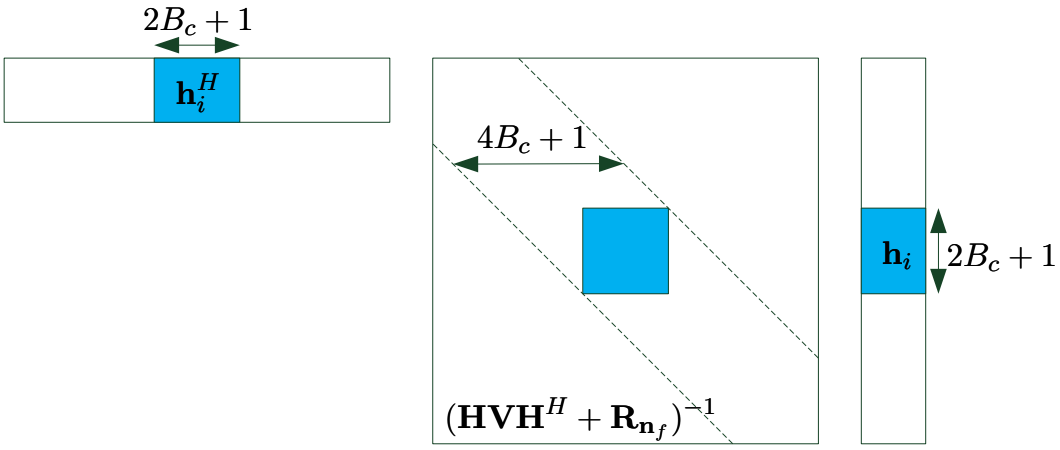

Figure 3.4: Structure of t_i.

Although solving a banded linear system requires a complexity that is only linear in N, this is not sufficient to guarantee that the full equalization procedure presented in the previous section has a linear complexity. Indeed, for all equalizers, we also need to calculate $t_i = \mathbf{h}_i^H \mathbf{A}^{-1} \mathbf{h}_i$ for each subcarrier i. Intuitively, a linear system solver for $\mathbf{A}\mathbf{c}_i = \mathbf{b}_i$ based on the band LDL^H factorization of $\mathbf{A}$, should be repeated for each subcarrier, leading to a complexity that is quadratic in N. Similarly, exploiting the banded structure of $\mathbf{A}$, an explicit calculation of the inverse $\mathbf{A}^{-1}$ would also require a quadratic complexity [29].

To reduce the complexity of the t_i calculations from quadratic to linear, we exploit the fact that the vector $\mathbf{h}_i$ is the ith column of the banded matrix $\mathbf{H}$, which is characterized by $2B_c + 1$ non-zero diagonals. This means that $\mathbf{h}_i$ has only $2B_c + 1$ non-zero elements, from $i - B_c$ to $i + B_c$. Since these non-zero elements are contiguous, we will refer to $\mathbf{h}_i$ as a *banded vector*. Hence, to calculate a specific $t_i = \mathbf{h}_i^H \mathbf{A}^{-1} \mathbf{h}_i$, we only need a square subblock of $\mathbf{A}^{-1}$ of dimension $2B_c + 1$. More specifically, by defining $\mathbf{O} = \mathbf{A}^{-1}$, only the $4B_c + 1$ diagonals in the main band of $\mathbf{O}$ are necessary in order to calculate the t_i values (see Fig. 3.4). Now, we split the complexity calculation in two parts: computing the main band of $\mathbf{O}$, and computing the t_i values from the knowledge of the main band of $\mathbf{O}$.

The calculation of the main band of $\mathbf{O}$ can be done from the band LDL^H factorization of $\mathbf{A}$, which is already available, with complexity $O(N)$ [29]. Let us define $o_{i,j}$ as the (i, j)th element of $\mathbf{O}$, $l_{i,j}$ as the (i, j)th element of $\mathbf{L}$, and

$d_{i,i}$ as the (i,i)th element of $\mathbf{D}$. The algorithm starts from calculating $o_{N,N}$, which is at the bottom right corner of $\mathbf{O}$, and then calculates the elements from the bottom to the top. Within each row, each element is calculated from the right to the left. The algorithm is adapted from [29], and is summarized in Table 3.2.

Table 3.2: Calculation of the main band of $\mathbf{O}$

$o_{N,N} = 1/d_{N,N}$
for $i = (N-1) : (-1) : 1$
  $M_i = \min(N, i + 2B_c)$
  for $j = M_i : (-1) : (i+1)$
    $o_{i,j} = -\sum_{k=i+1}^{M_i} l_{k,i}^* o_{k,j}$
    $o_{j,i} = o_{i,j}^*$
  end
  $o_{i,i} = 1/d_{i,i} - \sum_{k=i+1}^{M_i} l_{k,i} o_{i,k}$
end

Let us now evaluate the complexity of the algorithm described above. In the following analysis, we do not differentiate between data symbols and pilot symbols, and we assume the entire N-length block of symbols need to be estimated. Calculating the main band of $\mathbf{O}$ requires $(4B_c^2 + 2B_c)(N-1)$ complex multiplications (CM), $(4B_c^2 + 2B_c)(N-1)$ complex additions (CA) and N complex divisions (CD). The computation of each t_i requires $(2B_c + 1)(2B_c + 2)$ CM and $2B_c(2B_c + 2)$ CA. Hence, in total, approximately $(8B_c^2 + 8B_c + 2)N$ CM, $(8B_c^2 + 6B_c)N$ CA and N CD are needed to calculate all the t_i's. For the complexity of the block turbo equalizer I, we use the results of [11], and we observe that computing (4.1) requires $(4B_c^2 + 16B_c + 6)N$ CM, $(4B_c^2 + 12B_c + 3)N$ CA and $(2B_c + 1)N$ CD. Calculating the extrinsic information in (3.37) requires $6N$ CM, $2N$ CA and $2N$ CD. Updating the soft information in (3.7) requires N CM, $3N$ CA, N CD, and $2N$ hyperbolic tangent calculations. The hyperbolic tangent function can be evaluated by using a look-up table or a low-complexity numerical algorithm. The complexity analysis of the other block turbo equalizers is similar to that of equalizer I. Table 3.3 gives a comprehensive overview of the complexity of a generic iteration for the three block turbo equalizers. Please observe that the complexity of the first iteration is even smaller, because the prior means m_i and variances v_i are 0 and 1, respectively, and hence some additions and multiplications can be omitted. Summarizing, the proposed block turbo MMSE equalizers are characterized by a low complexity, which is linear in the number of active

Table 3.3: Complexity analysis (per subcarrier)

	CA	CM	CD	tanh
equalizer I	$12B_c^2 + 18B_c + 8$	$12B_c^2 + 24B_c + 15$	$2B_c + 5$	2
equalizer II/III	$12B_c^2 + 18B_c + 10$	$12B_c^2 + 24B_c + 17$	$2B_c + 7$	2

subcarriers N. A complexity analysis of the SIE/BIE has been derived in [9], which showed similar $O(B_c^2 N)$ computational complexity. However, in the simulation section we demonstrate that the proposed block turbo MMSE equalizers have a performance advantage over the SIE/BIE for OFDM systems.

By exploiting a smart algorithm for the calculation of t_i, it can be shown that, for each OFDM block, the computational complexity of the described equalization algorithm is $\mathcal{O}(B_c^2 N)$ per iteration, that is, linear in the number of subcarriers N and quadratic in the matrix bandwidth B_c. On the contrary, the complexity of a time-domain equalizer would be $\mathcal{O}(L^2 N)$. Therefore, since the Doppler support is usually much lower than the maximum delay spread, our frequency-domain equalizer is computationally cheaper than the corresponding time-domain equalizer.

3.4 Block Turbo Equalization for SC systems

In SC systems, the precoder is absent and therefore it is set to $\mathbf{P} = \mathbf{I}$. In this case, (3.2) can be rewritten as

$$\mathbf{y}_f = \mathbf{F}\mathbf{W}\mathbf{H}_t\mathbf{F}^H\mathbf{F}\mathbf{s} + \mathbf{F}\mathbf{W}\mathbf{n}_t = \mathbf{H}_f\mathbf{F}\mathbf{s} + \mathbf{F}\mathbf{W}\mathbf{n}_t \approx \mathbf{H}\mathbf{s}_f + \mathbf{n}_f, \tag{3.33}$$

where we approximate $\mathbf{H}_f$ by its banded version as in (3.3), $\mathbf{s}_f = \mathbf{F}\mathbf{s}$, and $\mathbf{n}_f = \mathbf{F}\mathbf{W}\mathbf{n}_t$. Similarly to our previous notation, we define $s_{f,i}$ as the ith symbol of $\mathbf{s}_f$, $m_{f,i} = \mathrm{E}(s_{f,i})$ and $v_{f,i} = \mathrm{Cov}(s_{f,i}, s_{f,i})$ as the means and the variances of the frequency-domain signals.

Given $\mathbf{m}$ and $\mathbf{V}$ as prior information, the equalizer exploits the means and the variances of the frequency-domain symbols. Since $\mathbf{s}_f = \mathbf{F}\mathbf{s}$, we have $\mathbf{m}_f = \mathrm{E}(\mathbf{s}_f) = \mathbf{F}\mathbf{m} = [m_{f,1}, \ldots, m_{f,N}]^T$, and $\mathbf{V}_f = \mathrm{Cov}(\mathbf{s}_f, \mathbf{s}_f) = \mathbf{F}\mathbf{V}\mathbf{F}^H$. In general, $\mathbf{V}_f$ is not a diagonal matrix, and can not be written as $\mathrm{diag}([v_{f,1}, \ldots, v_{f,N}]^T)$. Therefore, to save complexity, we use its approximated version obtained by setting its off-diagonal elements to zero. This approximation leads to $\mathbf{V}_f = \bar{v}_t \cdot \mathbf{I}_N$ due to the properties of $\mathbf{F}$, where $\bar{v}_t = \frac{1}{N}\sum_{i=1}^{N} v_i$, and basically annihilates

the frequency variability of the variance. A similar approximation is used also in time-domain equalizers [19, 20].

By using $m_{f,i}$ and $v_{f,i}$ as prior information, a frequency-domain linear MMSE equalizer can be obtained using the previously developed unbiased Equalizer III for OFDM systems. In SC systems, this approach leads to

$$\hat{s}_{f,i} = \frac{1}{t_i}\mathbf{h}_i^H \mathbf{A}^{-1}(\mathbf{y}_f - \mathbf{H}\mathbf{m}_f) + m_{f,i}, \tag{3.34}$$

where $\mathbf{h}_i$ is the ith column of $\mathbf{H}$, $\mathbf{A} = \mathbf{H}\mathbf{V}_f\mathbf{H}^H + \mathbf{R}_{\mathbf{n}_f}$, $t_i = \mathbf{h}_i^H\mathbf{A}^{-1}\mathbf{h}_i$, and $\mathbf{R}_{\mathbf{n}_f} = E(\mathbf{n}_f\mathbf{n}_f^H)$. Since the matrix $\mathbf{A}$ is banded, the computations in (3.34) can be performed using special routines designed to solve banded linear systems, with linear complexity in the block size N. On the contrary, without the diagonal approximation on $\mathbf{V}_f$, $\mathbf{A}$ would not be banded anymore, and therefore the complexity order would increase.

The estimated time-domain data-symbol vector is successively obtained by $\hat{\mathbf{s}} = \mathbf{F}^H\hat{\mathbf{s}}_f$, which leads to

$$\begin{aligned}
\hat{s}_i &= \mathbf{i}_i^H\mathbf{F}^H\hat{\mathbf{s}}_f = \mathbf{i}_i^H\mathbf{F}^H\sum_{k=1}^{N}\mathbf{i}_k\hat{s}_{f,k} \\
&= \mathbf{i}_i^H\mathbf{F}^H\sum_{k=1}^{N}\frac{1}{t_k}\mathbf{i}_k\mathbf{h}_k^H\mathbf{A}^{-1}\mathbf{H}\mathbf{F}(\mathbf{s}-\mathbf{m}) + \mathbf{i}_i^H\mathbf{F}^H\sum_{k=1}^{N}\mathbf{i}_k m_{f,k} \\
&\quad + \mathbf{i}_i^H\mathbf{F}^H\sum_{k=1}^{N}\frac{1}{t_k}\mathbf{i}_k\mathbf{h}_k^H\mathbf{A}^{-1}\mathbf{F}\mathbf{n}_t \\
&= \mathbf{i}_i^H\mathbf{F}^H\sum_{k=1}^{N}\frac{1}{t_k}\mathbf{i}_k\mathbf{h}_k^H\mathbf{A}^{-1}\mathbf{H}\mathbf{F}(\mathbf{s}-\mathbf{m}) + \mathbf{i}_i^H\mathbf{F}^H\sum_{k=1}^{N}\mathbf{i}_k\mathbf{i}_k^H\mathbf{F}\mathbf{m} \\
&\quad + \mathbf{i}_i^H\mathbf{F}^H\sum_{k=1}^{N}\frac{1}{t_k}\mathbf{i}_k\mathbf{h}_k^H\mathbf{A}^{-1}\mathbf{F}\mathbf{n}_t \\
&= m_i + \mathbf{i}_i^H\mathbf{F}^H\mathbf{T}\mathbf{\Sigma}\mathbf{F}(\mathbf{s}-\mathbf{m}) + \mathbf{i}_i^H\mathbf{F}^H\mathbf{T}\mathbf{H}^H\mathbf{A}^{-1}\mathbf{F}\mathbf{n}_t,
\end{aligned} \tag{3.35}$$

where $\mathbf{i}_k$ is the $N \times 1$ unit vector, defined as the kth column of $\mathbf{I}_N$, $\mathbf{T} = \sum_{k=1}^{N}\frac{1}{t_k}\mathbf{i}_k\mathbf{i}_k^H$, and $\mathbf{\Sigma} = \mathbf{H}^H\mathbf{A}^{-1}\mathbf{H}$.

The mean μ_i and the variance σ_i^2 of the Gaussian PDF $p(\hat{s}_i|s_i = s)$ can

be calculated from (3.35) as

$$\begin{aligned}
\mu_i &= \mathrm{E}(\hat{s}_i|s_i = s) \\
&= \mathbf{i}_i^H \mathbf{F}^H \mathbf{T}\boldsymbol{\Sigma}\mathbf{F}\mathrm{E}(\mathbf{s} - (\mathbf{m} - m_i\mathbf{i}_i)|s_i = s) \\
&= \mathbf{i}_i^H \mathbf{F}^H \mathbf{T}\boldsymbol{\Sigma}\mathbf{F}\mathbf{i}_i s \\
&\approx s, \\
\sigma_i^2 &= \mathrm{Cov}(\hat{s}_i, \hat{s}_i|s_i = s) \\
&= \mathrm{E}(|\hat{s}_i - \mu_i|^2 \mid s_i = s) \\
&= \mathrm{E}(|\mathbf{i}_i^H \mathbf{F}^H \mathbf{T}\boldsymbol{\Sigma}\mathbf{F}[\mathbf{s} - \mathbf{m} - \mathbf{i}_i(s - m_i)] + \mathbf{i}_i^H \mathbf{F}^H \mathbf{T}\mathbf{H}^H \mathbf{A}^{-1}\mathbf{F}\mathbf{n}_t|^2) \\
&= \mathbf{i}_i^H \mathbf{F}^H \mathbf{T}\boldsymbol{\Sigma}\mathbf{F}(\mathbf{V} - v_i\mathbf{i}_i\mathbf{i}_i^H)\mathbf{F}^H \boldsymbol{\Sigma}^H \mathbf{T}^H \mathbf{F}\mathbf{i}_i + \sigma_n^2 \mathbf{i}_i^H \mathbf{F}^H \mathbf{T}\boldsymbol{\Sigma}\mathbf{H}^{-1}\mathbf{H}^{-H}\boldsymbol{\Sigma}^H \mathbf{T}^H \mathbf{F}\mathbf{i}_i \\
&\approx \bar{v}_i + |\bar{\mathbf{h}}|^2,
\end{aligned} \tag{3.36}$$

where $\bar{v}_i = \frac{1}{N}(\sum_{k=1}^{N} v_k - v_i)$ and $|\bar{\mathbf{h}}|^2 = \frac{\sigma_n^2}{N}\sum_{k=1}^{N} |\mathbf{h}_k^H \mathbf{h}_k|^{-1}$. In (3.36), we have approximated the matrices $\mathbf{F}(\mathbf{V} - \mathbf{i}_i\mathbf{i}_i^H v_i)\mathbf{F}^H$, $\mathbf{H}^H\mathbf{H}$ and $\boldsymbol{\Sigma}$ by diagonal matrices, by setting their off-diagonal elements to zero. Hence, we now discuss these three approximations. *First*, the approximation of $\mathbf{F}(\mathbf{V} - v_i\mathbf{i}_i\mathbf{i}_i^H)\mathbf{F}^H$ is similar to that of $\mathbf{V}_f$ already discussed. An alternative approximation approach is to set $\bar{v}_i = \max\{v_i\}, i = 1, \ldots, N$, which assigns to all the symbols the reliability of the worst-estimated symbol. *Second*, since $\mathbf{H}$ is banded, the off-diagonal elements of $\mathbf{H}^H\mathbf{H}$ decay to zero very rapidly. Hence, a diagonal approximation should not introduce too much performance degradation. *Third*, the matrix $\boldsymbol{\Sigma} = \mathbf{H}^H\mathbf{A}^{-1}\mathbf{H}$ represents the effect of a linear MMSE equalizer $\mathbf{H}^H\mathbf{A}^{-1}$ applied to the channel matrix $\mathbf{H}$. Assuming that the equalizer highly mitigates the ICI, then $\boldsymbol{\Sigma}$ should be very close to a diagonal matrix. This last approximation also leads to $\mathbf{T}\boldsymbol{\Sigma} \approx \mathbf{I}_N$, which justifies the equalizer unbiasedness $\mu_i \approx s_i$.

Using the results of (3.36), the extrinsic LLR can be expressed as [19,37]

$$\begin{aligned}
L_e(s_{i,1}) &= \ln \frac{p(\hat{s}_i|s_i = \alpha_1)P_2(0) + p(\hat{s}_i|s_i = \alpha_3)P_2(1)}{p(\hat{s}_i|s_i = \alpha_2)P_2(0) + p(\hat{s}_i|s_i = \alpha_4)P_2(1)} \\
&= \frac{\sqrt{8}\mathrm{Re}(\hat{s}_i)}{\bar{v}_i + |\bar{\mathbf{h}}|^2}, \\
L_e(s_{i,2}) &= \ln \frac{p(\hat{s}_i|s_i = \alpha_1)P_1(0) + p(\hat{s}_i|s_i = \alpha_2)P_1(1)}{p(\hat{s}_i|s_i = \alpha_3)P_1(0) + p(\hat{s}_i|s_i = \alpha_4)P_1(1)} \\
&= \frac{\sqrt{8}\mathrm{Im}(\hat{s}_i)}{\bar{v}_i + |\bar{\mathbf{h}}|^2},
\end{aligned} \tag{3.37}$$

where $P_j(0) = P(s_{i,j} = 0)$ and $P_j(1) = P(s_{i,j} = 1)$.

Similarly to the equalization algorithm for OFDM [37], it can be shown that the proposed block turbo equalization algorithm has linear complexity in the block size N. Specifically, the equalization step in (3.34) and the calculation of the t_i's have complexity $\mathcal{O}(B_c^2 N)$, while calculating the extrinsic information in (3.37) has complexity $\mathcal{O}(B_c N)$. Therefore, taking into account FFT operations, the overall computational complexity per iteration for each block of N symbols is $\mathcal{O}((B_c^2+\log(N))N)$. As in the OFDM case, this complexity is independent of the channel length L. On the other hand, the complexity of the time-domain equalizer of [35] is $\mathcal{O}(L^2 N)$. Therefore, for long multipath channels, we obtain a significant complexity saving.

We highlight that the diagonal approximations introduced so far highly reduce the computational complexity. For instance, if the matrix $\mathbf{\Sigma}$ is not approximated as diagonal, the computation of σ_i^2 in (3.36) involves full (non-banded) matrices, and therefore the computational complexity would be at least $\mathcal{O}(N^2)$. Therefore, the non-approximated equalizer is useful only when the block size N is small, which is impossible in long multipath channels due to the constraint $N > L$. We also observe that our diagonal approximations, though derived for complexity reasons, seem intuitively reasonable, and therefore we expect a reasonably-good performance. Anyway, we do not claim any performance optimality, since many different reasonable approximations are possible. In the simulation section in the next chapter, the performance of the proposed equalizer for coded SC system is compared with another equalizer obtained using a different approximation.

3.5 Simulation Results

In this section, the proposed algorithms are examined and compared by simulations. We only show the simulation results for uncoded OFDM systems with perfect CSI at the receiver here, simulations for coded OFDM and SC systems will be shown in next chapter together with iterative channel estimators. We consider an OFDM system with $N = 128$ subcarriers. The maximum channel delay spread and the CP length are the same and equal to $L = 32$. We denote with $h_{n,l}^t$ the lth channel tap at the nth time instant. The channel is assumed to be Rayleigh distributed with uniform $\mathrm{E}\{|h_{n,l}^t|^2\} = 1/L$ or exponential $\mathrm{E}\{|h_{n,l}^t|^2\} = e^{-0.6l}/\sum_{l'=1}^{L} e^{-0.6l'}$ power delay profile, and a U-shaped Doppler spectrum. As indicated before, the unbiased equalizer III has the same BER

performance as the biased equalizer II for constant-modulus constellations such as the QPSK used in our simulation.

We consider a high-mobility case where the normalized Doppler frequency is $f_d/\Delta f = 0.15$ with f_d the Doppler frequency and Δf the subcarrier spacing. As indicated in [2], the subcarrier spacing is approximately 4464/2232/1116 Hz for the 2K/4K/8K mode operation in DVB-H. The Doppler frequency f_d can be as high as 120 Hz corresponding to a speed of 160km/h @ 800MHz (upper part of Band V) to 650km/h @ 200 MHz (lower part of band III). Such a speed range could cover most of the vehicle and high-speed train velocities.

Figs. 3.5-3.6 compare the BER performances of equalizers I, II and III with the SIE of [10], in channels with uniform and exponential power-delay profile, respectively. We do not compare with the BIE of [10], since it has a worse performance than the SIE. The time-domain receiver window is designed for a bandwidth parameter $B_c = 3$. As a reference, the BER performances of the traditional receiver ($B_c = 0$) and the non-banded MMSE receiver ($B_c = N-1$) are also shown in Figs. 3.7-3.8, for a uniform and exponential power delay profile, respectively. It can be seen that with $B_c = 3$, the banded equalizers are very close to the non-banded MMSE equalizer ($B_c = N - 1$).

The simulation results in Figs. 3.5-3.8 show that the block turbo equalizer outperforms the serial turbo equalizer. This result, which corroborates our initial expectation, is mainly due to the window design, which is done over the entire OFDM block. Further, we observe that both methods converge slowly after two iterations. In the first iteration, when no a priori information is available, equalizers I, II and III have the same performance since they are simply the standard MMSE BLE of [11]. Because of the additive term into its residual bias, equalizer I produces worse BER performance than equalizers II and III. All the banded equalizers have an error floor due to the band approximation error of the channel. The error floor can be decreased by increasing the bandwidth parameter B_c, as shown in Fig. 3.9 for the uniform power delay profile.

We have also tested our equalizers for various normalized Doppler frequencies ranging from $f_d/\Delta f = 0.05$ to $f_d/\Delta f = 0.25$. We assume a uniform power delay profile and $L = 32$ with bandwidth parameter $B_c = 3$. The BER performance curves are rather flat as a function of $f_d/\Delta f$, as shown in Fig. 3.10 for some specific SNR's. These results testify that our algorithms are robust to different Doppler spreads.

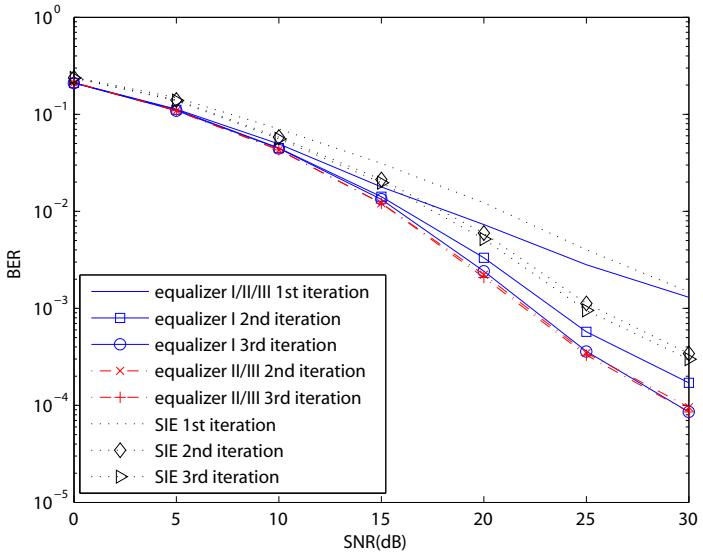

Figure 3.5: BER comparison of equalizer I/II/III and SIE, uniform power delay profile.

3.6 Summary

We have proposed low-complexity MMSE block turbo equalizers for OFDM and SC systems in time-varying channels. By exploiting the banded structure of the frequency-domain channel matrix, as well as receiver windowing to enforce this band assumption, the complexity of the equalizers is linear in the block length. We have derived turbo equalizers operating on the entire block, showing better performance than the serial turbo equalizer for uncoded OFDM systems. Three turbo equalizers have been proposed for OFDM systems. The first and second are both based on a unbiased MMSE criterion. The difference between these two equalizers is that the first does not achieve independence between the extrinsic and a priori information, whereas the second does. Simulation results show that introducing this independence reduces the error floor. The third equalizer, on the other hand, is based on the unbiased MMSE criterion and is equivalent to the second equalizer for constant-modulus constellations.

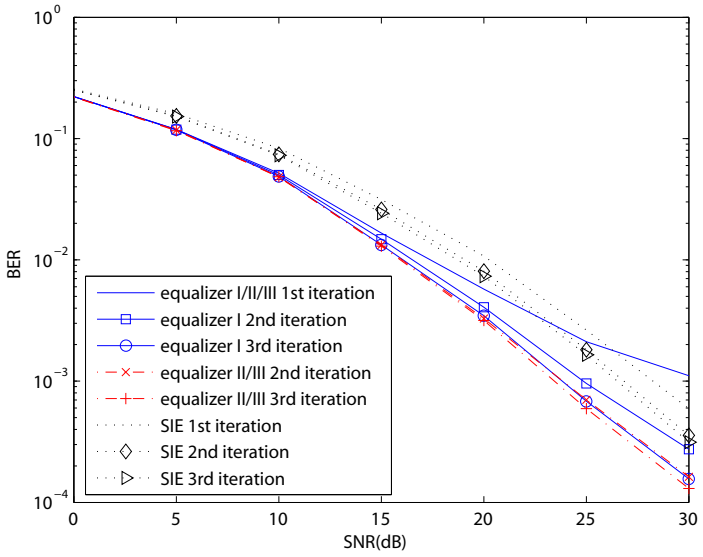

Figure 3.6: BER comparison of equalizer I/II/III and SIE, exponential power delay profile.

Appendix 3.1: Derivation of extrinsic information

For simplicity, we only derive the expression of $L_e(s_{I,i,1})$ in (3.16). The derivation of $L_e(s_{I,i,2})$ is similar. We define $P(0) = P(s_{I,i,2} = 0)$ and $P(1) = P(s_{I,i,2} = 1)$, and omit the subscript I. From (3.6), we can derive $L_e(s_{i,1})$ as in (3.38). Defining $c = [\hat{s}_i - m_i(1 - v_i t_i)]^* v_i t_i$, we can further simplify (3.38), as illustrated in (3.39), where we have used the fact that all the $\sigma^2_{i,k}, k = 1, \ldots, 4$ have the same value.

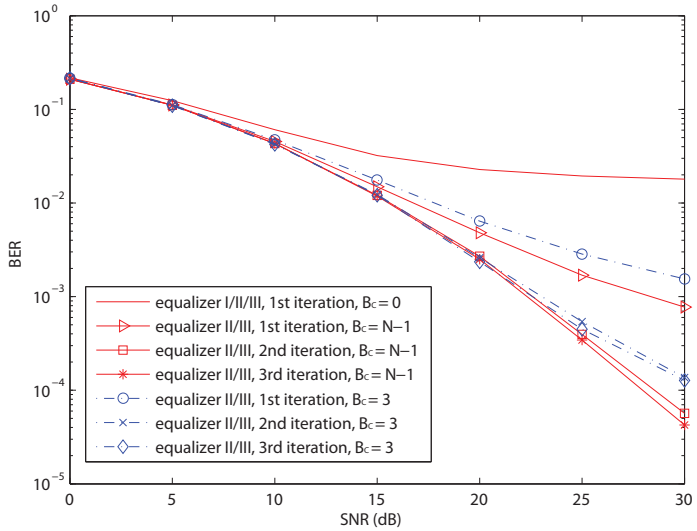

Figure 3.7: BER reference for equalizer II/III, uniform power delay profile.

$$
\begin{aligned}
L_e(s_{i,1}) &= \ln \frac{p(\hat{s}_i|s_i=\alpha_1)P(0)+p(\hat{s}_i|s_i=\alpha_3)P(1)}{p(\hat{s}_i|s_i=\alpha_2)P(0)+p(\hat{s}_i|s_i=\alpha_4)P(1)} \\
&= \ln \frac{\exp(-\frac{|\hat{s}_i-\mu_{i,1}|^2}{\sigma_{i,1}^2})P(0)+\exp(-\frac{|\hat{s}_i-\mu_{i,3}|^2}{\sigma_{i,3}^2})P(1)}{\exp(-\frac{|\hat{s}_i-\mu_{i,2}|^2}{\sigma_{i,2}^2})P(0)+\exp(-\frac{|\hat{s}_i-\mu_{i,4}|^2}{\sigma_{i,4}^2})P(1)} \\
&= \ln \frac{\exp(-\frac{|[\hat{s}_i-m_i(1-v_it_i)]-v_it_i\alpha_1|^2}{\sigma_{i,1}^2})P(0)+\exp(-\frac{|[\hat{s}_i-m_i(1-v_it_i)]-v_it_i\alpha_3|^2}{\sigma_{i,3}^2})P(1)}{\exp(-\frac{|[\hat{s}_i-m_i(1-v_it_i)]-v_it_i\alpha_2|^2}{\sigma_{i,2}^2})P(0)+\exp(-\frac{|[\hat{s}_i-m_i(1-v_it_i)]-v_it_i\alpha_4|^2}{\sigma_{i,4}^2})P(1)} \\
&= \ln \frac{\exp(\frac{2\mathrm{Re}\{[\hat{s}_i-m_i(1-v_it_i)]^*\cdot v_it_i\alpha_1\}}{\sigma_{i,1}^2})P(0)+\exp(\frac{2\mathrm{Re}\{[\hat{s}_i-m_i(1-v_it_i)]^*\cdot v_it_i\alpha_3\}}{\sigma_{i,3}^2})P(1)}{\exp(\frac{2\mathrm{Re}\{[\hat{s}_i-m_i(1-v_it_i)]^*\cdot v_it_i\alpha_2\}}{\sigma_{i,2}^2})P(0)+\exp(\frac{2\mathrm{Re}\{[\hat{s}_i-m_i(1-v_it_i)]^*\cdot v_it_i\alpha_4\}}{\sigma_{i,4}^2})P(1)}.
\end{aligned}
\tag{3.38}
$$

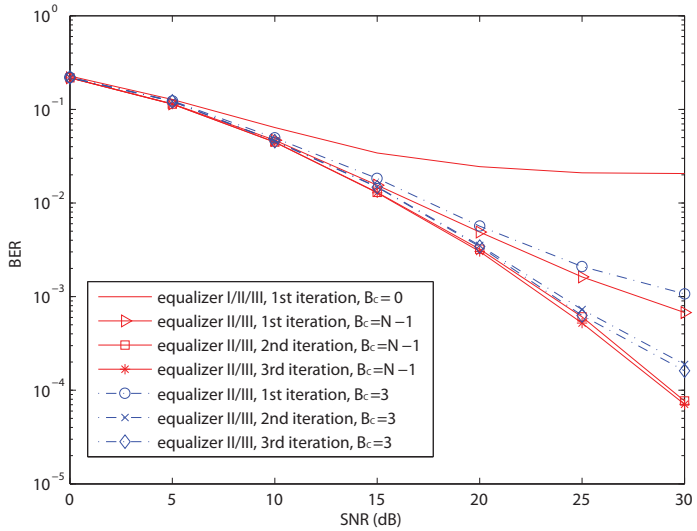

Figure 3.8: BER reference for equalizer II/III, exponential power delay profile.

$$
\begin{aligned}
L_e(s_{i,1}) &= \ln \frac{\exp(\frac{2\mathrm{Re}\{c\alpha_1\}}{\sigma^2_{i,1}})P(0) + \exp(\frac{2\mathrm{Re}\{c\alpha_3\}}{\sigma^2_{i,3}})P(1)}{\exp(\frac{2\mathrm{Re}\{c\alpha_2\}}{\sigma^2_{i,2}})P(0) + \exp(\frac{2\mathrm{Re}\{c\alpha_4\}}{\sigma^2_{i,4}})P(1)} \\
&= \ln \frac{\exp(\frac{\sqrt{2}}{\sigma^2_{i,1}}\mathrm{Re}\{c(1+j)\})P(0) + \exp(\frac{\sqrt{2}}{\sigma^2_{i,3}}\mathrm{Re}\{c(1-j)\})P(1)}{\exp(\frac{\sqrt{2}}{\sigma^2_{i,2}}\mathrm{Re}\{c(-1+j)\})P(0) + \exp(\frac{\sqrt{2}}{\sigma^2_{i,4}}\mathrm{Re}\{c(-1-j)\})P(1)} \\
&= \ln \frac{\exp(\frac{\sqrt{2}}{\sigma^2_{i,1}}[\mathrm{Re}\{c\} - \mathrm{Im}\{c\}])P(0) + \exp(\frac{\sqrt{2}}{\sigma^2_{i,3}}[\mathrm{Re}\{c\} + \mathrm{Im}\{c\}])P(1)}{\exp(\frac{\sqrt{2}}{\sigma^2_{i,2}}[-\mathrm{Re}\{c\} - \mathrm{Im}\{c\}])P(0) + \exp(\frac{\sqrt{2}}{\sigma^2_{i,4}}[-\mathrm{Re}\{c\} + \mathrm{Im}\{c\}])P(1)} \\
&= \ln \frac{\exp(\frac{\sqrt{2}}{\sigma^2_{i,1}}\mathrm{Re}\{c\})[\exp(-\frac{\sqrt{2}}{\sigma^2_{i,1}}\mathrm{Im}\{c\})P(0) + \exp(\frac{\sqrt{2}}{\sigma^2_{i,3}}\mathrm{Im}\{c\})P(1)]}{\exp(-\frac{\sqrt{2}}{\sigma^2_{i,1}}\mathrm{Re}\{c\})[\exp(-\frac{\sqrt{2}}{\sigma^2_{i,2}}\mathrm{Im}\{c\})P(0) + \exp(\frac{\sqrt{2}}{\sigma^2_{i,4}}\mathrm{Im}\{c\})P(1)]} \\
&= \ln[\exp(\frac{2\sqrt{2}}{\sigma^2_{i,1}}\mathrm{Re}\{c\})] \\
&= \frac{2\sqrt{2}}{\sigma^2_{i,1}}\mathrm{Re}\{[\hat{s}_i - m_i(1 - v_i t_i)]^* v_i t_i\} \\
&= \frac{\sqrt{8}\mathrm{Re}(\hat{s}_i - m_i(1 - v_i t_i))}{v_i(1 - v_i t_i)}
\end{aligned}
\tag{3.39}
$$

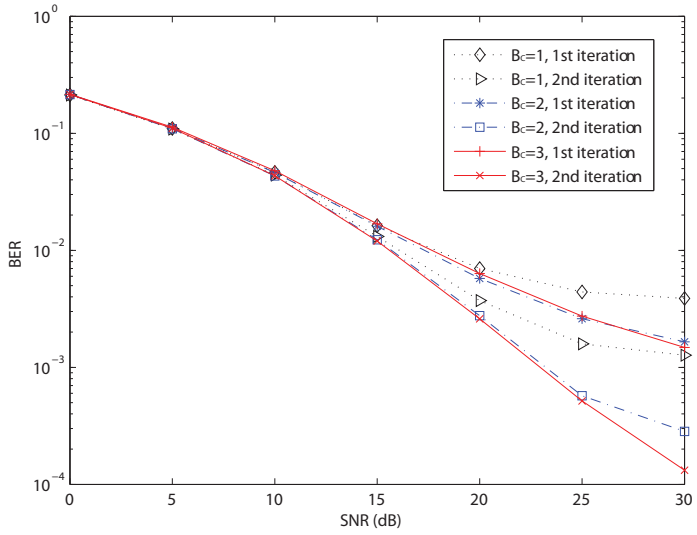

Figure 3.9: BER performance of equalizer II/III for different Q's.

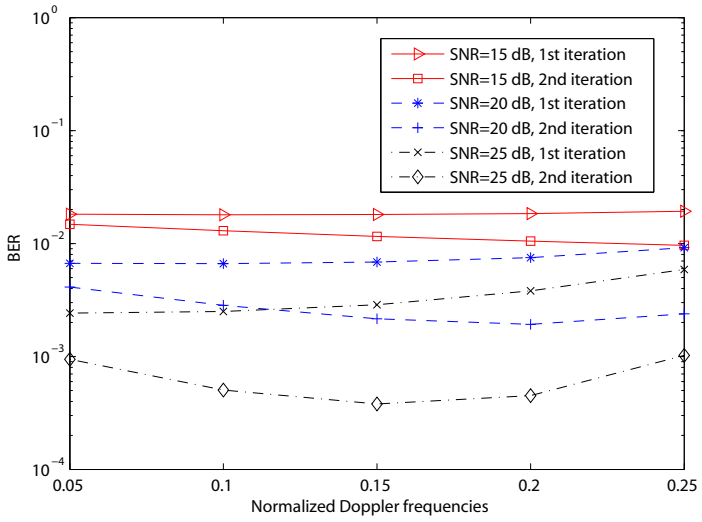

Figure 3.10: BER performance of equalizer II/III for different normalized Doppler frequencies.

Chapter 4

Iterative Channel Estimation

4.1 Introduction

In the previous chapter, the turbo equalization algorithm requires an accurate channel estimation at the receiver. The ICI caused by Doppler spreads makes the channel estimation problem more challenging. Pilot-assisted channel estimation algorithms have been developed to model and estimate time-varying flat fading channels in [48, 49], and doubly-selective channels in [23, 39, 43, 44] using the BEM for OFDM and SC systems. A superimposed training method has been developed in [38]. Besides pilot symbols, soft data estimates can be used to improve the quality of channel estimation, as shown in [24] using recursive least squares (RLS) algorithms.

In this chapter, we present iterative pilot-assisted channel estimators for both OFDM and SC systems. Specifically, in each channel estimation iteration, we also exploit the soft data estimates obtained from the turbo equalizer. These data estimates are used as additional virtual pilots, and their reliability, also obtained from the turbo equalizer, is included in the channel estimation process. As a result, the proposed channel estimators are well matched to the proposed turbo equalizers, since both channel estimation and equalization are performed iteratively, with mutual exchange of soft information. For both OFDM and SC cases, the proposed channel estimators firstly estimate the time-domain channel exploiting the BEM, and then transform the time-domain channel into the frequency-domain for equalization purposes. It should be observed that the pilot-aided BEM channel estimation is a well known method for OFDM in doubly-selective channels, as it has been exploited in [23, 39].

However, differently from [23, 39], we incorporate into our channel estimators the reliability of the estimated data. A similar idea has been used in adaptive channel estimation algorithms, such as [24] which develops an RLS algorithm and [41] which proposes Kalman filtering with an autoregressive model. In addition, to keep low-complexity processing, we simplify our channel estimators by locating the pilot symbols in the same domain as where the data symbols are placed. This means that we assume frequency-domain pilot tones in OFDM systems, and time-domain pilot symbols in SC systems. Although this choice is mainly dictated by computational benefits, it is consistent with known pilot allocation strategies in doubly-selective channels, which suggest time-domain pilots for SC systems [43, 44], and frequency-domain pilots for OFDM systems [43].

Notice that the channel model used in this chapter is the same as that in the previous chapter. Thus, we omit the channel model section here and refer to Section 3.2.

4.2 Iterative Channel Estimation

The turbo equalizers presented in the previous chapter require CSI at the receiver. To acquire the CSI, we propose a modification of a pilot-assisted channel estimator presented in [23] for OFDM. Specifically, we modify the iterative linear MMSE channel estimator of [23] in a such a way that it can operate in a turbo fashion. Therefore, besides the pilot symbols, we also use the soft data estimates originating from the turbo equalizer and the decoder. Indeed, after the first iteration, the soft data symbol estimates can be used as auxiliary pilot symbols, in order to improve the quality of the subsequent channel estimates [42]. For both OFDM and SC systems, our channel estimators produce an estimate $\hat{\mathbf{H}}_t$ of the time-domain channel matrix $\mathbf{H}_t$, and then translate $\hat{\mathbf{H}}_t$ into the frequency-domain banded matrix estimate $\hat{\mathbf{H}}$. The channel estimators are assumed to have perfect knowledge of the channel statistics, i.e., the Doppler spectrum and the power-delay profile. We highlight that the channel estimators considered in this chapter are non-adaptive, that is, the CSI is newly estimated in each transmitted block, using both pilots and data. This way, severe time variation can be handled.

In pilot-assisted transmissions, there exist various approaches to design the pilot pattern. We can distinguish between two broad categories: multiplexed training and superimposed training [38]. In the multiplexed training

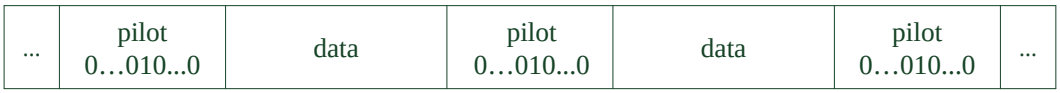

Figure 4.1: Pilot structure.

case, each element of the transmitted vector contains either a pilot symbol or a data symbol, while in the superimposed case both pilot and data symbols are located in the same positions, typically distributed over the whole transmitted vector. In this chapter, we assume multiplexed training, which is also known as periodic training when the pilots are placed in the time domain, or as orthogonal training when the pilots are located in the frequency domain. In particular, we focus on the pilot placement schemes developed in [43,44], which have been proved to be optimal in the MMSE sense under certain channel conditions. In these schemes, pilot symbols are interleaved with the data symbols to form the transmitted signal vector. For OFDM systems, we employ the frequency-domain Kronecker delta (FDKD) pilot structure [43], while, its dual scheme [44], identified as time-domain Kronecker delta (TDKD), is adopted for SC systems, as shown in Fig. 4.1. In both cases, the pilot symbols are grouped into equidistant clusters, each having the same length. Within each cluster, a unique non-zero pilot symbol is located in the middle of the cluster, while null pilot symbols are placed on both sides. Therefore, the FDKD scheme coincides with equispaced pilot tones with guard frequency bands, while the TDKD scheme uses periodic training with guard time intervals.

Suppose that there are M pilot clusters, each containing L_p (odd) pilots, denoted by the vector $\mathbf{s}_m^p$ of size L_p, for $m = 0, \ldots, M-1$. These vectors are interleaved with the data clusters $\mathbf{s}_m^d$, $m = 0, \ldots, M$, to form the transmitted vector $\mathbf{s}$, as expressed by

$$\mathbf{s} = [(\mathbf{s}_0^d)^T, (\mathbf{s}_0^p)^T, \ldots, (\mathbf{s}_{M-1}^d)^T, (\mathbf{s}_{M-1}^p)^T, (\mathbf{s}_M^d)^T]^T. \tag{4.1}$$

Therefore, by denoting with n_m the starting position of the mth pilot cluster, the mth pilot vector contains the elements of $\mathbf{s}$ with index starting from n_m up to $n_m + L_p - 1$. We also define the aggregate pilot vector and the aggregate data vector as

$$\begin{aligned} \mathbf{s}^p &= [(\mathbf{s}_0^p)^T, \ldots, (\mathbf{s}_{M-1}^p)^T]^T, \\ \mathbf{s}^d &= [(\mathbf{s}_0^d)^T, \ldots, (\mathbf{s}_M^d)^T]^T, \end{aligned} \tag{4.2}$$

respectively, with size ML_p and $N - ML_p$, respectively.

In addition, we define $h_{n,l}^t$ as the lth channel tap at the nth time instant, where $h_{n,l}^t = 0$ for $l < 0$ or $l > L$, since the maximal channel order is equal to the CP length, both denoted by L. Thus the elements of $\mathbf{H}_t$ can be expressed as $[\mathbf{H}_t]_{p,q} = h_{L+p,(p-q) \bmod N}^t$,

$$\mathbf{H}_t = \begin{pmatrix} h_{L,0}^t & & 0 & h_{L,L}^t & \cdots & h_{L,1}^t \\ \vdots & \ddots & & & \ddots & \vdots \\ h_{2L-1,L-1}^t & & \ddots & \ddots & & h_{2L-1,L}^t \\ & \ddots & & \ddots & \ddots & \\ 0 & & \ddots & & \ddots & 0 \\ & & & h_{N+L-1,L}^t & \cdots & h_{N+L-1,0}^t \end{pmatrix}, \tag{4.3}$$

which means that our channel estimation problem has $N(L+1)$ unknowns. However, these unknowns are correlated in the time domain. The BEM can be used to reduce the number of unknowns from $N(L+1)$ to $(2Q+1)(L+1)$, where $2Q+1$ is the number of basis functions [23]. By stacking all the channel taps within the block in a single $N(L+1) \times 1$ vector $\mathbf{h}_t$,

$$\mathbf{h}_t = [h_{L+1,0}^t, \ldots, h_{L+1,L}^t, \ldots, h_{L+N,0}^t, \ldots, h_{L+N,L}^t]^T, \tag{4.4}$$

the BEM permits to express this vector as

$$\mathbf{h}_t = (\mathbf{B} \otimes \mathbf{I}_{L+1})\mathbf{h}, \tag{4.5}$$

where $\mathbf{B} = [\mathbf{b}_{-Q}, \ldots, \mathbf{b}_Q]$ is an $N \times (2Q+1)$ matrix that has $2Q+1$ orthonormal basis functions $\mathbf{b}_q$ as columns, and $\mathbf{h}$ is a $(2Q+1)(L+1)$ vector that collects all the BEM coefficients of all the channel taps.

In order to derive our MMSE channel estimator, the following assumptions are made.

Assumption 1

The wireless channel can be regarded as a wide-sense stationary uncorrelated scattering (WSSUS) process, which has the following statistics

$$\mathrm{E}(h_{n,l}^t h_{n-n',l-l'}^t) = \sigma_l^2 \delta_{l'} \gamma_{n'}, \tag{4.6}$$

where σ_l^2 denotes the variance of the lth channel tap, γ_t is the normalized time correlation, and δ_n stands for the Kronecker delta function.

Assumption 2

The data symbols in $\mathbf{s}^d$ are assumed to be uncorrelated with zero mean and variance σ_s^2. The noise at the receiver is assumed to be uncorrelated with the transmitted symbols.

$$\begin{aligned} \mathrm{E}(\mathbf{s}^d(\mathbf{s}^d)^H) &= \sigma_s^2 \mathbf{I}_{N-ML_p}, \\ \mathrm{E}(\mathbf{s}\mathbf{n}_t^H) &= \mathbf{0}. \end{aligned} \tag{4.7}$$

Assumption 3

The BEM coefficients $\mathbf{h}$ are assumed to be uncorrelated with the transmitted signal $\mathbf{s}$ and the noise, respectively.

$$\begin{aligned} \mathrm{E}(\mathbf{h}\mathbf{s}^H) &= \mathbf{0}, \\ \mathrm{E}(\mathbf{h}\mathbf{n}_t^H) &= \mathbf{0}. \end{aligned} \tag{4.8}$$

Assumption 4

The covariance matrix of the BEM coefficients is assumed known to the receiver, and it is calculated as [23]

$$\mathbf{R}_{\mathbf{h}} = \mathrm{E}(\mathbf{h}\mathbf{h}^H) = \mathbf{R}_{\mathbf{h},l} \otimes \mathrm{diag}(\sigma_0^2, \ldots, \sigma_L^2), \tag{4.9}$$

where $\mathbf{R}_{\mathbf{h},l} = \mathrm{E}(\mathbf{h}_l \mathbf{h}_l^H) = \mathbf{B}^\dagger \mathbf{R}_{\mathbf{h},l}^{\{t\}} \mathbf{B}^{\dagger H}$, with $\mathbf{h}_l = [h_{-Q,l}, \ldots, h_{Q,l}]^T$ and $[\mathbf{R}_{\mathbf{h},l}^{\{t\}}]_{p,q} = \mathrm{E}(h_{p,l}^t (h_{q,l}^t)^*)$.

Assumption 5

The average power of the pilot symbols is the same as that of the data symbols

$$\sigma_s^2 = (\mathbf{s}^p)^H \mathbf{s}^p / (ML_p) \tag{4.10}$$

4.2.1 Iterative Channel Estimation for OFDM Systems

For OFDM systems, the pilot and data symbols are interleaved in the frequency domain. Since the frequency-domain channel matrix is only approximately

banded, the received samples used for channel estimation are always contaminated by ICI, independently of the length of the null guard bands inserted. To be precise, the frequency-domain channel matrix is (with high probability) a full matrix, and hence the power of the pilot symbols is spread over all the received samples. While a time-domain receiver window can reduce the ICI to get a better equalization performance, it is still unknown whether the same window can improve the channel estimation quality or not. Thus, to estimate the time-domain channel matrix $\mathbf{H}_t$, we use the frequency-domain received signal *without* applying the time-domain receiver window.

By substituting (4.5) in (3.8), we can rewrite (3.8) as

$$\begin{aligned}\mathbf{y}_f &= \mathbf{F}\mathbf{H}_t\mathbf{F}^H\mathbf{s} + \mathbf{F}\mathbf{n}_t \\ &= \mathbf{F}(\sum_{q=-Q}^{Q} \mathrm{diag}\{\mathbf{b}_q\}\mathbf{H}_{t,q})\mathbf{F}^H\mathbf{s} + \mathbf{n}_f \\ &= \sum_{q=-Q}^{Q} (\mathbf{F}\mathrm{diag}\{\mathbf{b}_q\}\mathbf{F}^H)(\mathbf{F}\mathbf{H}_{t,q}\mathbf{F}^H) + \mathbf{n}_f \\ &= \sum_{q=-Q}^{Q} \mathbf{D}_q\mathbf{\Delta}_q\mathbf{s} + \mathbf{n}_f,\end{aligned} \tag{4.11}$$

where $\mathbf{D}_q = \mathbf{F}\mathrm{diag}\{\mathbf{b}_q\}\mathbf{F}^H$, $\mathbf{\Delta}_q = \mathrm{diag}\{\mathbf{F}_L[h_{q,0}, \ldots, h_{q,L}]^T\}$, $\mathbf{F}_L$ represents the first $L+1$ columns of the matrix $\sqrt{N}\mathbf{F}$, and $\mathbf{H}_{t,q}$ is a circulant matrix which can be expressed as

$$\mathbf{H}_{t,q} = \begin{pmatrix} h_{q,0} & & & h_{q,L} & \cdots & h_{q,1} \\ \vdots & \ddots & & & \ddots & \vdots \\ h_{q,L} & & \ddots & & & h_{q,L} \\ & \ddots & & \ddots & & \\ & & \ddots & & \ddots & \\ & & & h_{q,L} & \cdots & h_{q,0} \end{pmatrix}, \tag{4.12}$$

where we use the result that $\mathbf{F}\mathbf{H}_{t,q}\mathbf{F}^H$ is a diagonal matrix, with the diagonal elements being the Fourier transform of the first column of $\mathbf{H}_{t,q}$.

It is noteworthy that, for channel estimation purposes, it is not necessary to process all the received samples. Indeed, similarly to [23], the computational complexity of the channel estimator can be highly reduced by extracting a

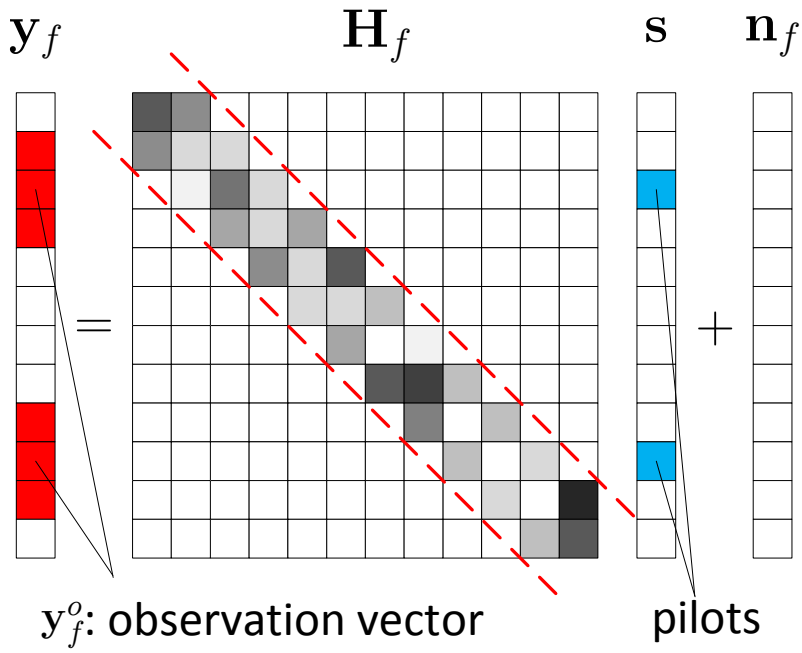

Figure 4.2: Reduced size received vector for channel estimation.

subvector of $\mathbf{y}_f$ before channel estimation. Obviously, this subvector should contain the relevant information given by the pilot symbols as shown in Fig. 4.2. Therefore, with reference to the mth pilot cluster $\mathbf{s}_m^p$, we consider the following observation subvector

$$\mathbf{y}_{f,m} = [[\mathbf{y}_f]_{n_m-\Delta}, \ldots, [\mathbf{y}_f]_{n_m+L_p-1+\Delta}]^T, \tag{4.13}$$

where Δ is a smoothing parameter used to control the amount of interference taken into account for channel estimation. Please observe that Δ can be positive as well as negative, or zero: When Δ is positive, the channel estimator is actually enlarging the observation window, which in this case monitors also 2Δ data symbol locations, i.e., the positions closest to the pilot symbols. The received signal in (4.13) can also be expressed as

$$\mathbf{y}_{f,m} = \sum_{q=-Q}^{Q} \mathbf{D}_{q,m}\boldsymbol{\Delta}_q\mathbf{m} + \sum_{q=-Q}^{Q} \mathbf{D}_{q,m}\boldsymbol{\Delta}_q(\mathbf{s}-\mathbf{m}) + \mathbf{n}_{f,m}, \tag{4.14}$$

where $\mathbf{D}_{q,m}$ is an $(L_p + 2\Delta) \times N$ matrix consisting of the $L_p + 2\Delta$ rows of $\mathbf{D}_q$ with indices from $n_m - \Delta$ to $n_m + L_p - 1 + \Delta$, and $\mathbf{m} = \mathrm{E}(\mathbf{s})$. It can be observed that the received signal $\mathbf{y}_{f,m}$ contains information from both pilot

and data symbols if Δ is positive. Thus, the pilot symbols, as well as the soft data estimates $\mathbf{m}$, are used to estimate the CSI, which could help to achieve a better performance than [23], which uses the pilot symbols only. The second term in (4.14) reflects the uncertainty of the soft data estimates and can be regarded as interference, whose covariance can be taken into account into the channel estimator.

After some tedious manipulations, we can rewrite (4.14) as a function of $\mathbf{h}$ as

$$\begin{aligned}\mathbf{y}_{f,m} &= \mathbf{D}_m \left\{\mathbf{I}_{2Q+1} \otimes [\mathrm{diag}(\mathbf{m})\mathbf{F}_{\mathrm{L}}]\right\} \mathbf{h} \\ &\quad + \mathbf{D}_m \left\{\mathbf{I}_{2Q+1} \otimes [\mathrm{diag}(\mathbf{s}-\mathbf{m})\mathbf{F}_{\mathrm{L}}]\right\} \mathbf{h} + \mathbf{n}_{f,m} \\ &= \mathbf{P}_m \mathbf{h} + \mathbf{d}_{f,m} + \mathbf{n}_{f,m},\end{aligned} \tag{4.15}$$

where

$$\begin{aligned}\mathbf{D}_m &= [\mathbf{D}_{-Q,m}, \ldots, \mathbf{D}_{Q,m}], \\ \mathbf{P}_m &= \mathbf{D}_m \left\{\mathbf{I}_{2Q+1} \otimes [\mathrm{diag}(\mathbf{m})\mathbf{F}_{\mathrm{L}}]\right\}, \\ \mathbf{d}_{f,m} &= \mathbf{D}_m \left\{\mathbf{I}_{2Q+1} \otimes [\mathrm{diag}(\mathbf{s}-\mathbf{m})\mathbf{F}_{\mathrm{L}}]\right\} \mathbf{h}.\end{aligned}$$

Although $\mathbf{d}_{f,m}$ also contains information from the channel coefficients $\mathbf{h}$, we will regard it as interference later, as $(\mathbf{s}-\mathbf{m})$ measures the symbol estimation uncertainty. Stacking the M observation clusters together, we obtain the reduced-size frequency-domain received signal expressed by

$$\begin{aligned}\mathbf{y}_f^o &= \mathbf{D}^o \left\{\mathbf{I}_{2Q+1} \otimes [\mathrm{diag}(\mathbf{m})\mathbf{F}_{\mathrm{L}}]\right\} \mathbf{h} \\ &\quad + \mathbf{D}^o \left\{\mathbf{I}_{2Q+1} \otimes [\mathrm{diag}(\mathbf{s}-\mathbf{m})\mathbf{F}_{\mathrm{L}}]\right\} \mathbf{h} + \mathbf{n}_f^o \\ &= \mathbf{P}^o \mathbf{h} + \mathbf{d}_f^o + \mathbf{n}_f^o,\end{aligned} \tag{4.16}$$

where

$$\begin{aligned}\mathbf{y}_f^o &= [\mathbf{y}_{f,0}^T, \ldots, \mathbf{y}_{f,M-1}^T]^T, \\ \mathbf{d}_f^o &= [\mathbf{d}_{f,0}^T, \ldots, \mathbf{d}_{f,M-1}^T]^T, \\ \mathbf{n}_f^o &= [\mathbf{n}_{f,0}^T, \ldots, \mathbf{n}_{f,M-1}^T]^T,\end{aligned}$$

are vectors of size $M(L_p + 2\Delta)$, and

$$\begin{aligned}\mathbf{D}^o &= [\mathbf{D}_0^T, \ldots, \mathbf{D}_{M-1}^T]^T, \\ \mathbf{P}^o &= \mathbf{D}^o \left\{\mathbf{I}_{2Q+1} \otimes [\mathrm{diag}(\mathbf{m})\mathbf{F}_{\mathrm{L}}]\right\}.\end{aligned}$$

As a result of (4.16), the linear MMSE estimation of the BEM channel coefficients can be expressed by (2.24)

$$\hat{\mathbf{h}} = \mathbf{R}_{\mathbf{h}}\mathbf{P}^{oH}(\mathbf{P}^{o}\mathbf{R}_{\mathbf{h}}\mathbf{P}^{oH} + \mathbf{R}_{\mathbf{d}_f^o} + \mathbf{R}_{\mathbf{n}_f^o})^{-1}\mathbf{y}_f^o, \tag{4.17}$$

where $\mathbf{R}_{\mathbf{d}_f^o} = \mathrm{E}(\mathbf{d}_f^o\mathbf{d}_f^{oH})$, and $\mathbf{R}_{\mathbf{n}_f^o} = \mathrm{E}(\mathbf{n}_f^o\mathbf{n}_f^{oH})$. We can express $\mathbf{R}_{\mathbf{d}_f^o}$ as

$$\mathbf{R}_{\mathbf{d}_f^o} = \mathbf{D}^{o}\mathbf{R}_x\mathbf{D}^{oH}, \tag{4.18}$$

where

$$\begin{aligned}\mathbf{R}_x =&\{\mathbf{I}_{2Q+1} \otimes [\mathrm{diag}(\mathbf{s}-\mathbf{m})\mathbf{F}_L]\}\mathbf{R}_{\mathbf{h}}\{\mathbf{I}_{2Q+1} \otimes [\mathrm{diag}(\mathbf{s}-\mathbf{m})\mathbf{F}_L]^H\}\\ =&[\mathbf{I}_{2Q+1} \otimes \mathrm{diag}(\mathbf{s}-\mathbf{m})]\{(\mathbf{I}_{2Q+1} \otimes \mathbf{F}_L)\mathbf{R}_{\mathbf{h}}(\mathbf{I}_{2Q+1} \otimes \mathbf{F}_L)^H\}[\mathbf{I}_{2Q+1} \otimes \mathrm{diag}(\mathbf{s}-\mathbf{m})^H]\\ =&[\mathbf{I}_{2Q+1} \otimes \mathrm{diag}(\mathbf{s}-\mathbf{m})]\mathbf{X}[\mathbf{I}_{2Q+1} \otimes \mathrm{diag}(\mathbf{s}-\mathbf{m})^H],\end{aligned} \tag{4.19}$$

where $\mathbf{X} = (\mathbf{I}_{2Q+1} \otimes \mathbf{F}_L)\mathbf{R}_{\mathbf{h}}(\mathbf{I}_{2Q+1} \otimes \mathbf{F}_L)^H$, which can be further simplified using the assumptions in (4.7)-(4.9) as

$$[\mathbf{R}_x]_{m,n}\begin{cases} v_{m \bmod N}[\mathbf{X}]_{m,n} & \text{if } (m-n)\bmod N = 0,\\ 0 & \text{otherwise.}\end{cases} \tag{4.20}$$

After the estimation of the BEM coefficients in $\hat{\mathbf{h}}$, the time-domain channel vector can be reconstructed by (4.5) as $\hat{\mathbf{h}}_t = (\mathbf{B}\otimes\mathbf{I}_{L+1})\hat{\mathbf{h}}$, whose elements form the estimated time-domain channel matrix $\hat{\mathbf{H}}_t$.

In [23], it has been shown that the BEM-based LMMSE channel estimator can achieve a better performance by using a larger number of observation samples, i.e., when all elements of $\mathbf{y}_f$ are included in the observation vector $\mathbf{y}_f^o$. Obviously, the same behavior is expected in our case: Indeed, our channel estimator additionally includes the reliability of the turbo equalized data symbols by the symbol estimation uncertainty term $(\mathbf{s}-\mathbf{m})$ in $\mathbf{d}_f^o$, and $\mathbf{d}_f^o$ is modeled as extra interference other than noise in the MMSE channel estimator. Hence additional benefit should be obtained by including more data locations into the observation window. However, the main complexity of our channel estimator comes from the matrix inverse in (4.17), which requires the observation vector length to be small. Thus, the observation parameter Δ allows for a trade-off between channel estimation complexity and performance.

4.2.2 Iterative Channel Estimation for SC Systems

Unlike OFDM systems, where the pilots are inserted in the frequency domain, and the frequency-domain channel matrix is only approximately banded, in SC systems the pilots are positioned in the time domain, and the time-domain channel matrix is strictly banded, due to the FIR channel assumption. Therefore, using sufficiently long guard intervals, the ISI between pilots and data is completely eliminated [44], thereby simplifying the channel estimation procedure.

Due to the strictly-banded structure of the time-domain channel matrix, when the guard intervals are large enough, the mth pilot cluster only contributes to the time-domain received signal $[[\mathbf{y}_t]_{n_m}, \ldots, [\mathbf{y}_t]_{n_m+L_p-1+L}]^T$. Similarly to the OFDM case, we consider the mth observation vector

$$\mathbf{y}_{t,m} = [[\mathbf{y}_t]_{n_m-\Delta}, \ldots, [\mathbf{y}_t]_{n_m+L_p-1+L+\Delta}]^T, \tag{4.21}$$

where the smoothing parameter Δ is defined as in (4.13), but now operates in the time domain. Using the expressions (4.3) and (4.5), we can rewrite the time-domain received signal (3.1) as [23]

$$\begin{aligned}\mathbf{y}_{t,m} =& \mathbf{H}_{t,m}\mathbf{m} + \mathbf{H}_{t,m}(\mathbf{s}-\mathbf{m}) + \mathbf{n}_{t,m} \\ =& \sum_{q=-Q}^{Q} \mathrm{diag}\{\mathbf{b}_{q,m}\}\mathbf{C}_{q,m}\mathbf{m} + \sum_{q=-Q}^{Q} \mathrm{diag}\{\mathbf{b}_{q,m}\}\mathbf{C}_{q,m}(\mathbf{s}-\mathbf{m}) + \mathbf{n}_{t,m} \\ =& \mathbf{P}_m\mathbf{h} + \mathbf{d}_{t,m} + \mathbf{n}_{t,m},\end{aligned} \tag{4.22}$$

where $\mathbf{H}_{t,m}$ consists of the corresponding rows of $\mathbf{H}_t$, with indices from $n_m - \Delta$ to $n_m + L_p - 1 + L + \Delta$, $\mathbf{b}_{q,m} = [[\mathbf{b}_q]_{n_m-\Delta}, \ldots, [\mathbf{b}_q]_{n_m+L_p-1+L+\Delta}]^T$, $\mathbf{C}_{q,m}$ is an $(L_p + L + 2\Delta) \times N$ Toeplitz matrix defined as in (4.23),

$$\mathbf{C}_{q,m} = \begin{pmatrix} \mathbf{0}_{1\times(n_m-L-1)} & h_{q,L} & \cdots & h_{q,0} & & \mathbf{0}_{1\times(N-n_m)} \\ \vdots & & \ddots & & \ddots & \vdots \\ \mathbf{0}_{1\times(n_m+L_p+\Delta-2)} & & & h_{q,L} & \cdots & h_{q,0} \quad \mathbf{0}_{1\times[(N-(n_m+L_p-1+L+\Delta)]} \end{pmatrix}, \tag{4.23}$$

and $\mathbf{P}_m = \mathbf{Z}_m \mathbf{U}_m$, where

$$\begin{aligned} \mathbf{Z}_m &= [\mathrm{diag}(\mathbf{b}_{-Q,m}), \ldots, \mathrm{diag}(\mathbf{b}_{Q,m})], \\ \mathbf{U}_m &= \mathbf{I}_{2Q+1} \otimes \mathbf{T}_m, \\ \mathbf{T}_m &= \begin{pmatrix} m_{n_m-\Delta} & \cdots & m_{n_m-L-\Delta} \\ \vdots & \ddots & \vdots \\ m_{n_m+L_p-1+L+\Delta} & \cdots & m_{n_m+L_p-1+\Delta} \end{pmatrix}. \end{aligned} \tag{4.24}$$

The covariance matrix of the interference term $\mathbf{R}_{\mathbf{d}_{t,m}}$ can be calculated using assumptions 1 and 2 as

$$\begin{aligned} \mathbf{R}_{\mathbf{d}_{t,m}} &= \mathrm{E}(\mathbf{d}_{t,m}\mathbf{d}_{t,m}^H) \\ &= \mathrm{E}[\mathbf{H}_{t,m}(\mathbf{s}-\mathbf{m})(\mathbf{s}-\mathbf{m})^H \mathbf{H}_{t,m}^H] \\ &= \mathrm{diag}(\sum_{i=0}^{L} v_{n_m-\Delta+i}^2 \sigma_{L-i}^2, \ldots, \sum_{i=0}^{L} v_{n_m+\Delta+L+L_p-1+i}^2 \sigma_{L-i}^2), \end{aligned} \tag{4.25}$$

where v_i is the variance of the symbol s_i. Stacking the M observation clusters together, we get the reduced-size time-domain received signal

$$\mathbf{y}_t^o = \mathbf{P}^o \mathbf{h} + \mathbf{d}_t^o + \mathbf{n}_t^o, \tag{4.26}$$

where $\mathbf{P}^o = \mathbf{Z}\mathbf{U}$, with

$$\begin{aligned} \mathbf{Z} &= \mathrm{diag}[\mathbf{Z}_0, \ldots, \mathbf{Z}_{M-1}], \\ \mathbf{U} &= [\mathbf{U}_0^T, \ldots, \mathbf{U}_{M-1}^T], \end{aligned}$$

and $\mathbf{d}_t^o$ and $\mathbf{n}_t^o$ are the stacking vectors of $\{\mathbf{d}_{t,m}\}_{m=0}^{M-1}$ and $\{\mathbf{n}_{t,m}\}_{m=0}^{M-1}$, respectively.

Like in the OFDM case, the linear MMSE estimate of the BEM channel coefficients can be derived as

$$\hat{\mathbf{h}} = \mathbf{R}_{\mathbf{h}} \mathbf{P}^{oH} (\mathbf{P}^o \mathbf{R}_{\mathbf{h}} \mathbf{P}^{oH} + \mathbf{R}_{\mathbf{d}_t^o} + \mathbf{R}_{\mathbf{n}_t^o})^{-1} \mathbf{y}_t^o, \tag{4.27}$$

where $\mathbf{R}_{\mathbf{d}_t^o} = \mathrm{E}(\mathbf{d}_t^o \mathbf{d}_t^{oH})$ and $\mathbf{R}_{\mathbf{n}_t^o} = \mathrm{E}(\mathbf{n}_t^o \mathbf{n}_t^{oH})$ are similarly defined as in (4.17), and $\mathbf{R}_{\mathbf{d}_t^o} = \mathrm{diag}(\mathbf{R}_{\mathbf{d}_{t,0}}, \ldots, \mathbf{R}_{\mathbf{d}_{t,M-1}})$. It is easy to understand that, also in this case, a better performance is achieved by including a larger number of observation samples [23], i.e., by increasing the smoothing parameter Δ, at the price of increased complexity. Different from the equalization, where a low complexity algorithm can be derived, the channel estimation process needs to invert a $M(L_p + L + 2\Delta) \times M(L_p + L + 2\Delta)$ matrix, which has a $\mathcal{O}([M(L_p + L + 2\Delta)]^3)$ complexity.

4.3 Simulation Results

In this section, the proposed algorithms are examined and compared by simulations. We consider a block transmission system with block length $N = 256$. The maximum channel delay spread and the CP length are equal to $L = 7$. The channel is assumed to be Rayleigh distributed with uniform $\mathrm{E}\{|h_{n,l}^t|^2\} = 1/L$ power delay profile, and with Jakes' Doppler spectrum [46]. We consider a high-mobility case where the normalized Doppler frequency is $f_d T = 0.15/N$ with f_d the absolute Doppler frequency shift and T the symbol period. It can be interpreted as $f_d/\Delta f = 0.15$ with Δf the subcarrier spacing in OFDM systems. The time-domain receiver window of [11], as well as the banded equalizers, are designed for a matrix bandwidth parameter $B_c = 3$. A rate 1/2 convolutional code with generator polynomials [5,7] (in octal notation) and codeword length of 16384 is used. We employ random interleaving. The channel decoder in Fig. 3.1 employs a linear approximation to the log-MAP decoding algorithm.

Fig. 4.3 shows the BER performance of the proposed iterative block equalization algorithm for OFDM systems, as a function of the signal-to-noise ratio (SNR), which is defined as $\frac{1}{\sigma_n^2}$. We insert 10 frequency-domain pilot symbols, grouped into $M = 10$ clusters, which means $L_p = 1$, i.e., there are no guard bands around the non-zero pilot in each cluster. Therefore, the efficiency is $\eta = (N - ML_p)/(N + L)$=0.94. We use the generalized complex-exponential BEM with $Q = 2$ to model the time-varying channel [23]. The observation length parameter is set to $\Delta = 2$, which leads to a total observation length of $M(L_p + 2\Delta) = 50$ for each block. It is clear that most of the performance gain is obtained when passing from one iteration, which represents the non-iterative equalizer, to two iterations. In addition, it is relevant that the performance gain obtained by iterative equalization with respect to the non-iterative equalizer is higher in case of estimated CSI: For instance, at BER=10^{-3}, the performance gain is about 3 dB. The performance gain with respect to non-iterative approaches is confirmed by Fig. 4.4, which displays the normalized mean square error NMSE = $E\{||\mathbf{h}_t - (\mathbf{B} \otimes \mathbf{I}_{L+1})\hat{\mathbf{h}}||^2/N\}$ of the MMSE channel estimator. Notably, the first iteration of our channel estimator coincides with the LMMSE channel estimator of [23].

Fig. 4.5 shows the BER performance comparison for the SC systems with perfect CSI. It can be seen that the time-domain receiver windowing can improve the BER performance over the system without windowing [50] under doubly-selective channels. With time-domain receiver windowing, the BER

performances of the average approximation of $\bar{v}_i = \frac{1}{N}(\sum_{k=1}^{N} v_k - v_i)$ and the maximum approximation of $\bar{v}_i = \max\{v_i\}, i = 1, \ldots, N$ in (3.36) are almost the same after three iterations.

Fig. 4.6 illustrates the BER performance of the proposed iterative frequency-domain block turbo equalizer for SC systems with average approximation of $\bar{v}_i = \frac{1}{N}(\sum_{k=1}^{N} v_k - v_i)$, with both perfect and estimated CSI. We employ 60 time-domain pilot symbols, grouped into $M = 4$ clusters, which means $L_p = 15$ and there are $(L_p - 1)/2 = 7$ guard time symbols on each side of the non-zero pilot in each cluster. In this case, the efficiency is $\eta = (N - ML_p)/(N + L)$=0.75. To model the time-varying channel, we use the generalized complex-exponential BEM with $Q = 1$. The observation length parameter is set to $\Delta = -7$, which means we do not include all the received signals containing pilot information, and it leads to a total observation length of $M(L_p + L + 2\Delta) = 32$ for each block. It is shown that our block turbo equalizer achieves about 1-dB gain with respect to the first iteration, which corresponds to the output of a non-iterative equalizer. After two iterations, however, the BER improvement is small. Fig. 4.7 plots the NMSE of the MMSE channel estimator. In this SC case, the channel estimation performance does not improve with more iterations, since the length of the time-domain guard intervals are equal to the channel length, so that the ISI from data symbols is completely eliminated. Note that, differently, in OFDM systems we have not used any guard bands around the non-zero pilot tone. The reason is that in OFDM systems, the ICI power has a rapid decay. On the contrary, the considered channel, whose power-delay profile is uniform, generates significant ISI. Thus, the iterative process is not capable of suppressing such large interference, and large guard intervals are needed to accurately estimate the CSI.

It is interesting to compare the SC and OFDM systems in doubly-selective channels. Previous work has shown some performance comparisons for frequency-selective channels [33, 45]. We first consider uncoded systems. For a wireless channel with significant multipath, OFDM systems cannot exploit frequency diversity, since each data symbol is placed on a single frequency, while SC systems can achieve frequency diversity by spreading each data symbol over many frequencies. In a fast time-varying channel, a high Doppler spread gives time diversity. However, SC systems do not exploit the time diversity, because each data symbol is placed on a single time period, whereas OFDM exploits the time diversity, since it precodes the symbols (by the IDFT) so that each data symbol is spread over the whole OFDM block period. Applying channel coding over OFDM subcarriers offers some frequency diversity, and coding

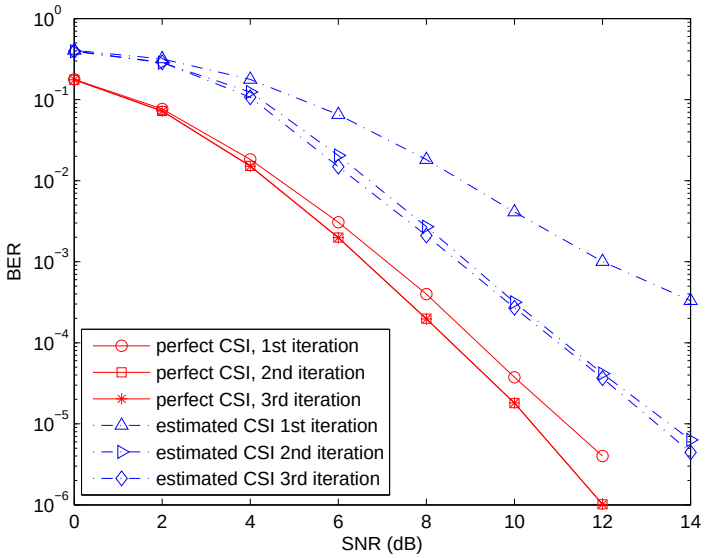

Figure 4.3: BER performance of OFDM systems.

over many OFDM blocks can gain additional time diversity. Similarly, SC system can obtain time diversity by channel coding. Fig. 4.8 and 4.9 illustrate the BER performance comparisons for SC and OFDM systems with different Doppler spreads and different channel lengths, respectively. The BER curves are for the turbo equalizers with perfect CSI after three iterations. The bandwidth parameter $B_c = 3$ is the same for both SC and OFDM systems. It can be shown that, as the values of Doppler spread and channel length increase, a lower BER can be achieved at high SNR. The simulation results confirm that both SC and OFDM systems benefit from channel coding, by obtaining delay and Doppler diversity, respectively, which is not fully exploited in the uncoded case. However, the achievable diversity gain is difficult to analyze, since the band approximation error impairs the performance at high SNR, and the amount of diversity also depends on the specific error correction code used [33, 45].

4.4 Summary

We have proposed Linear MMSE pilot-assisted channel estimators, where the soft data estimates from the turbo equalizers are used to improve the quality

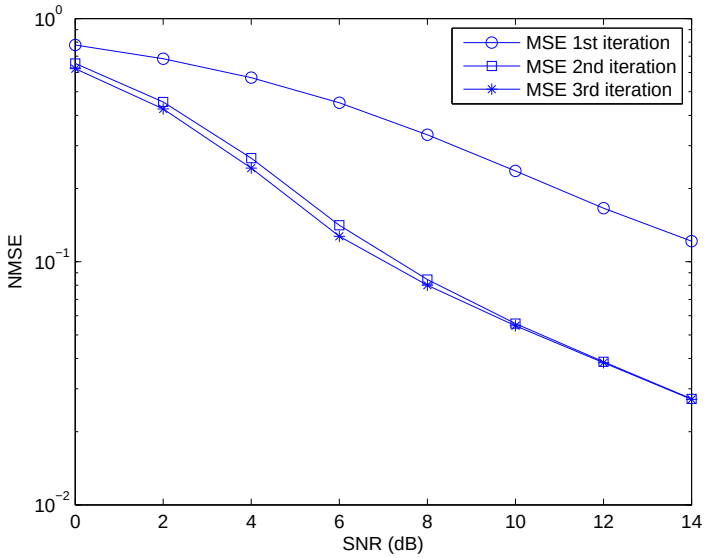

Figure 4.4: Channel estimation performance of OFDM systems.

of the channel estimates. Combined with error correction coding, both OFDM and SC systems can effectively exploit the delay-Doppler diversity provided by doubly-selective channels.

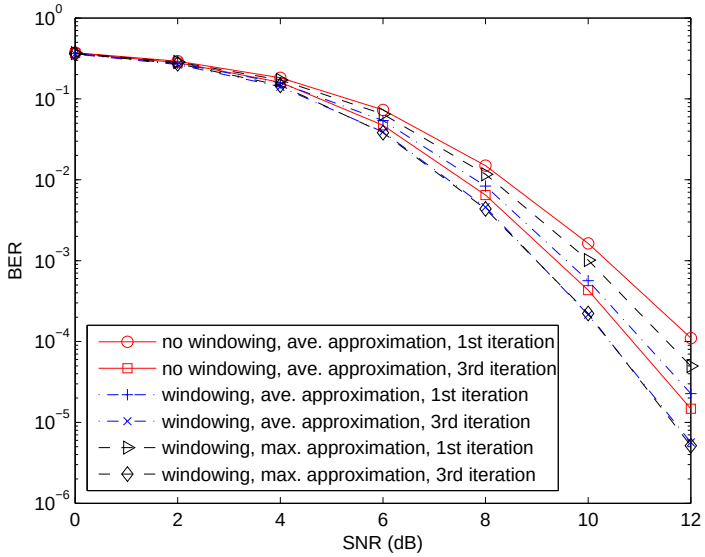

Figure 4.5: BER performance comparison of different equalization approaches for SC systems.

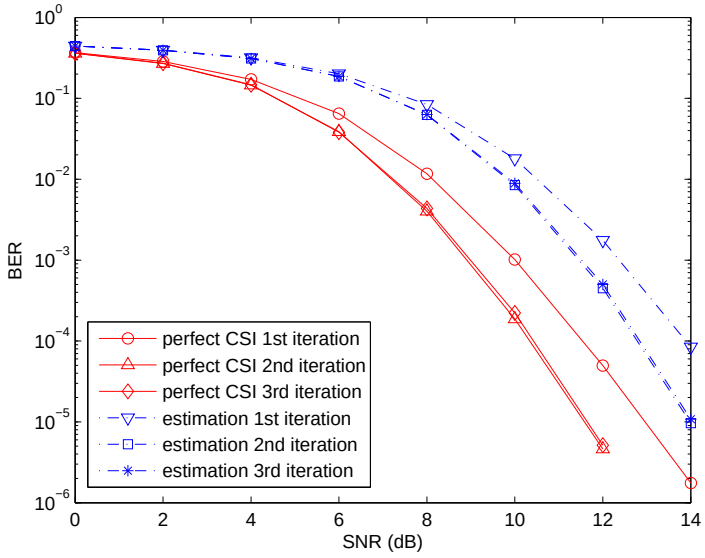

Figure 4.6: BER performance of SC systems.

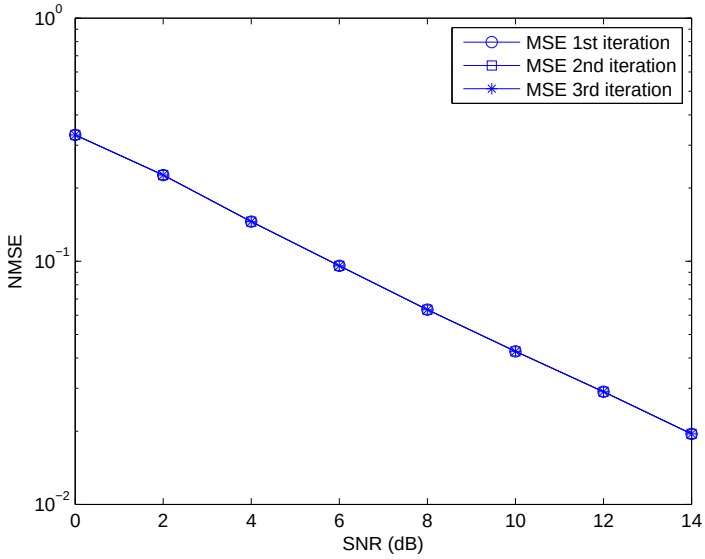

Figure 4.7: Channel estimation performance of SC systems.

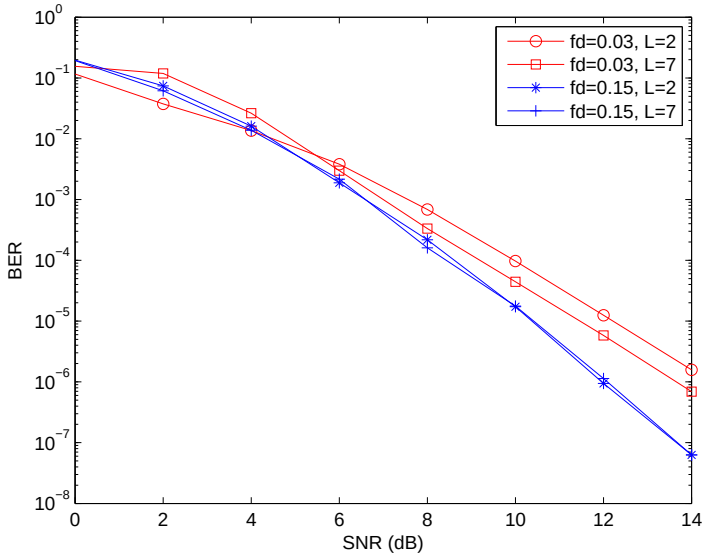

Figure 4.8: BER comparison of OFDM systems with different Doppler spreads and different channel lengths.

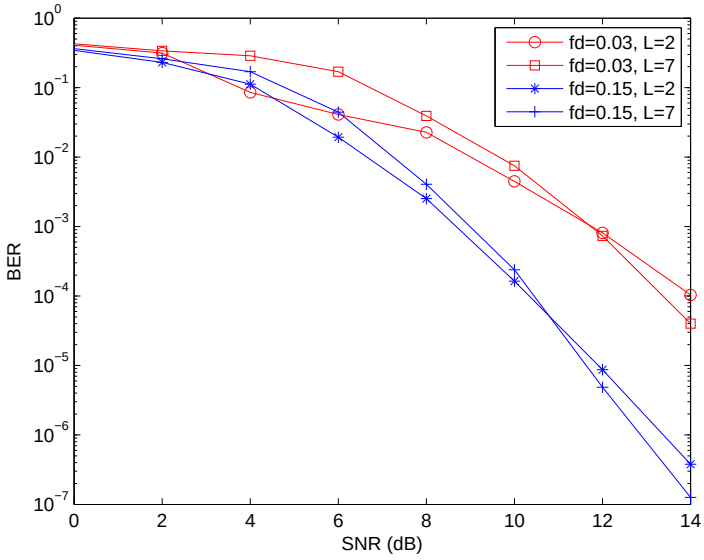

Figure 4.9: BER comparison of SC systems with different Doppler spreads and different channel lengths.

Chapter 5

STBC for Doubly-Selective Channels

The second part of the thesis focuses on the design of STBC which is used to jointly explore the degrees of freedom in the time, frequency and spatial domains for a multi-antenna systems under doubly-selective channels.

5.1 Introduction

In the last decade, multi-antenna systems have attracted a lot of research interest for future wireless systems. Using multiple transmit and/or receive antennas can significantly enhance communication system performances such as channel capacity and reliability [53]. STBC [54, 55] has been introduced to achieve the spatial diversity offered by multiple transmit and/or receive antennas. However, as STBC is typically designed for flat-fading channels, the time- and frequency-selectivity of wideband channels as studied in this thesis will seriously degrade the system performance. Thus, it is crucial to accurately model the doubly-selective channel and to design efficient STBC schemes to counteract its effects. Doubly-selective channels can also provide multiplicative delay-Doppler diversity gains if the transceiver is properly designed [51, 52], with diversity being an effective way to combat fading channels.

Many papers have extended STBC design to frequency-selective channels. In [56], STBC has been proposed for single-carrier transmission, which corresponds to orthogonal STBC for frequency-selective channels, and it can achieve maximum space-delay diversity in rich scattering channels. The transmission formats proposed in [56] subsume those of [57, 58], which present time-

reversal STBC at the transmitter to achieve transmit diversity, with either time domain equalization [57] or frequency domain equalization [58]. Multicarrier transmission systems have been considered in [59–61], where [59] derives the design criteria for space-frequency codes, by coding across OFDM tones and employing a spatial broadband channel model. An explicit construction of a class of space-frequency codes is provided in [60], with full space-delay diversity at the expense of spectral efficiency. Space-time-frequency (STF) coding is proposed in [61] for multi-antenna OFDM systems which also achieves full space-delay diversity. [62] developed space-time-multipath coded systems using digital phase sweeping (DPS) in the frequency domain or circular delaying in the time domain, which converts multiple frequency-selective channels into a single longer frequency-selective channel. It guarantees the maximum possible space-delay diversity, and has full rate for any number of transmit-receive antennas. Note that the aforementioned algorithms all require the channel to be constant over the entire space-time codeword.

Among the papers considering time-selective channels, [63] designs STBC for purely time-selective channels by transforming the time-selective channels into frequency-selective channels, and by adjusting existing space-time code designs over frequency-selective MIMO channels to collect joint space-Doppler gains over purely time-selective MIMO channels. Further, [64] uses the ideas of [62] to develop a space-time code that can achieve full space-delay-Doppler diversity for any number of transmit-receive antennas. However, to quantify the maximum Doppler diversity order [52], the above papers rely on a parsimonious critically sampled complex-exponential basis expansion model (CCE-BEM) for the underlying purely time-selective or doubly-selective channels [68]. The CCE-BEM gained a lot of attention because of its special algebraic structure [52, 62, 64], which is used to prove the achievable diversity of the considered system. However, the CCE-BEM may have a large modeling error under certain channel conditions [69], especially for channels with large Doppler spreads. Next to the BEM approaches, short-time Fourier basis signaling over doubly-dispersive channels has been proposed in [70, 71], which is generated from a prototype pulse via time-frequency shifts. Finally note that the time-reversal STBC [56] has been extended to doubly-selective channels in [72]. This is done by shortening the data block length without inserting new guard bands and/or adapting the decoding to the time-varying channel assuming it changes from subblock to subblock within a space-time codeword. In any case, the performance of the above scheme will be upper bounded by [56], using the appropriate space-time codeword length and using a decoder that is adapted to the time-varying channel by modeling its variation on a sample-

by-sample basis. It is this latter scheme that we will adopt as a benchmark for our proposed design.

In this chapter, we develop a novel STBC for multi-antenna transmissions over doubly-selective channels. The proposed STBC is designed for a MISO system with 2 transmit antennas and 1 receive antenna, i.e., a 2×1 system, but it is straightforward to extend the ideas to a general MIMO system. The proposed technique can be interpreted as the extension of the Alamouti code to doubly-selective channels, and relies on a joint time-frequency reversal of the transmitted sequences. Assuming a block fading channel where the time-variation from subblock to subblock is modeled by a CCE-BEM (we will label such a channel as a *block fading CCE-BEM channel*), the proposed STBC belongs to the class that achieves full spatial, delay, and Doppler diversity using a ML receiver, as well as a LZF or LMMSE receiver. For realistic doubly-selective channels, which cannot be exactly modeled by a block fading CCE-BEM channel, a real-valued linear data model is presented, for which different receiver structures can be developed. In that case, it is difficult to make any diversity claims, but comparing the proposed STBC with existing approaches by simulation we notice great improvements. However, note that our STBC relies on the orthogonal structure of [54], which incurs a rate loss of up to 50% when more than 2 transmit antennas and complex constellations are used.

The Doppler spread caused by the high mobility also makes the channel estimation problem more challenging. This chapter assumes that the receiver has perfect CSI, as well as perfect knowledge of the maximum delay spread τ_{max} and the maximum Doppler spread f_{max} which can be derived from the wireless transmission channel. The transmitter on the other hand has no access to CSI. In practice, the receiver can use the estimated CSI, obtained for instance by using the techniques developed in the previous chapter.

5.2 System Model

For simplicity reasons, we consider a single-user MISO communication system with 2 transmit antennas and 1 receive antenna, i.e., a 2×1 system, as shown in Fig. 5.1, where $\mathbf{C}_1$ and $\mathbf{C}_2$ are the precoder matrices and $\mathbf{P}_{\text{er}}$ is a permutation matrix which will be explained in Sec. 5.3.2, S/P and P/S represent serial/parallel and parallel/serial conversion, respectively. However, the proposed methods can be easily adapted to a general MIMO system. More specifically, extensions to multiple transmit antennas can be obtained by fol-

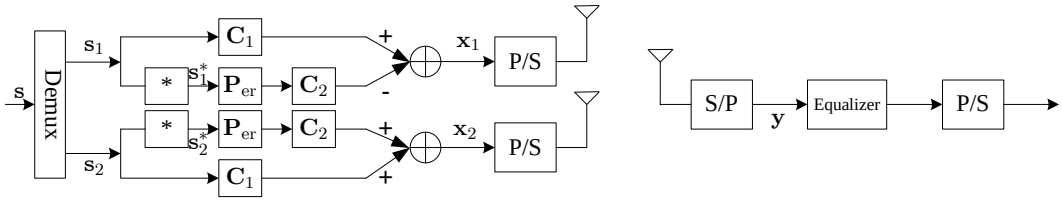

Figure 5.1: System model of the proposed STBC system.

lowing the generalizations of the Alamouti code to more than 2 transmit antennas, whereas extensions to multiple receive antennas can be realized by applying the proposed methods to a stack of the different receive antennas. Such generalizations will be discussed later on. We focus on a discrete-time baseband-equivalent description, with details that can be found in [75, chap. 1], [5]. Suppose x_n^k is the symbol sequence transmitted over the k-th transmit antenna. The received signal related to the k-th transmit antenna without noise can then be written as

$$y_n^k = \sum_{l=0}^{L} h_{n,l}^k x_{n-l}^k, \tag{5.1}$$

where $h_{n,l}^k$ is the order-L time- and frequency-selective channel from the k-th transmit antenna to the receive antenna. As we always use the time domain channel coefficients in this chapter, we omit the time domain superscript t, instead, the superscript k is used to indicate antenna index. The channel order L depends on the channel delay spread and should be chosen to satisfy $LT \geq \tau_{max}$, with T being the symbol period as well as the sampling period, and τ_{max} is the maximal delay spread. The overall received signal is then given by

$$y_n = \sum_{k=1}^{2} y_n^k + \eta_n, \tag{5.2}$$

where η_n is the additive noise.

Suppose now that the STBC has a length of N. In order to avoid inter block interference (IBI), we design our STBC codewords in such a way that the last L symbols within each codeword are zero (as shown in the next section). Since IBI is then avoided, the equalizer at the receiver can be designed for each codeword separately. For simplicity reasons, we here focus on the first codeword. The other codewords can be treated in a similar fashion.

Parsing x_n^k and y_n^k into blocks of length N, the first transmitted and received block from the k-th transmit antenna can be denoted as $\mathbf{x}_k = [x_0^k, x_1^k, \ldots, x_{N-1}^k]^T$ and $\mathbf{y}_k = [y_0^k, y_1^k, \ldots, y_{N-1}^k]^T$, respectively. They are connected through the following noiseless input-output relationship

$$\mathbf{y}_k = \mathbf{H}_k \mathbf{x}_k, \tag{5.3}$$

where $\mathbf{H}_k$ is the $N \times N$ channel matrix with $[\mathbf{H}_k]_{n,n'} = h^k_{n,(n-n') \bmod N}$ (we may use the modulo operator here since every codeword has L zeros at the end). Parsing y_n into blocks of length N and denoting $\mathbf{y} = [y_0, y_1, \ldots, y_{N-1}]^T$ as the first overall received block, we finally obtain

$$\mathbf{y} = \sum_{k=1}^{2} \mathbf{y}_k + \boldsymbol{\eta}, \tag{5.4}$$

where $\boldsymbol{\eta} = [\eta_0, \eta_1, \ldots, \eta_{N-1}]^T$. For simplicity, we assume that $\boldsymbol{\eta}$ is a circular complex Gaussian noise vector with zero mean and covariance matrix $\mathrm{E}\{\boldsymbol{\eta}\boldsymbol{\eta}^H\} = \sigma_\eta^2 \mathbf{I}_N$.

5.3 Space-Time Block Coding

Orthogonal STBC [54, 55] has been designed to achieve the spatial diversity offered by multiple transmit and/or receive antennas. The STBC schemes proposed in [54,55] are designed for flat-fading channels, which leads to a performance degradation in time- and frequency-selective channels. Our goal is to design efficient STBC schemes to counteract the effects of doubly-selective channels. The basic idea of the proposed STBC for a 2×1 system is to multiplex the data sequence in two data subsequences and to generate two orthogonal full-diversity subchannels over doubly-selective channels. Then, we apply a scheme that is similar to the Alamouti code. On the first antenna, we send the first data subsequence in the first subchannel and a negative permuted version of the complex conjugate of the second data subsequence in the second subchannel. On the second antenna, we send the second data subsequence in the first subchannel and a permuted version of the complex conjugate of the first data subsequence in the second subchannel. The questions that now remain are how we can generate two orthogonal full-diversity subchannels over doubly-selective channels, and how the permutations should look like in order to obtain a good performance. Both these questions can be answered by

assuming a restrictive yet simple doubly-selective channel model. More specifically, we assume a *block fading CCE-BEM* channel, which is defined as a block fading channel where the time-variation from subblock to subblock is modeled by a CCE-BEM. Hence, in this section, we develop and analyze the STBC under this block fading CCE-BEM channel model, and in the next section, we show how to decode the STBC for real-life channels, which do not exactly fit this block fading CCE-BEM channel model.

5.3.1 Block Fading CCE-BEM Channel Model

Let us start by defining what we exactly mean by a block fading CCE-BEM channel model. We assume that within the span of one STBC codeword, the doubly-selective channel behaves like a block fading channel, where the fading from subblock to subblock can be described by a CCE-BEM. Assume for instance that the span of the STBC codeword can be split into $2P'$ subblocks of length K', i.e., $N = 2P'K'$. Every channel is then assumed to be constant within every subblock of length K' and to vary over the $2P'$ subblocks as a CCE-BEM, which uses $2Q+1$ complex exponential basis functions to model the time variation over the $2P'$ subblocks:

$$h_{n,l}^{k} = \sum_{q=-Q}^{Q} e^{j2\pi(\lfloor n/K' \rfloor)q/(2P')} h_{q,l}^{k}, \tag{5.5}$$

where $h_{q,l}^{k}$ is the q-th CCE-BEM coefficient of the l-th channel tap within the STBC codeword. The $(L+1)(2Q+1)$ BEM coefficients $\{\{h_{q,l}^{k}\}_{l=0}^{L}\}_{q=-Q}^{Q}$ remain constant during each length-N block, and are allowed to change over different length-N blocks. The $2Q+1$ CCE-BEM basis functions used to capture the time variations are the same for every length-N block. Q can be regarded as the discrete Doppler spread index with frequency-domain resolution $1/(NT)$, and it needs to satisfy $Q/(NT) \geq f_{max}$. Different from [52, 65], where the CCE-BEM is used to model the time-variation of the channel from sample to sample, we now use it to model the time-variation of the channel from subblock to subblock. Note that in a rich scattering scenario, the CCE-BEM coefficients may be assumed to be zero-mean complex Gaussian distributed.

Under the block fading CCE-BEM channel model, the channel matrix

$\mathbf{H}_k$ from (5.3) can be written as

$$\mathbf{H}_k = \sum_{q=-Q}^{Q} (\mathbf{\Lambda}_{2P',q} \otimes \mathbf{I}_{K'}) \mathbf{H}_{N,q}^k, \tag{5.6}$$

where $\mathbf{\Lambda}_{2P',q}$ is the $2P' \times 2P'$ diagonal matrix given by $[\mathbf{\Lambda}_{2P',q}]_{p,p} = e^{j2\pi pq/(2P')}$ and $\mathbf{H}_{N,q}^k$ is the $N \times N$ circulant matrix given by $[\mathbf{H}_{N,q}^k]_{n,n'} = h_{q,(n-n') \bmod N}^k$.

5.3.2 Code Design

In [65], it has been shown how to generate orthogonal full-diversity subchannels in case the CCE-BEM is adopted to model the time-variation of the channel from sample to sample. It has been introduced there to develop a multi-user communications scheme where users remain orthogonal after propagation over a doubly-selective channel and where the full delay-Doppler diversity of a doubly-selective channel is enabled. Similarly, the same transmission scheme can be used to generate two orthogonal full-diversity subchannels in case the CCE-BEM is used to model the time-variation of the channel from subblock to subblock, i.e., in case we have a block fading CCE-BEM channel. This will be the basis of our STBC design.

The proposed STBC now proceeds as mentioned earlier. We start by demultiplexing a $2PK \times 1$ data vector $\mathbf{s}$ into two $PK \times 1$ data subvectors $\mathbf{s}_1$ and $\mathbf{s}_2$, where the data symbols are assumed to be circular complex with zero mean and covariance matrix $\mathrm{E}\{\mathbf{s}\mathbf{s}^H\} = \sigma_s^2 \mathbf{I}_{2PK}$. On the first and second antenna, we then send

$$\begin{aligned} \mathbf{x}_1 &= \mathbf{C}_1 \mathbf{s}_1 - \mathbf{C}_2 \mathbf{P}_{\mathrm{er}} \mathbf{s}_2^*, \\ \mathbf{x}_2 &= \mathbf{C}_1 \mathbf{s}_2 + \mathbf{C}_2 \mathbf{P}_{\mathrm{er}} \mathbf{s}_1^*, \end{aligned} \tag{5.7}$$

where $\mathbf{P}_{\mathrm{er}}$ is a $PK \times PK$ permutation matrix that will be determined later on. Assuming $K' > L$ and $P' > 2Q$, and defining $K = K' - L$ and $P = P' - 2Q$, let us introduce the channel-independent $N \times PK$ spreading matrices $\mathbf{C}_u$ and $N \times P'K'$ despreading matrices $\mathbf{D}_u$ defined as [65]

$$\mathbf{C}_u = [\mathbf{F}_{2P'}^H (\mathbf{c}_u \otimes \mathbf{T}_2)] \otimes \mathbf{T}_1, \tag{5.8}$$

$$\mathbf{D}_u = [\mathbf{F}_{2P'}^H (\mathbf{c}_u \otimes \mathbf{I}_{P'})] \otimes \mathbf{I}_{K'}, \tag{5.9}$$

where $\mathbf{T}_1 = [\mathbf{I}_K, \mathbf{0}_{K \times L}]^T$ is a $K' \times K$ zero padding matrix, $\mathbf{T}_2 = [\mathbf{0}_{P \times Q}, \mathbf{I}_P, \mathbf{0}_{P \times Q}]^T$ is a $P' \times P$ two-sided zero inserting matrix, $\mathbf{F}_N$ is the N-point unitary DFT

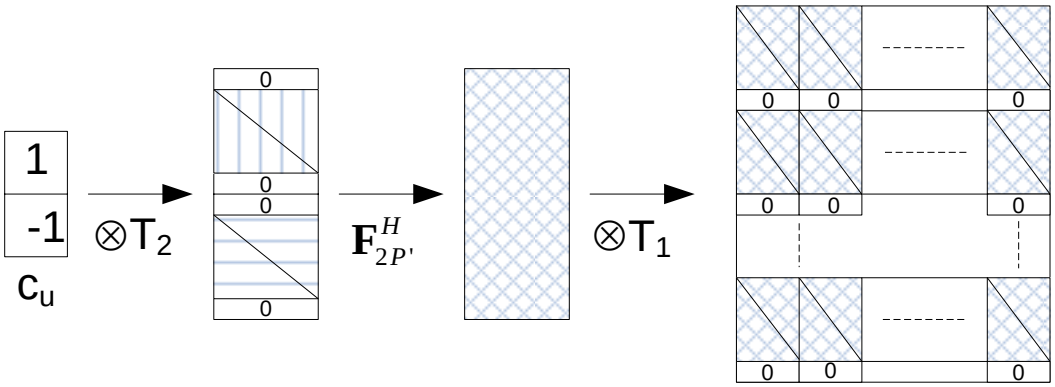

Figure 5.2: Block spreading by $\mathbf{C}_u$.

matrix, and $\{\mathbf{c}_u\}_{u=1}^{2}$ is an arbitrary set of 2 orthonormal code vectors. The spreading procedure implemented by the precoder $\mathbf{C}_u$ can be illustrated as in Fig. 5.2, and the despreading procedure is similar. Notice that the last L rows of the spreading matrix $\mathbf{C}_u$ are set to zero, which avoids the IBI. Since there are $2PK$ information symbols sent over $2P'K'$ symbol periods, the spectral efficiency can be written as

$$\varepsilon = \frac{PK}{(P+2Q)(K+L)}, \tag{5.10}$$

where $2Q$ and L are the number of time and frequency guard bands in the spreading matrices.

Similar to [65], it is possible to show that these spreading matrices $\mathbf{C}_u$ and despreading matrices $\mathbf{D}_u$ can be used to create two orthogonal full-diversity subchannels under the assumption of a block fading CCE-BEM channel model. The composite channel matrix consisting of the block fading CCE-BEM channel as well as the spreading and despreading operations can be expressed as

$$\mathbf{D}_{u'}^{H}\mathbf{H}_k\mathbf{C}_u = \begin{cases} \sum_{q=-Q}^{Q}(\mathbf{J}_{P',q}\mathbf{T}_2)\otimes(\mathbf{H}_{K',q}^{k}\mathbf{T}_1) = \tilde{\boldsymbol{\mathcal{H}}}_k, & u'=u; \\ \mathbf{0}, & u'\neq u, \end{cases} \tag{5.11}$$

where $\mathbf{J}_{P',q}$ is the $P'\times P'$ circulant matrix given by $[\mathbf{J}_{P',q}]_{p,p'} = \delta[(p-p'-q) \bmod P']$ and $\mathbf{H}_{K',q}^{k}$ is the $K'\times K'$ circulant matrix given by $[\mathbf{H}_{K',q}^{k}]_{p,p'} = h_{q,p-p' \bmod K'}^{k}$. A proof of (5.11) is given in Appendix 5.1.

Using the Kronecker product property $(\mathbf{A}_1\otimes\mathbf{A}_2)(\mathbf{A}_3\otimes\mathbf{A}_4) = (\mathbf{A}_1\mathbf{A}_3)\otimes$

$(\mathbf{A}_2\mathbf{A}_4)$, we can rewrite $\tilde{\boldsymbol{\mathcal{H}}}_k$ in (5.11) also as

$$\begin{aligned}\tilde{\boldsymbol{\mathcal{H}}}_k &= \sum_{q=-Q}^{Q} \mathbf{J}_{P',q}\mathbf{T}_2 \otimes \mathbf{H}^k_{K',q}\mathbf{T}_1 \\ &= (\sum_{q=-Q}^{Q} \mathbf{J}_{P',q} \otimes \mathbf{H}^k_{K',q})(\mathbf{T}_2 \otimes \mathbf{T}_1) \\ &= \boldsymbol{\mathcal{H}}_k\mathbf{T},\end{aligned} \tag{5.12}$$

where $\boldsymbol{\mathcal{H}}_k = \sum_{q=-Q}^{Q} \mathbf{J}_{P',q} \otimes \mathbf{H}^k_{K',q}$, and $\mathbf{T} = \mathbf{T}_2 \otimes \mathbf{T}_1$.

The received signal can now be expressed as

$$\begin{aligned}\mathbf{y} &= \mathbf{H}_1\mathbf{x}_1 + \mathbf{H}_2\mathbf{x}_2 + \boldsymbol{\eta} \\ &= \mathbf{H}_1\mathbf{C}_1\mathbf{s}_1 - \mathbf{H}_1\mathbf{C}_2\mathbf{P}_{\text{er}}\mathbf{s}_2^* + \mathbf{H}_2\mathbf{C}_1\mathbf{s}_2 + \mathbf{H}_2\mathbf{C}_2\mathbf{P}_{\text{er}}\mathbf{s}_1^* + \boldsymbol{\eta}.\end{aligned} \tag{5.13}$$

Applying the despreading operations $\mathbf{D}_1$ and $\mathbf{D}_2$ at the receiver, we obtain (using (5.11))

$$\begin{aligned}\bar{\mathbf{y}}_1 &= \mathbf{D}_1^H\mathbf{y} \\ &= \tilde{\boldsymbol{\mathcal{H}}}_1\mathbf{s}_1 + \tilde{\boldsymbol{\mathcal{H}}}_2\mathbf{s}_2 + \mathbf{D}_1^H\boldsymbol{\eta} \\ &= \boldsymbol{\mathcal{H}}_1\mathbf{T}\mathbf{s}_1 + \boldsymbol{\mathcal{H}}_2\mathbf{T}\mathbf{s}_2 + \bar{\boldsymbol{\eta}}_1,\end{aligned} \tag{5.14}$$

$$\begin{aligned}\bar{\mathbf{y}}_2 &= \mathbf{D}_2^H\mathbf{y} \\ &= \tilde{\boldsymbol{\mathcal{H}}}_2\mathbf{P}_{\text{er}}\mathbf{s}_1^* - \tilde{\boldsymbol{\mathcal{H}}}_1\mathbf{P}_{\text{er}}\mathbf{s}_2^* + \mathbf{D}_2^H\boldsymbol{\eta} \\ &= \boldsymbol{\mathcal{H}}_2\mathbf{T}\mathbf{P}_{\text{er}}\mathbf{s}_1^* - \boldsymbol{\mathcal{H}}_1\mathbf{T}\mathbf{P}_{\text{er}}\mathbf{s}_2^* + \bar{\boldsymbol{\eta}}_2.\end{aligned} \tag{5.15}$$

Since the $N \times P'K'$ despreading matrix $\mathbf{D}_u$ is a tall matrix and $\mathbf{D}_u^H\mathbf{D}_u = \mathbf{I}_{P'K'}$ [65], $\bar{\boldsymbol{\eta}}_u$ is still a complex Gaussian noise vector with zero mean and covariance matrix $\text{E}\{\bar{\boldsymbol{\eta}}_u\bar{\boldsymbol{\eta}}_u^H\} = \sigma_\eta^2\mathbf{I}_{P'K'}$.

We wish to be able to decode the two multiplexed transmitted data streams $\mathbf{s}_1$ and $\mathbf{s}_2$ separately at the receiver, similar to the scalar case for Alamouti decoding [55]. In order to achieve that, we now have to find the $PK \times PK$ permutation matrix $\mathbf{P}_{\text{er}}$ such that there exists a $P'K' \times P'K'$ permutation matrix $\mathbf{P}'_{\text{er}}$ for which

$$\mathbf{P}'_{\text{er}}\boldsymbol{\mathcal{H}}_k\mathbf{T}\mathbf{P}_{\text{er}} = \boldsymbol{\mathcal{H}}_k^T\mathbf{T}. \tag{5.16}$$

Since $\boldsymbol{\mathcal{H}}_k$ is a block circulant matrix of circulant matrices, it is easy to show similar to [56] that the permutation matrices that satisfy this property are given by $\mathbf{P}_{\rm er} = \mathbf{P}_{{\rm er},2} \otimes \mathbf{P}_{{\rm er},1}$, where $\mathbf{P}_{{\rm er},1} = \mathbf{P}_{{\rm er}_K}^{(K-1)}$ and $\mathbf{P}_{{\rm er},2} = \mathbf{P}_{{\rm er}_P}^{(P-1)}$ perform a $K \times K$ and a $P \times P$ element reversal, respectively (this actually means that $\mathbf{P}_{\rm er}$ performs a $PK \times PK$ element reversal), and $\mathbf{P}'_{\rm er} = \mathbf{P}'_{{\rm er},2} \otimes \mathbf{P}'_{{\rm er},1}$, with $\mathbf{P}'_{{\rm er},1} = \mathbf{P}_{{\rm er}_{K'}}^{(K-1)}$ and $\mathbf{P}'_{{\rm er},2} = \mathbf{P}_{{\rm er}_{P'}}^{(P'-1)}$. As a result, (5.15) can be rewritten as

$$\mathbf{P}'_{\rm er}\bar{\mathbf{y}}_2^* = \boldsymbol{\mathcal{H}}_2^H \mathbf{T}\mathbf{s}_1 - \boldsymbol{\mathcal{H}}_1^H \mathbf{T}\mathbf{s}_2 + \mathbf{P}'_{\rm er}\bar{\boldsymbol{\eta}}_2^*, \tag{5.17}$$

Now applying $\mathbf{F} = \mathbf{F}_{P'} \otimes \mathbf{F}_{K'}$ to (5.14) and (5.17), we get

$$\mathbf{F}\bar{\mathbf{y}}_1 = \boldsymbol{\mathcal{G}}_1 \mathbf{F}\mathbf{T}\mathbf{s}_1 + \boldsymbol{\mathcal{G}}_2 \mathbf{F}\mathbf{T}\mathbf{s}_2 + \mathbf{F}\bar{\boldsymbol{\eta}}_1, \tag{5.18}$$

$$\mathbf{F}\mathbf{P}'_{\rm er}\bar{\mathbf{y}}_2^* = \boldsymbol{\mathcal{G}}_2^* \mathbf{F}\mathbf{T}\mathbf{s}_1 - \boldsymbol{\mathcal{G}}_1^* \mathbf{F}\mathbf{T}\mathbf{s}_2 + \mathbf{F}\mathbf{P}'_{\rm er}\bar{\boldsymbol{\eta}}_2^*. \tag{5.19}$$

In these formulas, $\boldsymbol{\mathcal{G}}_k = \mathbf{F}\boldsymbol{\mathcal{H}}_k\mathbf{F}^H$ is a $P'K' \times P'K'$ diagonal matrix given by

$$\boldsymbol{\mathcal{G}}_k = \sum_{q=-Q}^{Q} \boldsymbol{\Lambda}_{P',q} \otimes \mathbf{G}_{k,q}, \tag{5.20}$$

where $\boldsymbol{\Lambda}_{P',q}$ is the $P' \times P'$ diagonal matrix given by

$$[\boldsymbol{\Lambda}_{P',q}]_{p,p} = [\mathbf{F}_{P'}\mathbf{J}_{P',q}\mathbf{F}_{P'}^H]_{p,p} = e^{j2\pi pq/P'}, \tag{5.21}$$

and $\mathbf{G}_{k,q}$ is the $K' \times K'$ diagonal matrix given by

$$[\mathbf{G}_{k,q}]_{p,p} = [\mathbf{F}_{K'}\mathbf{H}_{K',q}^k\mathbf{F}_{K'}^H]_{p,p}. \tag{5.22}$$

Stacking (5.18) and (5.19), we obtain the following relationship

$$\begin{aligned} \check{\mathbf{y}} &= \begin{bmatrix} \mathbf{F}\bar{\mathbf{y}}_1 \\ \mathbf{F}\mathbf{P}'\bar{\mathbf{y}}_2^* \end{bmatrix} \\ &= \begin{bmatrix} \boldsymbol{\mathcal{G}}_1 & \boldsymbol{\mathcal{G}}_2 \\ \boldsymbol{\mathcal{G}}_2^* & -\boldsymbol{\mathcal{G}}_1^* \end{bmatrix} \begin{bmatrix} \mathbf{F}\mathbf{T}\mathbf{s}_1 \\ \mathbf{F}\mathbf{T}\mathbf{s}_2 \end{bmatrix} + \begin{bmatrix} \mathbf{F}\bar{\boldsymbol{\eta}}_1 \\ \mathbf{F}\mathbf{P}'\bar{\boldsymbol{\eta}}_2^* \end{bmatrix} \\ &= \boldsymbol{\mathcal{G}} \begin{bmatrix} \mathbf{F}\mathbf{T}\mathbf{s}_1 \\ \mathbf{F}\mathbf{T}\mathbf{s}_2 \end{bmatrix} + \check{\boldsymbol{\eta}}. \end{aligned} \tag{5.23}$$

Similar to [56], if we define $\boldsymbol{\mathcal{G}}_{12} = (\boldsymbol{\mathcal{G}}_1^*\boldsymbol{\mathcal{G}}_1 + \boldsymbol{\mathcal{G}}_2^*\boldsymbol{\mathcal{G}}_2)^{1/2}$ and apply the unitary matrix $\mathbf{U} = \boldsymbol{\mathcal{G}}(\mathbf{I}_2 \otimes \boldsymbol{\mathcal{G}}_{12}^{-1})$, we obtain

$$\mathbf{U}^H\check{\mathbf{y}} = \begin{bmatrix} \boldsymbol{\mathcal{G}}_{12}\mathbf{F}\mathbf{T}\mathbf{s}_1 \\ \boldsymbol{\mathcal{G}}_{12}\mathbf{F}\mathbf{T}\mathbf{s}_2 \end{bmatrix} + \mathbf{U}^H\check{\boldsymbol{\eta}}. \tag{5.24}$$

Note that if both $\boldsymbol{\mathcal{G}}_1$ and $\boldsymbol{\mathcal{G}}_2$ has a zero at the same position on the diagonal, we can still design a unitary $\mathbf{U}$ without compromising the validity of (5.24), by replacing either one of the common zeros by a one in the formula for $\mathbf{U}$, as explained in [56].

In conclusion, by applying linear unitary matrix operations, i.e., without loosing optimality, we can separate the two substreams, leading to two matrix equations of the form

$$\mathbf{z}_u = \boldsymbol{\mathcal{G}}_{12}\mathbf{F}\mathbf{T}\mathbf{s}_u + \boldsymbol{\zeta}_u = \mathbf{H}\mathbf{s}_u + \boldsymbol{\zeta}_u, \quad u = 1, 2. \tag{5.25}$$

Every stream can then be decoded using your favorite decoder. Note that all these derivations only hold under the assumption of a block fading CCE-BEM channel model.

5.3.3 Diversity Gain Analysis

Similar to [52,65], we can show that if a (near-)ML decoder is used, the delay-Doppler diversity order of $(2Q+1)(L+1)$, which is the number of degrees of freedom in the block fading CCE-BEM channel, can be reached, under the assumption that the CCE-BEM coefficients are independently zero-mean complex Gaussian distributed. Alamouti-like STBC offers an additional spatial diversity order of 2. Hence, the proposed STBC enables the maximum space-delay-Doppler diversity that the doubly-selective channel can offer, which is multiplicative in the degrees of freedom of the channel in space, time and frequency dimensions. The proof is an extension of that in [52, 65], and we only give a brief description here.

Since each data stream can be decoded separately in (5.25), we consider decoding $\mathbf{z}_1$ only. Define the error vector $\mathbf{e} = \mathbf{s}_1 - \mathbf{s}_1'$ between symbol blocks $\mathbf{s}_1$ and $\mathbf{s}_1'$. The Euclidean distance between $\mathbf{z}_1 = \mathbf{H}\mathbf{s}_1$ and $\mathbf{z}_1' = \mathbf{H}\mathbf{s}_1'$ can then be expressed as

$$d^2(\mathbf{z}_1, \mathbf{z}_1') = ||\mathbf{H}\mathbf{e}||^2 = ||\boldsymbol{\mathcal{E}}\mathbf{h}||^2, \tag{5.26}$$

where $\boldsymbol{\mathcal{E}}$ is an $N \times 2(2Q+1)(L+1)$ matrix that depends on $\mathbf{e}$ (the exact form is not important), and $\mathbf{h}$ is the vector containing all the CCE-BEM coefficients defined as $\mathbf{h} = [\mathbf{h}_1^T, \mathbf{h}_2^T]^T$, where $\mathbf{h}_k = [\mathbf{h}_{k,-Q}^T, \ldots, \mathbf{h}_{k,Q}^T]^T$, with $\mathbf{h}_{k,q} = [h_{q,0}^k, \ldots, h_{q,L}^k]^T$. In order to achieve the maximum space-delay-Doppler diversity the channel can provide, we require $||\boldsymbol{\mathcal{E}}\mathbf{h}|| > 0$ for all $\mathbf{e} \neq \mathbf{0}$, and for all $\mathbf{h} \neq \mathbf{0}$ [52, 65]. From (5.26), this corresponds to $||\mathbf{H}\mathbf{e}|| > 0$ for all $\mathbf{e} \neq \mathbf{0}$

and for all $\mathbf{h} \neq \mathbf{0}$. This is satisfied when $\mathbf{H}$ has full column rank PK for all $\mathbf{h} \neq \mathbf{0}$, which is proved in Appendix 5.2.

Using the results of [76], we can even show that if a LZF or LMMSE decoder is used, this full diversity order can still be achieved. It is shown in [76] that if $\det(\mathbf{H}^H\mathbf{H}) > 0, \forall \mathbf{H}$, i.e., $\mathbf{H}$ has full column rank for any channel realization, then the LZF and LMMSE decoder can obtain the same diversity order as the ML decoder.

5.3.4 Space-Time-Frequency Interpretation

Data symbols can be regarded as being modulated on waveforms that occupy a lattice in the time-frequency plane, up to some guard bands in time and frequency, and that preserve the orthogonality at the receiver in case of a block fading CCE-BEM channel as we discussed before. The transmitter first demultiplexes the data stream into two subchannels. By applying the spreading matrices $\mathbf{C}_u$, every subchannel spreads every data symbol over a $2P' \times 2K'$ lattice in the time-frequency plane. All the PK lattices related to all the PK data symbols sent over one subchannel are stacked in such a way that we obtain a $2P' \times 2K'$ raster of $K \times P$ boxes in the time-frequency plane [65]. By choosing different orthonormal code vectors $\mathbf{c}_u$, TDMA-like ($\mathbf{c}_u = \mathbf{f}_U[u]$, where $\mathbf{f}_U[u]$ is the uth column of $\mathbf{F}_U$), FDMA-like ($\mathbf{c}_u = \mathbf{i}_U[u]$, where $\mathbf{i}_U[u]$ is the uth column of $\mathbf{I}_U$), and CDMA-like ($\mathbf{c}_u$ is a Walsh-Hadamard code vector) transmission strategies can be realized. On top of the time-frequency spreading, data symbols are now also spread in the spatial dimension by the joint time-frequency reversal matrix $\mathbf{P}_{\text{er}}$. As shown in (5.7), the transmitted signal for each antenna is the superposition of the two data streams, with the second data stream being reversed and complex conjugated. With the help of the Alamouti structure, we can keep spatial orthogonality at the receiver in case of a block fading CCE-BEM channel and as a result achieve full spatial diversity.

5.3.5 Extension to MIMO Systems

The proposed STBC is designed for a 2×1 system. However, it is straightforward to extend the above ideas to a general MIMO system. For multiple transmit antennas, signals transmitted from different transmit antennas (5.7) can be designed according to the orthogonal structure in [54], with an appro-

priate permutation matrix $\mathbf{P}_{\rm er}$ and spreading matrices $\mathbf{C}_u$. However, note that this will incur a rate loss up to 50% when more than 2 transmit antennas and complex constellations are used. Consider a system with N_t transmit antennas, and an orthogonal structure with code rate N_s/N_T, where N_s symbols are transmitted over N_T time slots from N_t transmit antennas. The proposed STBC for doubly-selective channels can be adapted from this orthogonal structure, using N_T spreading matrices $\{\mathbf{C}_u\}_{u=1}^{N_T}$ of size $N \times N_s$ with $N = N_T P' K'$. Specifically, the N_t length-$(N_T P' K')$ transmitted vectors $\{\mathbf{x}_t\}_{t=1}^{N_t}$ are generated from N_s length-(PK) data subvectors $\{\mathbf{s}_t\}_{t=1}^{N_s}$ permuted and precoded by $\mathbf{P}_{\rm er}$ and $\{\mathbf{C}_u\}_{u=1}^{N_T}$, respectively.

We next show an example of an STBC designed for $N_t = 3$ transmit antennas. A rate 1/2 orthogonal structure for transmission using three transmit antennas is given by [54]

$$\boldsymbol{\mathcal{O}}_3 = \begin{pmatrix} s_1 & s_2 & s_3 \\ -s_2 & s_1 & -s_4 \\ -s_3 & s_4 & s_1 \\ -s_4 & -s_3 & s_2 \\ s_1^* & s_2^* & s_3^* \\ -s_2^* & s_1^* & -s_4^* \\ -s_3^* & s_4^* & s_1^* \\ -s_4^* & -s_3^* & s_2^* \end{pmatrix}, \tag{5.27}$$

with $N_s = 4$ and $N_T = 8$, where the element on the ith row and jth column being sent over jth transmit antenna at ith time slot. Following the same design philosophy as for a system with two transmit antennas, the signals transmitted from the three antennas can be expressed as

$$\begin{aligned} \mathbf{x}_1 &= \mathbf{C}_1\mathbf{s}_1 - \mathbf{C}_2\mathbf{s}_2 - \mathbf{C}_3\mathbf{s}_3 - \mathbf{C}_4\mathbf{s}_4 \\ &\quad + \mathbf{C}_5\mathbf{P}_{\rm er}\mathbf{s}_1^* - \mathbf{C}_6\mathbf{P}_{\rm er}\mathbf{s}_2^* - \mathbf{C}_7\mathbf{P}_{\rm er}\mathbf{s}_3^* - \mathbf{C}_8\mathbf{P}_{\rm er}\mathbf{s}_4^*, \\ \mathbf{x}_2 &= \mathbf{C}_1\mathbf{s}_2 + \mathbf{C}_2\mathbf{s}_1 + \mathbf{C}_3\mathbf{s}_4 - \mathbf{C}_4\mathbf{s}_3 \\ &\quad + \mathbf{C}_5\mathbf{P}_{\rm er}\mathbf{s}_2^* + \mathbf{C}_6\mathbf{P}_{\rm er}\mathbf{s}_1^* + \mathbf{C}_7\mathbf{P}_{\rm er}\mathbf{s}_4^* - \mathbf{C}_8\mathbf{P}_{\rm er}\mathbf{s}_3^*, \\ \mathbf{x}_3 &= \mathbf{C}_1\mathbf{s}_3 - \mathbf{C}_2\mathbf{s}_4 + \mathbf{C}_3\mathbf{s}_1 + \mathbf{C}_4\mathbf{s}_2 \\ &\quad + \mathbf{C}_5\mathbf{P}_{\rm er}\mathbf{s}_3^* - \mathbf{C}_6\mathbf{P}_{\rm er}\mathbf{s}_4^* + \mathbf{C}_7\mathbf{P}_{\rm er}\mathbf{s}_1^* + \mathbf{C}_8\mathbf{P}_{\rm er}\mathbf{s}_2^*, \end{aligned} \tag{5.28}$$

where $\{\mathbf{s}_t\}_{t=1}^4$ are the $PK \times 1$ data subvectors, $\mathbf{P}_{\rm er}$ is the $PK \times PK$ permutation matrix defined as before, and $\{\mathbf{C}_u\}_{u=1}^8$ are the spreading matrices defined in (5.8) with $\{\mathbf{c}_u\}_{u=1}^8$ being an arbitrary set of length-8 orthonormal code vectors. Notice that the block length has changed to $N = N_T P' K' = 8P' K'$.

At the receiver, the received signal can be expressed as

$$\mathbf{y} = \mathbf{H}_1\mathbf{x}_1 + \mathbf{H}_2\mathbf{x}_2 + \mathbf{H}_3\mathbf{x}_3 + \boldsymbol{\eta}. \tag{5.29}$$

In case of a block fading CCE-BEM channel, we then multiply $\mathbf{y}$ with the despreading matrix $\mathbf{D}_u^H$, which is similarly defined as in (5.9), and we obtain $\bar{\mathbf{y}}_u = \mathbf{D}_u^H\mathbf{y}$. After applying appropriate processing, and stacking the vectors together, the following equation can be obtained through a procedure similar to (5.13)-(5.23):

$$\begin{aligned}\begin{pmatrix} \mathbf{F}\bar{\mathbf{y}}_1 \\ \mathbf{F}\bar{\mathbf{y}}_2 \\ \mathbf{F}\bar{\mathbf{y}}_3 \\ \mathbf{F}\bar{\mathbf{y}}_4 \\ \mathbf{F}\mathbf{P}'\bar{\mathbf{y}}_1^* \\ \mathbf{F}\mathbf{P}'\bar{\mathbf{y}}_2^* \\ \mathbf{F}\mathbf{P}'\bar{\mathbf{y}}_3^* \\ \mathbf{F}\mathbf{P}'\bar{\mathbf{y}}_4^* \end{pmatrix} &= \begin{pmatrix} \boldsymbol{\mathcal{G}}_1 & \boldsymbol{\mathcal{G}}_2 & \boldsymbol{\mathcal{G}}_3 & \mathbf{0} \\ \boldsymbol{\mathcal{G}}_2 & -\boldsymbol{\mathcal{G}}_1 & \mathbf{0} & -\boldsymbol{\mathcal{G}}_3 \\ \boldsymbol{\mathcal{G}}_3 & \mathbf{0} & -\boldsymbol{\mathcal{G}}_1 & \boldsymbol{\mathcal{G}}_2 \\ \mathbf{0} & \boldsymbol{\mathcal{G}}_3 & -\boldsymbol{\mathcal{G}}_2 & -\boldsymbol{\mathcal{G}}_1 \\ \boldsymbol{\mathcal{G}}_1^* & \boldsymbol{\mathcal{G}}_2^* & \boldsymbol{\mathcal{G}}_3^* & \mathbf{0} \\ \boldsymbol{\mathcal{G}}_2^* & -\boldsymbol{\mathcal{G}}_1^* & \mathbf{0} & -\boldsymbol{\mathcal{G}}_3^* \\ \boldsymbol{\mathcal{G}}_3^* & \mathbf{0} & -\boldsymbol{\mathcal{G}}_1^* & \boldsymbol{\mathcal{G}}_2^* \\ \mathbf{0} & \boldsymbol{\mathcal{G}}_3^* & -\boldsymbol{\mathcal{G}}_2^* & -\boldsymbol{\mathcal{G}}_1^* \end{pmatrix} \begin{pmatrix} \mathbf{F}\mathbf{T}\mathbf{s}_1 \\ \mathbf{F}\mathbf{T}\mathbf{s}_2 \\ \mathbf{F}\mathbf{T}\mathbf{s}_3 \\ \mathbf{F}\mathbf{T}\mathbf{s}_4 \end{pmatrix} + \begin{pmatrix} \mathbf{F}\bar{\eta}_1 \\ \mathbf{F}\bar{\eta}_2 \\ \mathbf{F}\bar{\eta}_3 \\ \mathbf{F}\bar{\eta}_4 \\ \mathbf{F}\mathbf{P}'\bar{\eta}_1^* \\ \mathbf{F}\mathbf{P}'\bar{\eta}_2^* \\ \mathbf{F}\mathbf{P}'\bar{\eta}_3^* \\ \mathbf{F}\mathbf{P}'\bar{\eta}_4^* \end{pmatrix} \\ &= \boldsymbol{\mathcal{G}} \begin{pmatrix} \mathbf{F}\mathbf{T}\mathbf{s}_1 \\ \mathbf{F}\mathbf{T}\mathbf{s}_2 \\ \mathbf{F}\mathbf{T}\mathbf{s}_3 \\ \mathbf{F}\mathbf{T}\mathbf{s}_4 \end{pmatrix} + \check{\boldsymbol{\eta}}, \end{aligned} \tag{5.30}$$

where $\boldsymbol{\mathcal{G}}_k$ is defined in a similar way as in (5.23). It is then easy to show that the data streams can again be decoded separately as in (5.24)-(5.25).

With multiple antennas at the receiver, the maximum ratio combining (MRC) method can be applied as in [64]. It is a simple extension to prove that full transmit-receive diversity can be achieved using the above STBC and decoding method. We omit the details here.

5.3.6 Comparisons with Existing STBCs

In this subsection, we compare the proposed STBC with some existing works. A block precoded digital phase sweeping (DPS) transmission for any number of transmit-receive antennas is designed in [64]. By converting the multi-antenna time-selective channels into a single faster time-selective channel, full space-delay-Doppler diversity can be obtained for a CCE-BEM channel. DPS also applies a time-frequency spreading, but larger guard bands are required. For

a 2×1 system, the DPS algorithm has a block length of $N_{DPS} = (P + 4Q + 1)(K + L)$, and the corresponding spectral efficiency can be written as

$$\varepsilon_{DPS} = \frac{PK}{(P + 4Q + 1)(K + L)}, \tag{5.31}$$

which is smaller than the spectral efficiency of the proposed STBC scheme for the same P and K. Hence, if we compare the performance of our STBC with [64] for the same P and K, we actually disfavor our STBC. Note though that our STBC relies on the orthogonal structure of [54], which incurs a rate loss up to 50% when more than 2 transmit antennas and complex constellations are used, while [64] can be designed for any number of transmit antennas without rate loss.

STBCs for single-carrier block transmission over frequency-selective multipath fading channels are studied in [56]. The zero-padding only STBC in [56] can actually be regarded as a special case of the proposed STBC with $P = 1$ and $Q = 0$. Without data symbol spreading and guards in the frequency domain ($P = 1$, $Q = 0$), a higher spectral efficiency can be achieved, and the block length can be made smaller, which also leads to a lower complexity. A natural question is then if we can ignore the time-selectivity and only use the STBCs designed for a frequency-selective channel in doubly-selective channels. Later on we show that even without frequency guard bands ($Q = 0$), for moderate to high Doppler channels, it is better to spread the data symbols in frequency ($P > 1$). This is because the STBC designed for frequency-selective channels cannot exploit the Doppler diversity in doubly-selective channels. For moderate to high Doppler channels, the lack of frequency guard bands of course reduces the Doppler diversity benefit.

5.4 Proposed Receiver for Realistic Channels

The STBC design and analysis discussed before is based on the block fading CCE-BEM channel model. The nice algebraic structure of this block fading CCE-BEM channel model allows us to extend the Alamouti code to doubly-selective channels enabling the full space-delay-Doppler diversity, as shown in Section 5.3.2. Although this channel model was useful to design and analyze our STBC, it does not perfectly model real-life doubly-selective channels under all circumstances [69]. Hence, the receiver processing discussed in Section 5.3.2 can only be applied if we approximate the true channel by its best possible fit

to a block fading CCE-BEM channel. The related modeling error will of course introduce a bit-error-rate (BER) performance floor at medium to high SNR, and this floor will increase with the Doppler spread. To avoid this floor, we will next propose an alternative receiver for the proposed STBC that is suitable for realistic doubly-selective channels, which do not rely on any specific channel model, so that there is no channel modeling error.

First of all, we realize that in case of a block fading CCE-BEM channel, working with $\mathbf{z} = [\mathbf{z}_1^T, \mathbf{z}_2^T]^T$ (see (5.25)) is the same as working with $\tilde{\mathbf{z}} = [\Re\{\mathbf{z}^T\}, \Im\{\mathbf{z}^T\}]^T$, since the data and noise are circular complex white [91]. Further, it is easy to understand that working with $\tilde{\mathbf{z}}$ is also the same as working with $\tilde{\mathbf{y}}$, since $\mathbf{z}$ is obtained from $\mathbf{y}$ by applying complex conjugations and unitary matrix operations which has no effect on the receiver performance if the noise and the data are circular complex white. This shows that any receiver (ML, LZF, or LMMSE) applied to $\mathbf{z}$ would have the same performance as when we would apply a similar receiver to $\tilde{\mathbf{y}}$ in case of a block fading CCE-BEM channel. The advantage of designing a receiver for $\tilde{\mathbf{y}}$ however is that it can be generalized to realistic doubly-selective channels that do not necessarily fit into the block fading CCE-BEM channel model. To design such a receiver, we have to develop a data model for $\tilde{\mathbf{y}}$, which will be a real-valued data model.

Defining the $N \times PK$ matrix $\mathbf{K}_{k,u}$ as $\mathbf{K}_{k,u} = \mathbf{H}_k \mathbf{C}_u$, the received vector $\mathbf{y}$ can be written as

$$\mathbf{y} = \mathbf{K}_{1,1}\mathbf{s}_1 - \mathbf{K}_{1,2}\mathbf{P}_{\text{er}}\mathbf{s}_2^* + \mathbf{K}_{2,1}\mathbf{s}_2 + \mathbf{K}_{2,2}\mathbf{P}_{\text{er}}\mathbf{s}_1^* + \boldsymbol{\eta}. \tag{5.32}$$

Further defining

$$\tilde{\mathbf{K}}_{k,u} = \begin{bmatrix} \Re(\mathbf{K}_{k,u}) & -\Im(\mathbf{K}_{k,u}) \\ \Im(\mathbf{K}_{k,u}) & \Re(\mathbf{K}_{k,u}) \end{bmatrix}, \tag{5.33}$$

$$\tilde{\tilde{\mathbf{K}}}_{k,u} = \begin{bmatrix} \Re(\mathbf{K}_{k,u}) & \Im(\mathbf{K}_{k,u}) \\ \Im(\mathbf{K}_{k,u}) & -\Re(\mathbf{K}_{k,u}) \end{bmatrix}, \tag{5.34}$$

we can write $\tilde{\mathbf{y}}$ as

$$\begin{aligned} \tilde{\mathbf{y}} &= \tilde{\mathbf{K}}_{1,1}\tilde{\mathbf{s}}_1 - \tilde{\tilde{\mathbf{K}}}_{1,2}(\mathbf{I}_2 \otimes \mathbf{P}_{\text{er}})\tilde{\mathbf{s}}_2 + \tilde{\mathbf{K}}_{2,1}\tilde{\mathbf{s}}_2 + \tilde{\tilde{\mathbf{K}}}_{2,2}(\mathbf{I}_2 \otimes \mathbf{P}_{\text{er}})\tilde{\mathbf{s}}_1 + \tilde{\boldsymbol{\eta}} \\ &= \left[\tilde{\mathbf{K}}_{1,1} + \tilde{\tilde{\mathbf{K}}}_{2,2}(\mathbf{I}_2 \otimes \mathbf{P}_{\text{er}}) \quad \tilde{\mathbf{K}}_{2,1} - \tilde{\tilde{\mathbf{K}}}_{1,2}(\mathbf{I}_2 \otimes \mathbf{P}_{\text{er}})\right] \begin{bmatrix} \tilde{\mathbf{s}}_1 \\ \tilde{\mathbf{s}}_2 \end{bmatrix} + \tilde{\boldsymbol{\eta}} \\ &= \tilde{\mathbf{K}}\tilde{\mathbf{s}} + \tilde{\boldsymbol{\eta}}. \end{aligned} \tag{5.35}$$

On this real-valued data model, one can then apply any decoder, from a (near-)ML decoder to a LZF or LMMSE decoder. In this paper, we only consider

the LMMSE decoder, and the estimated transformed symbol sequence is then given by

$$\hat{\tilde{\mathbf{s}}} = \tilde{\mathbf{K}}^H (\tilde{\mathbf{K}}\tilde{\mathbf{K}}^H + \frac{\sigma_s^2}{\sigma_n^2}\mathbf{I}_{2N})^{-1}\tilde{\mathbf{y}}. \tag{5.36}$$

From $\hat{\tilde{\mathbf{s}}}$, the original transmitted symbols can be recovered.

5.5 Simulation Results

In this section, the proposed STBC is examined and compared with other coding schemes by simulations. We only consider a system with two transmit antennas and one receive antenna. The maximum channel delay spread is set to $L = 2$. The channel taps from each transmit antenna to the receive antenna are i.i.d. complex Gaussian distributed with zero mean and variance $\mathrm{E}\{|h_{n,l}^k|^2\} = 1/(L+1)$ (i.e., uniform power delay profile) and they follow Jakes' Doppler profile [46]. QPSK symbols with energy σ_s^2 are used for transmission. The 2 orthonormal code vectors are set to $\mathbf{c}_1 = [1/\sqrt{2},\ 1/\sqrt{2}]^T$ and $\mathbf{c}_2 = [1/\sqrt{2},\ -1/\sqrt{2}]^T$, which are the columns of the 2×2 unitary Hadamard matrix. The SNR is defined as σ_s^2/σ_η^2. The normalized Doppler spread is defined as $f_d = \frac{vf}{c}T$, where v denotes the mobile velocity, f is the carrier frequency, and c is the speed of light. The receiver applies the LMMSE decoder of (5.36).

Test Case 1: We first compare the BER performance of the proposed STBC applying the LMMSE decoder of (5.36), with the performance in case we approximate the true channel by the best possible block fading CCE-BEM channel and adopt the receiver processing of Section 5.3.2. We consider large normalized Doppler spreads so that the block fading CCE-BEM can not model the time-varying channel very well, in order to show the necessity of the real-valued linear data model. We especially focus on the achievable Doppler diversity order for different Doppler spreads. The symbol block lengths in the time and frequency domain are set to $P = 14$ and $K = 7$, respectively. Fig. 5.3 shows the BER performance of a system with normalized Doppler spread $f_d = 0.002$. It can be shown that a frequency domain guard band of $Q = 1$ is enough to suppress the interference due to the time-varying channel effects. However, when the approximate block fading CCE-BEM channel is considered, we observe an error floor even with $Q = 3$ due to the channel modeling error. In Fig. 5.4, the normalized Doppler spread is increased to

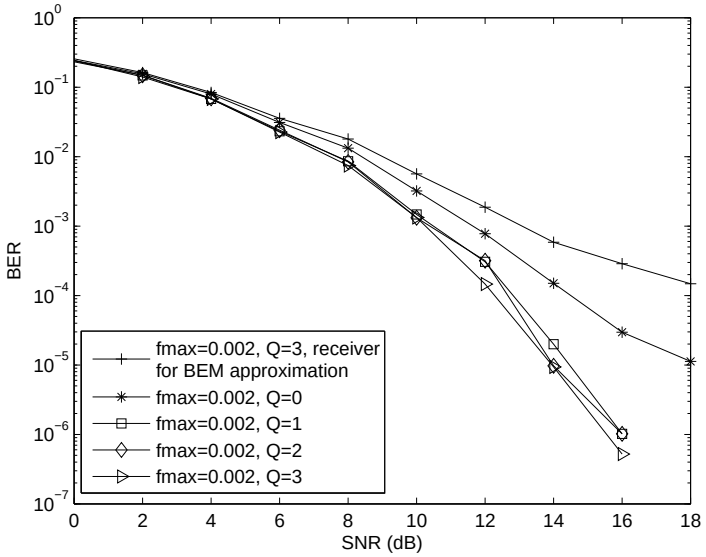

Figure 5.3: BER performance with normalized Doppler spread $f_d = 0.002$.

$f_d = 0.015$. The simulation result shows that a larger Q is required, as increasing Q leads to a better BER performance. Meanwhile, higher Doppler spreads lead to a lower BER because the Doppler diversity increases as the Doppler spread increases. On the other hand, when the approximate block fading CCE-BEM channel is considered, the receiver completely fails since it can not model such a rapidly time-varying channel. Notice that as we increase Q, the block length N increases and the spectral efficiency decreases.

Test Case 2: We next compare the proposed STBC with the DPS algorithm of [64] for doubly-selective channels. The symbol block lengths are set to $P = 27$ and $K = 8$. The frequency domain guard band length is set to $Q = 3$, which is large enough for the Doppler spread used in this simulation, for both approaches. The spectral efficiency of the proposed STBC is $\varepsilon = 0.65$, which is higher than the spectral efficiency of DPS $\varepsilon_{DPS} = 0.54$, meaning that we disfavor our approach. We use the LMMSE decoder for both algorithms. It is clearly shown in Fig. 5.5 that the proposed STBC can achieve a better BER performance due to a larger coding gain. The diversity order is almost the same for both approaches, which increases as the Doppler spread increases.

Test Case 3: Finally, we compare the proposed STBC with the STBC designed for frequency-selective channels in [56], in order to demonstrate the

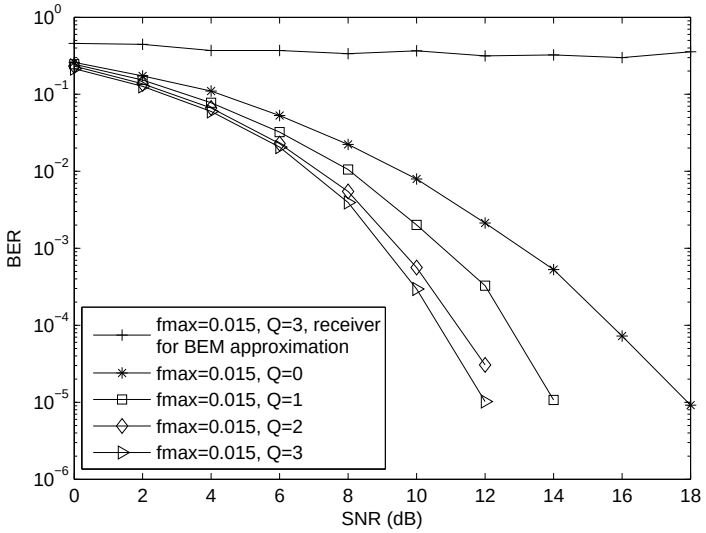

Figure 5.4: BER performance with normalized Doppler spread $f_d = 0.015$.

tradeoff between spectral efficiency, complexity, and Doppler diversity, as discussed in Section 5.3. To have the same spectral efficiency, we set $Q = 0$ for the proposed STBC, and keep $K = 5$ fixed for both approaches. Since [56] considers a purely frequency-selective channel, the decoder of [56] relies on the fact that the channel is constant during the entire space-time codeword. To obtain a fair comparison, we simulate the approach of [56] by using our receiver developed in Section 5.4, with $P = 1$ and $Q = 0$, so that the STBC design is the same as in [56], but the receiver does not require the channel to be constant. The simulation results in Fig. 5.6 show that we get a better BER performance as we increase P. But the BER performance is worse compared to the $Q > 0$ case shown in Fig. 5.5. This is due to the interference related to the lack of frequency-domain guard bands. However, Doppler diversity can still be exploited even without a frequency-domain guard band. As shown in the figure, when $P = 1$, i.e., when the data symbols are only spread in the time domain, a higher Doppler spread leads to a worse BER performance. When $P > 1$, a higher Doppler spread leads to a better BER performance, and as P increases, the BER becomes smaller due to an increasing Doppler diversity.

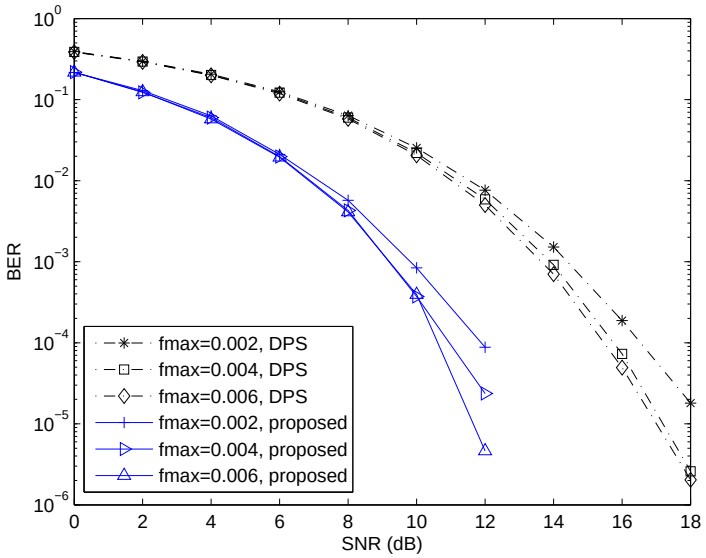

Figure 5.5: BER comparison of proposed STBC with DPS [64].

5.6 Summary

We have developed a novel STBC for multi-antenna transmissions over doubly-selective channels. By spreading the data symbols in the space-time-frequency dimensions with appropriate guard bands, the proposed STBC can achieve the full spatial, delay, and Doppler diversity, using the ML receiver as well as using a LZF or LMMSE receiver, under a specific channel model. Further, a real-valued linear data model has been presented for realistic doubly-selective channels, for which different receiver structures can be developed. Simulation results have shown significantly improved performance by jointly exploring the space-delay-Doppler diversity in doubly-selective channels.

Appendix 5.1: Proof of (5.11)

The following Kronecker product properties [78] are used throughout this appendix:

$$(\mathbf{A}_1 \otimes \mathbf{A}_2)(\mathbf{A}_3 \otimes \mathbf{A}_4) = (\mathbf{A}_1\mathbf{A}_3) \otimes (\mathbf{A}_2\mathbf{A}_4), \tag{5.37}$$

$$(\mathbf{A}_1 \otimes \mathbf{A}_2)^H = \mathbf{A}_1^H \otimes \mathbf{A}_2^H. \tag{5.38}$$

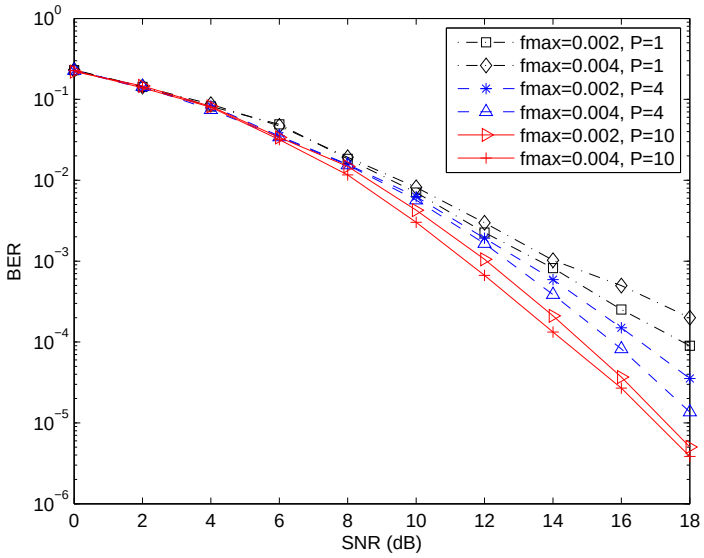

Figure 5.6: BER comparison of proposed STBC with the STBC of [56] (case $P = 1$).

First, similar to [65], we can show that $\mathbf{H}_{N,q}^{k}\mathbf{C}_u$ can be expressed as

$$\mathbf{H}_{N,q}^{k}\mathbf{C}_u = \{[\mathbf{F}_{2P'}^{H}(\mathbf{c}_u \otimes \mathbf{T}_2)] \otimes \mathbf{I}_{K'}\}(\mathbf{I}_P \otimes \mathbf{H}_{K',q}^{k}\mathbf{T}_1). \tag{5.39}$$

Then we can obtain

$$\begin{aligned}
&(\mathbf{\Lambda}_{2P',q} \otimes \mathbf{I}_{K'})\mathbf{H}_{N,q}^{k}\mathbf{C}_u \\
&= (\mathbf{\Lambda}_{2P',q} \otimes \mathbf{I}_{K'})\{[\mathbf{F}_{2P'}^{H}(\mathbf{c}_u \otimes \mathbf{T}_2)] \otimes \mathbf{I}_{K'}\}(\mathbf{I}_P \otimes \mathbf{H}_{K',q}^{k}\mathbf{T}_1) \\
&= \{\{\mathbf{\Lambda}_{2P',q}[\mathbf{F}_{2P'}^{H}(\mathbf{c}_u \otimes \mathbf{T}_2)]\} \otimes \mathbf{I}_{K'}\}(\mathbf{I}_P \otimes \mathbf{H}_{K',q}^{k}\mathbf{T}_1) \\
&= \{\mathbf{\Lambda}_{2P',q}[\mathbf{F}_{2P'}^{H}(\mathbf{c}_u \otimes \mathbf{T}_2)]\} \otimes \mathbf{H}_{K',q}^{k}\mathbf{T}_1.
\end{aligned} \tag{5.40}$$

Using the following equation, which has been proven in [65]

$$\mathbf{\Lambda}_{2P',q}[\mathbf{F}_{2P'}^{H}(\mathbf{c}_u \otimes \mathbf{T}_2)] = \mathbf{F}_{2P'}^{H}(\mathbf{c}_u \otimes \mathbf{J}_{P',q}\mathbf{T}_2), \tag{5.41}$$

we can continue deriving (5.40) as

$$\begin{aligned}
&(\mathbf{\Lambda}_{2P',q} \otimes \mathbf{I}_{K'})\mathbf{H}_{N,q}^{k}\mathbf{C}_u \\
&= [\mathbf{F}_{2P'}^{H}(\mathbf{c}_u \otimes \mathbf{J}_{P',q}\mathbf{T}_2)] \otimes \mathbf{H}_{K',q}^{k}\mathbf{T}_1 \\
&= [\mathbf{F}_{2P'}^{H}(\mathbf{c}_u \otimes \mathbf{I}_{P'})\mathbf{J}_{P',q}\mathbf{T}_2] \otimes \mathbf{H}_{K',q}^{k}\mathbf{T}_1 \\
&= \{[\mathbf{F}_{2P'}^{H}(\mathbf{c}_u \otimes \mathbf{I}_{P'})] \otimes \mathbf{I}_{K'}\}(\mathbf{J}_{P',q}\mathbf{T}_2 \otimes \mathbf{H}_{K',q}^{k}\mathbf{T}_1) \\
&= \mathbf{D}_u(\mathbf{J}_{P',q}\mathbf{T}_2 \otimes \mathbf{H}_{K',q}^{k}\mathbf{T}_1).
\end{aligned} \tag{5.42}$$

Thus, $\mathbf{H}_k\mathbf{C}_u$ can be calculated as

$$\begin{aligned}
\mathbf{H}_k\mathbf{C}_u &= \sum_{q=-Q}^{Q} (\mathbf{\Lambda}_{2P',q} \otimes \mathbf{I}_{K'})\mathbf{H}_{N,q}^{k}\mathbf{C}_u \\
&= \mathbf{D}_u \sum_{q=-Q}^{Q} (\mathbf{J}_{P',q}\mathbf{T}_2 \otimes \mathbf{H}_{K',q}^{k}\mathbf{T}_1). \\
&= \mathbf{D}_u\tilde{\boldsymbol{\mathcal{H}}}_k.
\end{aligned} \tag{5.43}$$

From [65], we know that the $N \times P'K'$ despreading matrices are mutually orthogonal tall unitary matrices, i.e.,

$$\mathbf{D}_{u'}^{H}\mathbf{D}_u = \begin{cases} \mathbf{0}_{P'K' \times P'K'}, & u' \neq u; \\ \mathbf{I}_{P'K'}, & u' = u. \end{cases} \tag{5.44}$$

Using (5.43) and (5.44), $\mathbf{D}_{u'}^{H}\mathbf{H}_k\mathbf{C}_u$ can finally be expressed as

$$\mathbf{D}_{u'}^{H}\mathbf{H}_k\mathbf{C}_u = \mathbf{D}_{u'}^{H}\mathbf{D}_u\tilde{\boldsymbol{\mathcal{H}}}_k = \begin{cases} \tilde{\boldsymbol{\mathcal{H}}}_k, & u' = u; \\ \mathbf{0}, & u' \neq u. \end{cases} \tag{5.45}$$

This concludes the proof of (5.11).

Appendix 5.2: Proof of full column rank PK for $\mathbf{H}$ in (5.25)

The compound channel matrix $\mathbf{H}$ can be expressed as

$$\begin{aligned}
\mathbf{H} &= \boldsymbol{\mathcal{G}}_{12}\mathbf{F}\mathbf{T} \\
&= (\boldsymbol{\mathcal{G}}_1^{*}\boldsymbol{\mathcal{G}}_1 + \boldsymbol{\mathcal{G}}_2^{*}\boldsymbol{\mathcal{G}}_2)^{1/2}(\mathbf{F}_{P'}\mathbf{T}_2 \otimes \mathbf{F}_{K'}\mathbf{T}_1),
\end{aligned} \tag{5.46}$$

where $\boldsymbol{\mathcal{G}}_k$ is a $P'K' \times P'K'$ diagonal matrix. We define $\boldsymbol{\mathcal{G}}_k = \text{diag}(\mathbf{V}_{1,k}, \ldots, \mathbf{V}_{P',k})$, where $\mathbf{V}_{p,k}$ is a $K' \times K'$ diagonal matrix. By stacking the diagonal elements of $\boldsymbol{\mathcal{G}}_k$ in a $P' \times K'$ matrix $\mathbf{V}_k$, we can rewrite (5.20) as

$$\mathbf{V}_k = \mathbf{B}\mathbf{G}_k, \tag{5.47}$$

where the pth row of $\mathbf{V}_k$ contains the diagonal elements of $\mathbf{V}_{p,k}$, and $\mathbf{B}$ and $\mathbf{G}_k$ are respectively a $P' \times (2Q+1)$ matrix and a $(2Q+1) \times K'$ matrix given by

$$\mathbf{B} = \begin{pmatrix} 1 & \cdots & 1 & \cdots & 1 \\ \alpha^{-Q} & \cdots & 1 & \cdots & \alpha^{Q} \\ \vdots & \ddots & \vdots & \ddots & \vdots \\ \alpha^{-(P'-1)Q} & \cdots & 1 & \cdots & \alpha^{(P'-1)Q} \end{pmatrix}, \tag{5.48}$$

$$\mathbf{G}_k = \begin{pmatrix} [\mathbf{G}_{k,-Q}]_{1,1} & \cdots & [\mathbf{G}_{k,-Q}]_{K',K'} \\ \vdots & \ddots & \vdots \\ [\mathbf{G}_{k,Q}]_{1,1} & \cdots & [\mathbf{G}_{k,Q}]_{K',K'} \end{pmatrix}, \tag{5.49}$$

where $\alpha = e^{j2\pi/P'}$. Since the diagonal elements of $\mathbf{G}_{k,q}$ and thus the elements of the qth row of $\mathbf{G}_k$ are the K'-point frequency response of $h^k_{q,l}$, and an order-L polynomial has at most L roots, it is easy to show that each row of $\mathbf{G}_k$ either contains at most L zeros, or is a full-zero row in case $\{h^k_{q,l}\}_{l=0}^{L} = 0$. This means there are at most L full-zero columns in$\mathbf{V}_k$, which occurs when each non-zero row of $\mathbf{G}_k$ has L zeros and they are located at the same position. Similarly, since an order-$2Q$ polynomial has at most $2Q$ roots, and $\mathbf{B}$ is a scaled $P' \times (2Q+1)$ Vandermonde matrix, there are at most $2Q$ zeros in each of the non-zero columns of the matrix $\mathbf{V}_k$. Finally, when $\boldsymbol{\mathcal{G}}_1$ and $\boldsymbol{\mathcal{G}}_2$ have zero elements at the same location, the corresponding elements of $\boldsymbol{\mathcal{G}}_{12}$ will be equal to zero.

We consider the case where $\boldsymbol{\mathcal{G}}_{12}$ has the maximum number of zeros, i.e., there are L full-zero columns in $\mathbf{V}_k$, and the remaining K columns of $\mathbf{V}_k$ all have $2Q$ zeros. For the zero elements in the diagonal matrix $\boldsymbol{\mathcal{G}}_{12}$, the corresponding rows of the matrix $\mathbf{F}_{P'}\mathbf{T}_2 \otimes \mathbf{F}_{K'}\mathbf{T}_1$ can be set to zero. Suppose that $\bar{\mathbf{P}}_{\text{er}}$ is a properly chosen permutation matrix that will group all the non-zero elements of $\boldsymbol{\mathcal{G}}_{12}$ at the top of the diagonal, then we can write (5.46) as

$$\mathbf{H} = \bar{\mathbf{P}}_{\text{er}}\bar{\mathbf{H}}, \tag{5.50}$$

where

$$\bar{\mathbf{H}} = \begin{pmatrix} \bar{\boldsymbol{\mathcal{G}}}_{12}\bar{\mathbf{F}}_{PK} \\ \mathbf{0}_{(P'L+2QK)\times PK} \end{pmatrix}, \tag{5.51}$$

with

$$\bar{\mathbf{F}}_{PK} = \begin{pmatrix} \mathbf{f}_K^1 \otimes \mathbf{F}_P^1 \\ \mathbf{f}_K^2 \otimes \mathbf{F}_P^2 \\ \vdots \\ \mathbf{f}_K^K \otimes \mathbf{F}_P^K \end{pmatrix}, \tag{5.52}$$

where the $PK \times PK$ diagonal matrix $\bar{\boldsymbol{\mathcal{G}}}_{12}$ contains the nonzero elements of $\boldsymbol{\mathcal{G}}_{12}$, $\{\mathbf{f}_K^k\}_{k=1}^K$ are the corresponding K nonzero rows of the matrix $\mathbf{F}_{K'}\mathbf{T}_1$, and $\{\mathbf{F}_P^k\}_{k=1}^K$ are the $P \times P$ matrices containing the corresponding nonzero rows of the matrix $\mathbf{F}_{P'}\mathbf{T}_2$. It can be shown that the only solution of $\bar{\mathbf{F}}_{PK}^T\mathbf{x} = \mathbf{0}$ is $\mathbf{x} = \mathbf{0}$, due to the Vandermonde structure of the matrices $\mathbf{F}_{K'}\mathbf{T}_1$ and $\mathbf{F}_{P'}\mathbf{T}_2$, which means that the rows of the matrix $\bar{\mathbf{F}}_{PK}$ are independent. As $\bar{\mathbf{F}}_{PK}$ is a $PK \times PK$ square matrix, $\bar{\mathbf{F}}_{PK}$ thus has full rank PK. Since left-multiplying with a non-singular matrix does not change the rank of the original matrix, we can conclude that the composite channel matrix $\bar{\mathbf{H}}$ and thus $\mathbf{H}$ are full column rank matrices when $\boldsymbol{\mathcal{G}}_{12}$ has the maximum number of zeros.

When $\boldsymbol{\mathcal{G}}_{12}$ has less zeros on the diagonal, and thus more rows of the matrix $\mathbf{F}_{P'}\mathbf{T}_2 \otimes \mathbf{F}_{K'}\mathbf{T}_1$ are included, the column rank of $\mathbf{H}$ will not reduce. Hence, $\mathbf{H}$ has full column rank PK for all $\mathbf{h} \neq \mathbf{0}$. This concludes the proof.

Chapter 6

Conclusions and Future Work

6.1 Conclusions

Modern wireless communication systems need to operate in frequency-selective and time-varying (doubly-selective) channels, as they require high transmission rates, as well as need to support high mobile speeds. In this thesis, we first focused on the receiver design for block transmission over doubly-selective channels, specifically, iterative channel estimation and turbo equalization for OFDM and single carrier (SC) systems. Later, we developed novel STBC for multi-antenna systems in doubly-selective channels.

6.1.1 Iterative Channel Estimation and Turbo Equalization

OFDM and SC with CP are important transmission schemes for next generation wireless communications. However, both SC and OFDM systems with CP suffer from doubly-selective channels, which require appropriate ICI mitigation methods. The problem is how to design equalization and channel estimation algorithms, which can achieve good performance, as well as have a low complexity.

We exploited the property that the frequency-domain channel matrix is almost banded, i.e., the most significant elements occur around the main diagonal, due to the limited support of the Doppler spread. We first derived block turbo MMSE equalizers for OFDM systems in time-varying channels, as an alternative to serial turbo MMSE equalization, to achieve a better per-

formance. The presented equalizers are based on a soft MMSE block linear equalizer, and exploit both the banded structure of the frequency-domain channel matrix and receiver windowing. Therefore, their complexities will be linear in the number of subcarriers. Later, we applied the block philosophy to design a soft MMSE turbo equalizer for SC systems in doubly-selective channels. Similarly to the OFDM case, we perform block equalization in the frequency domain, exploiting the banded structure of the frequency-domain channel matrix. An interesting feature of the proposed equalizer is its reduced computational complexity, which scales only linearly with the block length. As a result, in doubly-selective channels with significant multipath delay spread, our frequency-domain approach is less complex than time-domain equalizers.

The aforementioned equalization algorithms require an accurate channel estimation at the receiver. The ICI caused by Doppler spreading makes the channel estimation problem more challenging. We derived iterative pilot-assisted channel estimators for both OFDM and SC systems. Specifically, in each channel estimation iteration, we also exploit the soft data estimates obtained from the turbo equalizer. These data estimates are used as additional virtual pilots, and their reliability, also obtained from the turbo equalizer, is included in the channel estimation process. As a result, the proposed channel estimators are well matched to the proposed turbo equalizers, since both channel estimation and equalization are performed iteratively, with mutual exchange of soft information. For both OFDM and SC cases, the proposed channel estimators firstly estimate the time-domain channel exploiting the BEM, and then transform the time-domain channel into the frequency-domain for equalization purposes. In addition, to keep low-complexity processing, we simplify our channel estimators by locating the pilot symbols in the same domain as where the data symbols are placed. This means that we assume frequency-domain pilot tones in OFDM systems, and time-domain pilot symbols in SC systems.

6.1.2 STBC for Doubly-Selective Channels

The second part of the thesis focused on STBC design for multi-antenna systems in doubly-selective channels. STBC has been introduced to achieve the spatial diversity offered by multiple transmit and/or receive antennas. However, as STBC is typically designed for flat-fading channels, the time and frequency selectivity will seriously degrade the system performance. The challenge is how to design STBC which can still achieve a good performance under such hostile channel conditions.

The proposed technique can be interpreted as the extension of the Alamouti code to doubly-selective channels, and relies on a joint time-frequency reversal of the transmitted sequences. Assuming a block fading channel where the time-variation from subblock to subblock is modeled by a CCE-BEM, the proposed STBC belongs to the class that achieves full spatial, delay, and Doppler diversity using a ML receiver, as well as a LZF or LMMSE receiver. For realistic doubly-selective channels, which can not exactly be modeled by a block fading CCE-BEM channel, a real-valued linear data model is presented, for which different receiver structures can be developed.

6.2 Future Research

Optimal Training for Realistic BEMs

In this thesis, we focus on channel estimation, assuming a multiplexed training scheme with pilot symbols and data symbols being interleaved to form the transmitted signal vector. The FDKD pilot structure [43] for OFDM systems, and its dual scheme, the TDKD [44] pilot structure for SC systems, are proved to be optimal in minimizing the channel mean-square error as well as in maximizing the achievable rate. However, the above analysis relies on the CCE-BEM, which is not very accurate for modeling the doubly-selective channels. Thus, a further study on optimal pilot patterns under other and better channel models is necessary.

Exploiting Channel Tap Correlations

In most of the existing works, different channel taps are assumed to be independent in the channel model. However, under certain channel conditions, correlations between channel taps can be exploited to simplify the channel model and to improve the channel estimation accuracy. For example, in underwater acoustic communications, the transmitter may be constantly floating vertically, which leads to a time-varying channel even when the receiver is not moving. It has been shown in [92] that a similar phase shift is introduced across all the channel taps because of this effect. In some cases, it is therefore better to take possible correlations into account to improve the channel modeling accuracy.

Iterative Receiver Performance Analysis

In this thesis, we focus on the equalizer design only. On the other hand, error correction codes also plays an important role in the system performance. How to jointly design the iterative equalizer and decoder needs to be further investigated. Specifically, An extrinsic information transfer chart can be used to analyze the extrinsic information flow among different components of the receiver, i.e., equalizer, decoder, and channel estimator, which is very helpful to find the bottleneck which limits the iterative processing gains.

Compressive Sensing

Compressive sensing (CS) allows the efficient reconstruction of sparse signals from a limited number of measurement samples [84]. Recently, CS has been applied to the channel estimation problem under time-varying channels [85]. Compared to the conventional approach, the CS technique can exploit the sparsity of the channel in the time, frequency and spatial domain, which can potentially decrease the number of pilot symbols needed to get an accurate channel estimation. Thus, it could be interesting to study the inherent sparsity in doubly-selective channels, which could be used to optimize the basis functions to approximate the time-varying channel and to reduce the number of BEM coefficients.

Bibliography

[1] R. van Nee and R. Prasad, *OFDM for Wireless Multimedia Communications,* Artech House, 2000.

[2] G. Faria, J. A. Henriksson, E. Stare, and P. Talmola, "DVB-H: digital broadcasting sevices to handheld devices," *Proc. IEEE,* vol. 94, pp. 194-209, no. 1, Jan. 2006.

[3] Z. Wang and G. B. Giannakis, "Wireless multicarrier communications: where Fourier meets Shannon," *IEEE Signal Processing Mag.,* vol. 17, pp. 29-48, May 2000.

[4] T. Wang, J. G. Proakis, E. Masry, and J. R. Zeidler, "Performance degradation of OFDM systems due to Doppler spreading," in *IEEE Trans. Wireless Commun.*, vol. 5, pp. 1422-1432, Jun. 2006

[5] I. Barhumi, G.Leus, and M. Moonen, "Equalization for OFDM over doubly-selective channels," *IEEE Trans. Signal Processing,* vol. 54, pp. 1445-1458, Apr. 2006.

[6] A. Stamoulis, S. N. Diggavi, and N. Al-Dhahir, "Intercarrier interference in MIMO OFDM," *IEEE Trans. Signal Processing,* vol. 50, pp. 2451-2464, Oct. 2002.

[7] X. Huang and H.-C. Wu, "Robust and efficient intercarrier interference mitigation for OFDM systems in time-varying fading channels," *IEEE Trans. Veh. Technol.,* vol. 56, pp. 2517-2528, Sep. 2007.

[8] W. G. Jeon, K. H. Chang, and Y. S. Cho, "An equalization technique for orthogonal frequency-division multiplexing systems in time-variant multipath channels," *IEEE Trans. Commun.*, vol. 47, pp. 27-32, Jan. 1999.

[9] L. Rugini, P. Banelli, and G. Leus, "Simple equalization of time-varying channels for OFDM," *IEEE Commun. Lett.*, vol. 9, pp. 619-621, Jul. 2005.

[10] P. Schniter, "Low-complexity equalization of OFDM in doubly selective channels," *IEEE Trans. Signal Processing*, vol. 52, pp. 1002-1011, Apr. 2004.

[11] L. Rugini, P. Banelli, and G. Leus, "Low-complexity banded equalizers for OFDM systems in Doppler spread channels," *EURASIP J. Appl. Signal Processing*, vol. 2006, pp. 1-13, 2006, Article ID 67404.

[12] A. Gorokhov and J.P. Linnartz, "Robust OFDM receivers for dispersive time varying channels: Equalization and channel acquisition," *IEEE Trans. Commun.,* vol. 52, pp. 572-583, Apr. 2004.

[13] Y.-S. Choi, P. J. Voltz, and F. A. Cassara, "On channel estimation and detection for multicarrier signals in fast and selective Rayleigh fading channels," *IEEE Trans. Commun.,* vol. 49, pp. 1375-1387, Aug. 2001.

[14] X. Cai and G. B. Giannakis, "Bounding performance and suppressing intercarrier interference in wireless mobile OFDM," *IEEE Trans. Commun.,* vol. 51, pp. 2047-2056, Dec. 2003.

[15] S. Tomasin, A. Gorokhov, H. Yang and J. P. Linnartz, "Iterative interference cancellation and channel estimation for mobile OFDM," *IEEE Trans. Wireless Commun.*, vol. 4, pp. 238-245, Jan. 2005

[16] Y. Zhao and S.G. Haggman, "Intercarrier interference self-cancellation scheme for OFDM mobile communication systems," *IEEE Trans. Commun.,* vol. 49, pp. 1185-1191, Jul. 2001.

[17] S.-J. Hwang and P. Schniter, "Efficient sequence detection of multicarrier transmissions over doubly dispersive channels," *EURASIP J. Appl. Signal Processing,* vol. 2006, pp. 1-17, 2006, Article ID 93638.

[18] S. Ohno, "Maximum likelihood inter-carrier interference suppression for wireless OFDM with null subcarriers," *Proc. of ICASSP*, vol. 3, pp. 849-852, Mar. 2005.

[19] M. Tüchler, R. Koetter, and A. C. Singer, "Turbo equalization: principles and new results", *IEEE Trans. Commun.,* vol. 50, pp. 754-767, May 2002.

[20] M. Tüchler, A. C. Singer, and R. Koetter, " Minimum mean squared error equalization using a priori information," *IEEE Trans. Signal Processing,* vol. 50, pp. 673-683, Mar. 2002.

[21] M. A. Dangl, C. Sgraja, and J. Lindner, "An improved block equalization scheme for uncertain channel estimation," *IEEE Trans. Wireless Commun.*, vol. 6, pp. 146-156, Jan. 2007

[22] X. Wang and H. Poor, "Iterative (turbo) soft interference cancellation and decoding for coded CDMA," *IEEE Trans. Commun.,* vol. 47, pp. 1046-1061, Jul. 1999.

[23] Z. Tang, R. C. Cannizzaro, G. Leus, and P. Banelli, "Pilot-assisted time-varying channel estimation for OFDM systems," *IEEE Trans. Signal Processing,* vol. 55, pp. 2226-2238, May 2007.

[24] R. Otnes and M. Tüchler, "Iterative channel estimation for turbo equalization of time-varying frequency-selective channels," *IEEE Trans. Wireless Commun.*, vol. 3, pp. 146-156, Nov. 2004

[25] H. V. Poor, *An Introduction to Signal Detection and Estimation,* 2nd ed. New York: Springer-Verlag, 1994, pp. 221-229.

[26] H. V. Poor and S. Verdu, "Probability of error in MMSE multiuser detection," *IEEE Trans. Inf. Theory,* vol. 43, pp. 858-871, May 1997.

[27] J. M. Cioffi, G. P. Dudevoir, M. V. Eyuboglu, and G. D. Forney Jr., "MMSE decision-feedback equalizers and coding - Part I: Equalization results," *IEEE Trans. Commun.,* vol. 43, pp. 2582-2594, Oct. 1995.

[28] T. K. Moon and W. C. Stirling, *Mathematical methods and algorithms for signal processing.* Prentice Hall, 2000

[29] A. Asif and J. M. F. Moura, "Block matrices with L-block-banded inverse: Inversion algorithms," *IEEE Trans. Signal Processing,* vol. 53, pp. 630-642, Feb. 2005.

[30] Z. Tang, G. Leus and P. Banelli, "Pilot-assisted time-varying OFDM channel estimation based on multiple OFDM symbols," in *Proc. Workshop on Signal Processing Advances in Wireless Communications (SPAWC),* Cannes, France, Jul. 2006.

[31] M. Visintin, "Karhunen-Loeve expansion of a fast Rayleigh fading process," *IEEE Electron. Lett.,* vol. 32, pp. 1712-1713, Aug. 1996.

[32] 3GPP TS 36.201 - v1.0.0, "LTE Physical Layer - General Description", Mar. 2007.

[33] F. Pancaldi, G. Vitetta, R. Kalbasi, N. Al-Dhahir, M. Uysal, and H. Mheidat, "Single-carrier frequency-domain equalization: a review," *in IEEE Signal Processing Magazine,* pp. 37-56, Sep. 2008.

[34] M. Tüchler and J. Hagenauer, "Turbo equalization using frequency domain equalizers," in *Proc. Allerton Conf.,* Monticello, Oct. 2000.

[35] S. Ahmed, M. Sellathurai, S. Lambotharan, and J. Chambers, "Low-complexity iterative method of equalization for single carrier with cyclic prefix in doubly selective channels," *IEEE Signal Processing Letters,* pp. 5-8, Jan. 2006.

[36] K. Fang and G. Leus, "Space-time block coding for doubly-selective channels," *IEEE Trans. Signal Processing,* submitted.

[37] K. Fang, L. Rugini and G. Leus, "Low-complexity block turbo equalization for OFDM systems in time-varying channels," *IEEE Trans. Signal Processing,* vol. 56, no. 11, pp. 5555-5566, Nov. 2008.

[38] S. He and J.K. Tugnait, "On doubly selective channel estimation using superimposed training and discrete prolate spheroidal sequences," *IEEE Trans. Signal Processing,* vol. 56, no. 7, pp. 3214-3228, Jul. 2008.

[39] K. Teo and S. Ohno, "Pilot-aided channel estimation and viterbi equalization for OFDM over doubly-selective channel," *IEEE Global Telecommunications Conference (Globecom),* San Francisco, CA, Dec. 2008.

[40] P. Schniter and H. Liu, "Iterative frequency-domain equalization for single-carrier systems in doubly dispersive channels," *Proc. Asilomar Conf. on Signals, Systems, and Computers,* pp. 667-671, Nov. 2004.

[41] H. Liu and P. Schniter, "Iterative frequency-domain channel estimation and equalization for single-carrier transmissions without cyclic-prefix," *IEEE Trans. Wireless Commun.,* pp. 3686-3691, Oct. 2008.

[42] J. Bonnet and G. Auer, "Optimized iterative channel estimation for OFDM," *Proc. of VTC'F06*, Montreal, Canada, Sep. 2006.

[43] A. Kannu and P. Schniter, "Design and analysis of MMSE pilot-aided cyclic-prefixed block transmission for doubly selective channels", *IEEE Trans. Signal Processing,* vol. 56, no. 3, pp. 1148-1160, Mar. 2008.

[44] X. Ma, G. Giannakis and S. Ohno, "Optimal training for block transmissions over doubly selective wireless fading channels," *IEEE Trans. Signal Processing,* vol. 51, nr. 5, pp. 1351-1366, May. 2003.

[45] Z. Wang, X. Ma, and G. B. Giannakis, "OFDM or single-carrier block transmissions?," *IEEE Trans. Commun.,* pp. 380-394, Mar. 2004.

[46] W. C. Jakes, *Microwave Mobile Channels.* Wiley, 1974.

[47] B. K. Ng and D. Falconer, "A novel frequency domain equalization method for single-carrier wireless transmissions over doubly-selective fading channels," *Proc. of Globecom,* Dallas, TX, Nov. 2004.

[48] L. Tong, B.M. Sadler, and M. Dong, "Pilot assisted wireless transmissions - general model, design criteria, and signal processing," *IEEE Signal Processing Mag.,* vol. 21, no. 6, pp. 12-25, Nov. 2004.

[49] M. Dong, L. Tong, and Brian M. Sadler, "optimal insertion of pilot symbols for transmissions over time-varying flat fading channels," *IEEE Trans. Signal Processing,* vol. 52, no. 2, pp. 1403-1418, May 2004.

[50] K. Fang, L. Rugini and G. Leus, "Low-complexity frequency-domain turbo equalization for single-carrier transmissions over doubly-selective channels," *Proc. of Intl. Conf. on Acoustics, Speech and Signal Processing (ICASSP 2009)*, Taipei, Taiwan, Apr. 2009.

[51] A. M. Sayeed and B. Aazhang, "Joint Multipath-Doppler Diversity in Mobile Wireless Communications," *IEEE Trans. on Communications,* vol. 47, no. 1, pp. 123-132, Jan. 1999.

[52] X. Ma and G. B. Giannakis, "Maximum-diversity transmissions over doubly selective wireless channels," *IEEE Trans. Inform. Theory,* vol. 49, no. 7, pp. 1832-1840, Jul. 2003.

[53] L. Zheng and D.N.C. Tse, "Diversity and multiplexing: A fundamental tradeoff in mulitple antenna channels," *IEEE Trans. on Inform. Theory,* vol. 49, no. 5, pp. 1073-1096, May. 2003.

[54] V. Tarokh, H. Jafarkhani, and A. R. Calderbank, "Space-time block codes from orthogonal designs," *IEEE Trans. Inform. Theory*, vol. 45, no. 5, pp. 1456-1467, Jul. 1999.

[55] S. M. Alamouti, "A simple transmit diversity technique for wireless communications," *IEEE J. Select. Areas Commun.,* vol. 16, no. 8, pp. 1451-1458, Oct. 1998.

[56] S. Zhou and G. B. Giannakis, "Single-carrier space-time block coded transmissions over frequency-selective fading channels," *IEEE Trans. Inf. Theory,* vol. 49, no. 1, pp. 164-179, Jan. 2003.

[57] E. Lindskog and A. Paulraj, "A transmit diversity scheme for channels with intersymbol interference," in *Proc. IEEE International Conference on Communications (ICC),* New Orleans, USA, Jun. 2000.

[58] N. Al-Dhahir, "Single-carrier frequency-domain equalization for space time block-coded transmissions over frequency-selective fading channels," *IEEE Commun. Lett.,* vol. 5, no. 7, pp. 304-306, Jul. 2001.

[59] H. Bölcskei and A. J. Paulraj, "Space-frequency coded broadband OFDM systems," in *Proc. Wireless Commun. Networking Conf. (WCNC),* Chicago, IL, Sep. 2000.

[60] H. Bölcskei and A. J. Paulraj, "Space-frequency codes for broadband fading channels," in *Proc. IEEE Int. Symp. Inform. Theory (ISIT),* Washington, DC, Jun. 2001.

[61] Z. Liu, Y. Xin, and G. B. Giannakis, "Space-time-frequency coded OFDM over frequency-selective fading channels," *IEEE Trans. Signal Process.,* vol. 50, no. 10, pp. 2465-2476, Oct. 2002.

[62] X. Ma and G. B. Giannakis, "Space-time-multipath coding using digital phase sweeping or circular delay diversity," *IEEE Trans. Signal Processing,* vol. 53, no. 3, pp. 1121-1130, Mar. 2005.

[63] X. Ma, G. Leus and G. B. Giannakis, "Space-time-Doppler block coding for correlated time-selective fading channels," *IEEE Trans. Signal Process.,* vol. 53, no. 6, pp. 2167-2181, Jun. 2005.

[64] X. Ma and G. B. Giannakis, "Space-time coding for doubly selective channels," in *Proc. International Symposium on Circuits and Systems (ISCAS),* vol. 3, May 2002, pp. 647-650.

[65] G. Leus, S. Zhou, and G. B. Giannakis, "Orthogonal multiple access over time- and frequency-selective channels," *IEEE Trans. Inform. Theory,* vol. 49, no. 8, pp. 1942-1950, Aug. 2003.

[66] G. Leus, "On the estimation of rapidly time-varying channels," *IEEE Trans. Inform. Theory,* in *EUSIPCO*, Vienna, Austria, Sept. 2004

[67] D. K. Borah and B. D. Hart, "Frequency-selective fading channel estimation with a polynomial time-varying channel model," *IEEE Trans. on Commun.,* vol. 47, no. 6, pp. 862-873, Jun. 1999.

[68] G. B. Giannakis and C. Tepedelenlioglu, "Basis Expansion Models and Diversity Techniques for Blind Identification and Equalization of Time-Varying Channels," *Proc. IEEE,* vol. 86, no. 10, pp. 1969-1986, Oct. 1998.

[69] T. Zemen and C. F. Mecklenbraüker, "Time-variant channel estimation using discrete prolate spheroidal sequences," *IEEE Trans. Signal Process.,* vol. 53, no. 9, pp. 3597-3607, Sep. 2005.

[70] H. Bölcskei, R. Koetter, and S. Mallik, "Coding and modulation for underspread fading channels," in *Proc. IEEE Int. Symp. Inform. Theory (ISIT),* Lausanne, Switzerland, Jun. 2002.

[71] K. Liu, T. Kadous, and A. M. Sayeed, "Orthogonal time-frequency signaling over doubly dispersive channels," *IEEE Trans. Inform. Theory,* vol. 50, no. 11, pp. 2583-2603, Nov. 2004.

[72] S. Geirhofer, L. Tong, and A. Scaglione, "Time-Reversal Space-Time Coding for Doubly-Selective Channels," in *Proc. Wireless Commun. Networking Conf. (WCNC),* Las Vegas, NV, USA, Apr. 2006.

[73] K. Fang and G. Leus, "Iterative channel estimation and turbo equalization for time-varying OFDM systems," in *Proc. IEEE International Conference on Acoustics, Speech, and Signal Processing (ICASSP),* Las Vegas, NV, USA, Mar. 2008.

[74] K. Fang, L. Rugini and G. Leus, "Block Transmission over Doubly-Selective Channels: Iterative Channel Estimation and Turbo Equalization," *Eurasip J. Advances in Signal Processing,* submitted.

[75] G. B. Giannakis, Y. Hua, P. Stoica, and L. Tong, eds., *Signal Processing Advances in Wireless and Mobile Communications: Trends in Single- and Multi-user Systems.* vol. 2, Prentice Hall, 2000

[76] X. Ma, and W. Zhang, "Fundamental limits of linear equalizers: diversity, capacity and complexity," *IEEE Trans. Inform. Theory,* to appear.

[77] E.Telatar, "Capacity of Multi-antenna Gaussian Channels," *Euro. Transactions on Telecommunication*, vol. 10, pp. 585-595, Nov. 1999.

[78] R. A. Horn and C. R. Johnson, *Matrix Analysis.* Cambridge Univ. Press, 1991.

[79] T. Rappaport, *Wireless Communications Principles and Practice.* Prentice Hall, 2002

[80] P. A. Bello, "Characterization of randomly time-variant linear channels," *IEEE Trans. Circuits and Systems,* vol. CS-11, no. 4, pp. 360-393, Dec. 1963.

[81] P. A. van Walree, Trond Jenserud and Morten Smedsrud, "A discrete-time channel simulator driven by measured scattering functions," *IEEE J. Select. Areas Commun.,* vol. 26, no. 9, pp. 1628-1637, Dec. 2008.

[82] G. Leus and P. van Walree, "Multiband OFDM for Covert Acoustic Communications," *IEEE J. Select. Areas Commun.,* vol. 26, no. 9, pp. 1662-1673, Dec. 2008.

[83] S. Mason, C. R. Berger, S. Zhou, and P. Willett, "Detection, Synchronization, and Doppler Scale Estimation with Multicarrier Waveforms in Underwater Acoustic Communication," *IEEE J. Select. Areas Commun.,* vol. 26, no. 9, pp. 1638-1649, Dec. 2008.

[84] D. L. Donoho, "Compressed sensing," *IEEE Trans. Inform. Theory,* vol. 52, pp. 1289-1306, Apr. 2006.

[85] Georg Tauböck and Franz Hlawatsch, "A compressed sensing technique for OFDM channel estimation in mobile environments: Exploiting channel sparsity for reducing pilots," in *Proc. IEEE International Conference on Acoustics, Speech, and Signal Processing (ICASSP),* Las Vegas, NV, USA, Mar. 2008.

[86] S. M. Kay, *Fundamentals of Statistical Signal Processing, Vol. I - Estimation Theory,* Prentice Hall, 1993.

[87] L. Deneire, B. Gyselinckx, and M. Engels, "Training sequence versus cyclic prefix - a new look on single carrier communication," *IEEE Communications Letters,* vol. 7, no. 5, pp. 292-294, 2001.

[88] H. Boelcskei, D. Gesbert, C. Papadias, A. J. van der Veen, "Space-Time Wireless Systems: From Array Processing to MIMO Communications." Cambridge University Press, 2006.

[89] M. Visintin, "Karhunen-Loeve expansion of a fast Rayleigh fading process," *IET Electronics Letters,* 32(18):1712-1713, Aug. 1996.

[90] M. Dong, L. Tong, and B. Sadler, "Optimal insertion of pilot symbols for transmissions over time-varying flat fading channels," *IEEE Trans. Signal Processing,* vol. 52, pp. 1403-1418, May 2004.

[91] B. Picinbono, "On circularity," *IEEE Trans. Signal Processing,* vol. 42, no. 12, pp. 3473-3482, Dec. 1994.

[92] P. A. van Walree, T. Jenserud, and M. Smedsrud, "A discrete-time channel simulator driven by measured scattering functions," *IEEE J. Select. Areas Commun,* vol. 26, no. 8, pp. 1628-1637, Dec. 2008.

Samenvatting

Draadloze breedbandige communicatiesystemen vereisen hoge transmissiesnelheden, waarbij de bandbreedte van het verstuurde signaal groter is dan bandbreedte waarover de frequentieresponsie van het kanaal constant verondersteld kan worden. Hierdoor worden de verstuurde symbolen uitgesmeerd over de tijd, ofwel worden de verschillende frequentiecomponenten verschillend verzwakt (frequentie-selectiviteit). De verschillende ontvangen symbolen gaan elkaar storen, omdat de diverse transmissiepaden in het kanaal vertragingen ondervinden die groter zijn dan de tijdsduur van een symbool. Recente communicatiestandaarden zoals WiMAX en LTE eisen niet alleen hoge bitsnelheden, maar moeten ook hoge snelheden van de mobiele terminals toelaten. De resulterende Doppler-verschuivingen introduceren snelle variaties in het kanaal, waarbij de tijd dat het kanaal constant is korter is dan de duur van een symbool. De Dopplerspreiding geeft aanleiding tot frequentie-dispersie (tijd-selectiviteit).

LTE is een grote stap naar een nieuwe generatie van mobiele netwerken. De LTE fysieke laag heeft een toegangs-controlesysteem gebaseerd op OFDM met een cyclische prefix (CP) in de verbinding van het basisstation met de gebruiker, en een enkel-kanaals SC-FDMA met CP in de retourverbinding. OFDM is een van de belangrijkste technieken voor draadloze communicatie, en wordt al gebruikt in diverse standaarden zoals DVB-T/H, DAB, en IEEE 802.11. OFDM kan de onderlinge storingen tussen bits in een statisch frequentie-selectief kanaal voorkomen, doordat het deze omzet in een verzameling onafhankelijke niet-selectieve kanalen, zodat simpele egalisators van orde 1 per subband mogelijk zijn. Een enkelkanaals systeem kan ook beschouwd worden als een OFDM systeem met een DFT precoder. Zo'n systeem heeft een kleiner piekvermogen dan een regulier OFDM systeem. De prestatie en complexiteit is vergelijkbaar met OFDM, maar de complexiteit is verschoven van de zender naar de ontvanger. Hierdoor kunnen de mobiele terminals meer vermogens-efficient zenden. Echter, beide systemen hebben last van de door Doppler

veroorzaakte tijdvari erende kanalen, waardoor de onafhankelijkheid tussen de subbanden wordt verstoord. De resulterende storing tussen subbanden is erg nadelig voor de simpele egalisators. Tegelijkertijd is het ook moeilijker het kanaal te schatten, wat nodig is voor een coherente ontvanger waarbij de egalisator het kanaal inverteert. Hierdoor zijn meer geavanceerde technieken nodig om het tijd- en frequentieselectieve kanaal (ofwel dubbel-selectieve kanaal) te modelleren en de optredende verstoringen op te heffen.

In de laatste 10 jaar zijn systemen met meerdere antennes uitgebreid bestudeerd. Het gebruik van meerdere zend- of ontvangstantennes kan de prestatie van communicatiesystemen beduidend verbeteren, zoals de kanaalcapaciteit en de betrouwbaarheid. STBC is een ruimte-tijd coderingstechniek die de spatiele diversiteit die meerdere antennes bieden optimaal benut. Echter, zulke systemen zijn vooral bestudeerd voor frequentie-constante kanalen; tijd- en frequentieselectiviteit zullen de systeemprestatie significant verslechteren. Het is daarom van belang efficiente STBC technieken te ontwikkelen die hiermee om kunnen gaan.

Het eerste deel van het proefschrift kijkt naar het ontwerp van de ontvanger voor blok-transmissies over dubbel-selectieve kanalen. In het bijzonder worden algoritmes afgeleid voor iteratieve kanaalschatting en turbo-egalisatie met lage complexiteit voor OFDM en enkel-kanaalssystemen. Het tweede deel van het proefschrift kijkt naar STBC ontwerp voor een systeem met meerdere antennes en dubbel-selectieve kanalen. Het voorgestelde STBC ontwerp is afgeleid voor een systeem met 2 zendantennes en 1 ontvangstantenne, maar het is eenvoudig om de idee en uit te breiden naar algemene systemen met meer antennes.

Acknowledgment

I would like to thank my advisor Dr. Geert Leus for giving me the opportunity to start my PhD study at Delft. During the past four and half years, I learned how to conduct research under his guidance and support which led to this thesis. I also want to show my great gratitude to my promotor, Prof. Alle-Jan van der Veen, who has shown me a good example how to be a good researcher. Many thanks to the PhD committee members, for their time and comments to improve the quality of this thesis.

I have a great time in the Circuits and Systems group during my study at Delft. Special thanks to the CAS alumni, Dr. Luca Rugini and Dr. Zijian Tang, for the time they spent with me in discussing and helping me to transit from information theory to signal processing area in the early years of my PhD. I am lucky to have many nice colleagues and friends on the 17th floor, thank you Laura for helping me to solve many administrative works, and thank you Antoon for constantly helping me with the computer problems. My gratitude to all the other PhD students and colleagues, Claude, Yu, Yiyin, Zhifeng, Zoubir, Sina, Kees-Jan, Tao, Vijay, thank you for your help and the time being together.

During my studies at Univ. of Science and Technology of China, at ETH Zurich, and at TU Delft, I feel so fortunate to have many good friends, Thank you for lighting up my life.

List of Publications

Journal Papers:

1. K. Fang, L. Rugini and G. Leus, "Block Transmission over Doubly-Selective Channels: Iterative Channel Estimation and Turbo Equalization," *Eurasip J. Advances in Signal Processing,* submitted.

2. K. Fang and G. Leus, "Space-Time Block Coding for Doubly-Selective Channels," *IEEE Trans. Signal Processing,* Mar. 2009.

3. K. Fang, L. Rugini and G. Leus, "Low-complexity block turbo equalization for OFDM systems in time-varying channels," *IEEE Trans. Signal Processing,* vol. 56, no. 11, pp. 5555-5566, Nov. 2008.

Conference Papers:

1. K. Fang and G. Leus, "Space-Time Block Coding for Frequency-Selective and Time-Varying Channels," in *Proc. 43rd Asilomar Conf. Signals, Systems, and Computers,* Pacific Grove, CA, Nov. 2009.

2. L. Rugini, P. Banelli, K. Fang and G. Leus, "Enhanced Turbo MMSE Equalization for MIMO-OFDM over Rapidly Time-Varying Frequency-Selective Channels," in *Proc. of Intl. Workshop on Signal Processing Advances in Wireless Communication (SPAWC 2009),* Perugia, Italy, Jul. 2009.

3. K. Fang, L. Rugini and G. Leus, "Low-Complexity Frequency-Domain Turbo Equalization for Single-Carrier Transmissions over Doubly-Selective Channels," in *Proc. IEEE International Conference on Acoustics, Speech, and Signal Processing (ICASSP),* Taipei, Taiwan, Apr. 2009.

4. K. Fang, L. Rugini and G. Leus, "Iterative channel estimation and turbo equalization for time-varying OFDM systems," in *Proc. IEEE International Conference on Acoustics, Speech, and Signal Processing (ICASSP),* Las Vegas, NV, USA, Mar. 2008.

5. K. Fang and G. Leus, "Low-Complexity Block Turbo Equalization for OFDM Systems in Time-varying Channels," in *Proc. IEEE International Conference on Acoustics, Speech, and Signal Processing (ICASSP),* Honolulu, Hawaii, Apr. 2007.

6. K. Fang and G. Leus, "Low-Complexity Block Turbo Equalization for OFDM Systems in Time- and Frequency-Selective Channels," in *Proc. 3rd Annual IEEE Benelux/DSP Valley Signal Processing Symposium,* Antwerp, Belgium, pp. 83-87, Mar. 2007.

7. K. Fang, G. Leus, and L. Rugini, "Alamouti space-time coded OFDM systems in time- and frequency-selective channels," in *Proc. of Globecom Conf. (Globecom 2006),* St. Francisco, CA, Nov. 2006.

Curriculum Vitae

Kun Fang was born in Tianjin, China, on Jan. 5th, 1981. He graduated from Tianjin NanKai Hight School in 1999. He then received the B.E. degree in electrical engineering from University of Science and Technology of China in Jul. 2003, and the M.S. degree in electrical engineering from Swiss Federal Institute of Technology (ETH), Zurich, Switzerland in Jul. 2005. Since Aug. 2005, he has been working towards the Ph.D. degree at the Circuit and Systems group, Delft University of Technology, Delft, The Netherlands.